



<https://theses.gla.ac.uk/>

Theses Digitisation:

<https://www.gla.ac.uk/myglasgow/research/enlighten/theses/digitisation/>

This is a digitised version of the original print thesis.

Copyright and moral rights for this work are retained by the author

A copy can be downloaded for personal non-commercial research or study,
without prior permission or charge

This work cannot be reproduced or quoted extensively from without first
obtaining permission in writing from the author

The content must not be changed in any way or sold commercially in any
format or medium without the formal permission of the author

When referring to this work, full bibliographic details including the author,
title, awarding institution and date of the thesis must be given

Enlighten: Theses

<https://theses.gla.ac.uk/>
research-enlighten@glasgow.ac.uk

THE UNIVERSITY OF CHICAGO

DEPARTMENT OF CHEMISTRY

LABORATORY OF ORGANIC CHEMISTRY

CHICAGO, ILLINOIS

1954

RESEARCH REPORT

NO. 100

BY

ROBERT H. WOOD

AND

WALTER H. WOOD

IN

COLLABORATION WITH

THE UNIVERSITY OF CHICAGO

1954

CHICAGO, ILLINOIS

ProQuest Number: 10646274

All rights reserved

INFORMATION TO ALL USERS

The quality of this reproduction is dependent upon the quality of the copy submitted.

In the unlikely event that the author did not send a complete manuscript and there are missing pages, these will be noted. Also, if material had to be removed, a note will indicate the deletion.



ProQuest 10646274

Published by ProQuest LLC (2017). Copyright of the Dissertation is held by the Author.

All rights reserved.

This work is protected against unauthorized copying under Title 17, United States Code
Microform Edition © ProQuest LLC.

ProQuest LLC.
789 East Eisenhower Parkway
P.O. Box 1346
Ann Arbor, MI 48106 – 1346

SIMULTANEOUS CREEP AND OXIDATION OF NICKEL

William Alexander Abernethy

Submitted for the degree of Master of Science

Department of Mechanical Engineering
University of Glasgow

July, 1979

Thesis
5045
Copy 2.



ACKNOWLEDGMENT

The financial assistance of the Science Research Council, during the period of this research work, is gratefully acknowledged.

TABLE OF CONTENTS

	<u>Page</u>
SUMMARY	1
CHAPTER I THE EFFECT OF ENVIRONMENT ON CREEP BEHAVIOUR	
1.1 Introduction	3
1.2 Creep Testing Environment	3
1.3 The Creep/Environment Effect of Different Metals and Alloys	5
1.4 Oxidation Rate	5
1.5 Rupture Life	6
1.6 Creep Rate and Creep Curves	8
1.7 Creep Curve Form for Oxidation Strengthened Material	9
1.8 Ductility	10
1.9 Crack Formation	11
1.10 Weakening Mechanisms	12
1.11 Strengthening Mechanisms	13
1.12 Discussion of Weakening and Strengthening Mechanisms	16
CHAPTER II THE OXIDATION AND CREEP CHARACTERISTICS OF NICKEL	
2.1 Introduction	19
2.2 The High Temperature Oxidation of Nickel	19
2.3 The Creep of Nickel	25
2.4 Potential Interference of the Creep and Oxidation Mechanisms of Nickel	31
2.5 The Simultaneous Creep and Oxidation of Nickel - A Survey of Prior Work	33
2.6 Literature Review Summary	38
2.7 Aims of the Investigation	38

	<u>Page</u>
CHAPTER III	APPARATUS AND EXPERIMENTAL
3.1	Introduction 40
3.2	Constant Stress Creep Testing Apparatus 40
3.3	Constant Stress Loading Theory 45
3.4	Oxidation Apparatus 47
3.5	Other Apparatus and Facilities 48
3.6	Specimen Preparation 48
3.7	Test Conditions 49
CHAPTER IV	RESULTS AND METALLOGRAPHY
4.1	Introduction 51
4.2	Creep Rupture Tests at 950°C 52
4.3	Creep Rupture Tests at 700°C 53
4.4	Strain/Time Creep Curves 54
4.5	Comparison of Strain/Time Curves in Vacuum and Oxygen at 950°C 57
4.6	Creep of Pre Oxidised Specimens 59
4.7	Effect of Atmosphere Change during a Creep Test 60
4.8	External Appearance of Specimens 61
4.9	Metallography of Specimens Creep Tested at 700°C 62
4.10	Metallography of Specimens Creep Tested in Vacuum at 950°C 63
4.11	Metallography of Specimens Creep Tested in Oxygen at 950°C 64
4.12	Metallography of Unstressed Specimens 66
4.13	Metallographic Comparison of Stress _A ^{ed} and Unstressed Oxidation Specimens 68
4.14	Metallographic Illustration of Oxide Growth in a Simulated Crack 69
4.15	Metallography of the Oxide Layer 70
4.16	Scanning Electron Microscopy 71

	<u>Page</u>
CHAPTER V	DISCUSSION
5.1	Introduction 73
5.2	Primary Creep 74
5.3	Secondary Creep 75
5.4	Void Nucleation 77
5.5	Void Growth and Coalescence 79
5.6	Crack Initiation and Propagation 81
5.7	Fluctuating Creep Rate 83
5.8	Fracture 86
5.9	Rupture Life 87
5.10	Effect of Temperature and Stress on the Creep of Nickel in Oxygen 87
5.11	Prediction of an Atmosphere Effect on Creep 92
5.12	The Oxidation of Nickel at 950°C 93
5.13	Conclusions 97
LIST OF REFERENCES	99

LIST OF TABLES AND FIGURES

Tables and Figures are located, in that order, at the end of each relevant chapter.

	<u>Following Page</u>
CHAPTER I	18
Fig. 1	Relationship between Applied Stress and Creep Rupture Life
Fig. 2	Potential Differences between Creep Curves in Oxidising and Inert Atmospheres
Fig. 3	Creep Curve for Oxidation Strengthened Nickel
CHAPTER II	39
Table I	List of Published Creep Data for Nickel
CHAPTER III	50
Table II	Loading Parameters for Constant Stress Creep Tests
Table III	Analysis of Nickel 270
Fig. 4	Schematic View of Constant Stress Apparatus
Fig. 5	Simplified View of Constant Stress Apparatus showing Ancillary Equipment
Fig. 6	Vacuum Equipment for Constant Stress Apparatus
Fig. 7	Improved Version of Constant Stress Creep Apparatus
Fig. 8	n, δ Characteristics for Maximum Strain Rate Error of $\pm 5\%$
Fig. 9	Apparatus for the Oxidation of Stressed Specimens
Fig. 10	Nickel Specimens

CHAPTER IV

Table IV	Creep Data for Annealed Specimens tested at 950°C in Vacuum
Table V	Creep Data for Annealed Specimens tested at 950°C in Oxygen
Table VI	Creep Data for Annealed Specimens tested at 700°C
Table VII	Statistical Data of Creep Strain after 0.5 hrs. at 950°C
Table VIII	Creep Data for Pre Oxidised Specimens at 950°C
Table IX	Creep Data for Tests at 950°C started in Vacuum and continued in Oxygen
Table X	Creep Data for Tests at 950°C started in Oxygen and continued in Vacuum
Fig. 11	Relationship between Secondary Creep Rate and Rupture Life at 950°C
Fig. 12	Relationship between Stress and Rupture Life at 950°C
Fig. 13	Relationship between Stress and Secondary Creep Rate at 950°C
Fig. 14	Relationship between Secondary Creep Rate and Rupture Life at 700°C
Fig. 15	Relationship between Stress and Rupture Life at 700°C
Fig. 16	Relationship between Stress and Secondary Creep Rate at 700°C
Fig. 17	Creep Curves at 700°C
Fig. 18	Creep Curves at 950°C and Low Stress in Vacuum
Fig. 19	Creep Curves at 950°C and Low Stress in Oxygen
Fig. 20	Creep Curves at 950°C and 11.0 N/mm ² in Vacuum
Fig. 21	Creep Curves at 950°C and 11.0 N/mm ² in Oxygen
Fig. 22	Creep Curves at 950°C and 12.0 N/mm ² in Vacuum
Fig. 23	Creep Curves at 950°C and 12.0 N/mm ² in Oxygen

Fig. 24	Creep Curve at 950°C and 12.0 N/mm ² in Oxygen	72
Fig. 25	Early Stages of Creep at 950°C	
Fig. 26	Early Stages of Creep at 950°C and 11.0 N/mm ²	
Fig. 27	Early Stages of Creep at 950°C and 12.0 N/mm ²	
Fig. 28	Interrupted Creep at 950°C and 11.0 N/mm ²	
Fig. 29	Creep of Pre Oxidised Nickel at 950°C and 12.0 N/mm ²	
Fig. 30	Creep of Pre Oxidised Nickel at 950°C and 12.0 N/mm ² in Oxygen	
Fig. 31	Creep of Nickel at 950°C and 10.0 N/mm ² - Oxygen then Vacuum	
Fig. 32	Creep of Nickel at 950°C and 10.0 N/mm ² - Vacuum then Oxygen	
Fig. 33	Creep of Nickel at 950°C and 11.0 N/mm ² with Atmosphere Change	
Fig. 34	Annealed Specimen after Creep Testing	
Fig. 35	Pre Oxidised Specimen after Creep Testing	
Fig. 36	Failed Specimen in Creep Rig	
Fig. 37	Voids near Specimen Surface	
Fig. 38	Voids near Fracture Surface in Specimen Centre	
Fig. 39	Voids in Specimen Centre	
Fig. 40	Voids near Specimen Surface	
Fig. 41	Fracture Surface and Adjacent Cracking	
Fig. 42	Typical Grain Boundary Void Chain	
Fig. 43	Coalescence of Grain Boundary Voids	
Fig. 44	Serrations on Crack Faces	
Fig. 45	Serrations on Fracture Surface	
Fig. 46	Void Formation near Specimen Surface	

Fig. 47	Void Formation near Specimen Surface	72
Fig. 48	Void Distribution across Specimen	
Fig. 49	Voids near Specimen Surface	
Fig. 50	Voids in Centre of Specimen	
Fig. 51	Crack at Specimen Surface	
Fig. 52	Crack System near Specimen Surface	
Fig. 53	Crack System in Specimen Centre	
Fig. 54	Crack Formation at Specimen Surface	
Fig. 55	Fracture Surface	
Fig. 56	Cracks and Voids at Specimen Surface	
Fig. 57	Oxide Filled Crack at Specimen Surface	
Fig. 58	Crack System at Specimen Surface	
Fig. 59	Void Distribution across Specimen	
Fig. 60	Void Distribution across Specimen	
Fig. 61	Voids near Specimen Surface	
Fig. 62	Voids near Specimen Surface	
Fig. 63	Voids near Specimen Surface	
Fig. 64	Voids in Specimen Centre	
Fig. 65	Voids in Specimen Centre	
Fig. 66	Oxidation of Void Coalescence near Specimen Surface	
Fig. 67	Structure of Stressed Specimen	
Fig. 68	Structure of Unstressed Specimen	
Fig. 69	Structure of Stressed Specimen	
Fig. 70	Structure of Unstressed Specimen	
Fig. 71	Structure of Stressed Specimen	
Fig. 72	Structure of Unstressed Specimen	
Fig. 73	Structure of Stressed Specimen	

Fig. 74	Structure of Unstressed Specimen	72
Fig. 75	Oxide Growth in Simulated Crack	
Fig. 76	Oxide Growth in Simulated Crack	
Fig. 77	Oxide Growth in Simulated Crack	
Fig. 78	Oxide Growth in Simulated Crack	
Fig. 79	Surface Oxide on Stressed Specimen	
Fig. 80	Surface Oxide on Unstressed Specimen	
Fig. 81	Surface Oxide on Stressed Specimen	
Fig. 82	Surface Oxide on Stressed Specimen	
Fig. 83	Surface Oxide on Stressed Specimen	
Fig. 84	Surface Oxide on Unstressed Specimen	
Fig. 85	Specimen after Creep Testing	
Fig. 86	Typical Region of Fracture Surface	
Fig. 87	Typical Region of Fracture Surface	
Fig. 88	Typical Region of Fracture Surface	
Fig. 89	Typical Region of Fracture Surface	
Fig. 90	Oxide on Fracture Surface	
Fig. 91	Oxide on Fracture Surface	
Fig. 92	Feature on Fracture Surface	
Fig. 93	Plan View of Oxide on Specimen Surface	
Fig. 94	Plan View of Oxide on Specimen Surface	
Fig. 95	Plan View of Oxide on Specimen Surface	
Fig. 96	Plan View of Oxide on Specimen Surface	
Fig. 97	Fractured Section of Two Layer Oxide	
Fig. 98	Fractured Section of Outer Oxide Layer	
Fig. 99	Fractured Section of Inner Oxide Layer	

CHAPTER V

Fig. 100	Plot of Nickel Oxide Surface Advancement at 950°C	
----------	---	--

Key to Information Associated with Photographs in Figs. 34 to 99

The following information appears, in this order, in the line beneath the title of each figure:

- (1) Photograph Magnification
- (2) Test Atmosphere
- (3) Test Temperature
- (4) Applied Stress
- (5) Test Duration (the letters R.L. indicate that fracture occurred and the quoted time is a rupture life)

In addition, a double headed arrow shows the axis of applied stress, where applicable.

The etchant used was acid ferric chloride.

SUMMARY

A comprehensive literature review, covering the effect of environment on creep and the creep and oxidation of nickel is given.

The creep behaviour of high purity nickel is compared in atmospheres of oxygen (400 torr) and vacuum (10^{-1} torr from air). Constant stress creep tests were carried out in an apparatus of novel design due to Fletcher (J. Phys. E. Sci. Inst. vol 4. p 821. 1971). At 700°C , stresses in the range 23 N/mm^2 to 32 N/mm^2 were applied. At 950°C , stresses in the range 8 N/mm^2 to 12 N/mm^2 were applied. Oxidation experiments were also carried out.

There was no apparent effect of atmosphere on creep at 700°C . The bulk of the work was conducted at 950°C and at this temperature there were considerable differences between the creep behaviour of nickel in oxygen and vacuum. The creep data in terms of rupture life, secondary creep rate and elongation values are presented and discussed. The form of the creep curves is examined. Metallographic evidence from creep and oxidation specimens is presented and discussed.

Rupture life was increased from less than thirty hours in vacuum to several hundred hours in oxygen with a corresponding increase in elongation. The increase in rupture life was highly sensitive to stress. In oxygen, primary stage strain was reduced, no steady state stage existed and creep progressed directly from an extended primary stage of decreasing creep rate, directly into an extended tertiary stage of fluctuating creep rate.

It is suggested that simultaneous oxidation modifies the creep process in several ways. The occurrence of an oxide layer reflects dislocations at the surface, causing an increase in dislocation density and work hardening rate. The injection of vacancies into the metal by the oxidation process interferes with intragranular

deformation and prevents the attainment of a balance between work hardening and recovery. Vacancy injection also modifies the grain boundary void growth mechanism, reducing the tendency for coalescence and delaying crack initiation.

The major cause of delayed fracture is due to oxide formation in grain boundary cracks. The oxide inhibits crack propagation by forming load bearing bridges and blunting crack tips. A quantitative assessment is made of the dependence of this effect on temperature and stress. Extensive damage can be tolerated in an oxygen atmosphere and the nickel is transformed into a nickel/nickel oxide composite. A large proportion of the increased rupture life in oxygen is concerned with damage accumulation. The non-uniformity of this damage accumulation results in a fluctuating creep rate.

CHAPTER I

THE EFFECT OF ENVIRONMENT ON CREEP BEHAVIOUR

1.1 Introduction

The fact that atmosphere plays a role in determining the creep behaviour of metals has been known for a considerable time. A number of investigations into this effect have been carried out and reported. As yet no complete explanation has emerged and various conflicting theories and mechanisms have been published. Attention was first drawn to the subject in a review by H. H. Bleakney⁽¹⁾ in which he suggested that the effect of oxidation on intercrystalline failure in the stress rupture test deserved attention.

Results of investigations on various metals have been reported but most of the work concerned those metals used for high temperature service, i.e. nickel and the nickel base alloys. The general picture of the effect of environment on the creep behaviour of metals is at first sight extremely confused. Evidence of both increased and decreased creep resistance of metals in oxidising versus inert atmospheres has been reported and this must be examined in considerable detail to separate the various effects.

1.2 Creep Testing Environment

The term "environment" is taken to mean the gaseous atmosphere in which creep testing is carried out, although relevant investigations have used molten lead⁽²⁾ and sodium hydroxide⁽³⁾ in contact with the test pieces.

Early investigations, having highlighted an environment effect on creep behaviour^(2,4,5), underlined the need to conduct creep tests designed for service life prediction in atmospheres similar to those of actual service.

Creep testing in different atmospheres demands that a truly inert atmosphere be found on which to base comparisons. Reactive gases such as oxygen and hydrogen and even nitrogen, must be avoided, as must contamination by these gases, however slight, of a chosen inert atmosphere. Commonly used inert atmospheres are helium, argon and vacuum of sufficiently low pressure.

Shepard and Schalliol⁽²⁾ demonstrated the difficulty of obtaining sufficiently pure inert gases and most workers have used vacuum as the inert atmosphere. The environment effect considered here is based on a comparison of creep in oxidising atmospheres and in inert atmospheres.

Shepard and Schalliol⁽²⁾ considered the possibility of vacuum and helium atmospheres exerting a weakening effect on the metal, but the subsequent investigations^(3 to 21) accepted that it was the presence of oxygen which gave rise to any strengthening or weakening effects.

Shahinian⁽⁵⁾ conducted creep tests in atmospheres of air, oxygen, nitrogen, helium and vacuum. For several alloys the results generally showed that the longest rupture lives occurred in air followed by oxygen, nitrogen, helium and vacuum. In some cases contamination of the test atmosphere by traces of oxygen and nitrogen gave even longer rupture lives than found in air. This, and differences between helium and vacuum results, indicated the importance of impurities in the atmosphere affecting

creep behaviour. Minimum creep rate was usually lowest in air but other atmospheres did not exert a consistent effect.

Ductility appeared to be highest in vacuum but other atmospheres did not give consistent results. It was concluded that high rupture strength and also notch strengthening was associated with the presence of oxygen.

Stegman et al⁽⁶⁾ conducted creep tests in various "vacuum" pressures of oxygen and Hough and Rolls⁽⁷⁾ performed creep tests in argon with varying oxygen contents. Both found that as the oxygen pressure increased so the creep resistance decreased.

A considerable accumulation of evidence therefore exists to demonstrate that the presence of oxygen in the atmosphere is a major cause of any effect on creep behaviour.

1.3 The Creep/Environment Effect of Different Metals and Alloys

Steel has been reported to show both decreased^(1,3) and increased⁽⁵⁾ creep resistance in an oxidising atmosphere. Pure iron^(7,8) and cobalt⁽⁸⁾ have only been reported as showing decreased creep resistance in an oxidising atmosphere. Aluminium and copper⁽⁴⁾ and cobalt base alloys⁽⁵⁾ have only been reported as giving increased creep resistance in an oxidising atmosphere.

Nickel^(3,6,8 to 14) and the nickel base alloys^(2,5,10,12,15 to 18) have been reported as showing both increased and decreased creep resistance in an oxidising atmosphere dependent on the stress and temperature employed. Generally increased creep resistance is found at low stress and high temperature, with decreased creep resistance found at high stress and low temperature.

1.4 Oxidation Rate

The extent of occurring oxidation has been shown to be

related to the degree of environment effect on creep behaviour. Bleakney⁽¹⁾ quoted work which had shown the oxidation resistance of alloys to be proportional to the rupture life at which creep resistance was lowered in an oxidising atmosphere. He also referred to results which demonstrated that the ratio of the rupture lives of steel in steam and air was of the same order as the ratio of the extent of oxidation occurring in the two atmospheres.

Shahinian and Achter^(9,15) showed, for nickel and a nickel-chromium alloy, that the rupture lives at which the relative creep resistances in air and vacuum reversed were in accord with the corresponding oxidation rates. They also found, as did Shahinian⁽¹²⁾, that pronounced oxidation strengthening occurred in cases where long rupture lives are encountered. This indicates that the greater the exposure time to an oxidising atmosphere and therefore greater extent of oxidation, so the greater the atmosphere effect.

Hough and Rolls⁽⁷⁾ and Hancock and Fletcher⁽¹⁹⁾ found that pre-oxidation gave a reduction in creep resistance over and above a weakening effect caused by simultaneous oxidation and creep. Hough and Rolls also showed the extent of pre-oxidation to be proportional to the decrease in creep resistance. Thus it can be said that the extent of oxidation is closely related to the magnitude of any atmosphere effect on creep.

1.5 Rupture Life

Rupture life is possibly the most important parameter when judging creep strength. As referred to by Bleakney⁽¹⁾ there is a power function relationship between applied stress and creep rupture life. This can be demonstrated graphically on a log log

plot (Fig. 1). Any abrupt change of slope in this curve indicates a change in the relationship. Curve A shows a constant relationship where the creep behaviour is similar over the entire stress range. Curve B shows a sharp break in the curve with the region of increased slope showing the intrusion of some factor causing marked weakening at longer rupture lives. Curve C shows the same for a factor causing marked strengthening.

Several investigations^(1,3,9,12,15,16,17) have found such features when examining data for creep in an oxidising atmosphere. Several of these workers^(1,12,16,17) proposed that such breaks indicated a new factor coming into play under critical conditions. Where a material displays a reversal in the relative creep strengths in an oxidising atmosphere against inert atmosphere, the log rupture life versus log stress plot can be used to specify the reversal point, e.g. the point x on curves D and E in Fig. 1. Again this has been demonstrated by several investigators^(3,9,15,16).

Comparisons of the rupture lives of materials tested in oxidising and inert atmospheres show evidence of both longer and shorter life in the oxidising atmosphere. This can be due to an overall difference in the stress versus rupture life relationship between the two atmospheres or a change in the relationship at a certain rupture life for creep in an oxidising atmosphere. A combination of the two may be present in that the relationship for an inert atmosphere does not necessarily match either portion of an equivalent oxidising atmosphere curve containing a change of slope. Generally, where an oxidation strengthening effect is present, the magnitude of the effect on rupture life is greater at longer rupture lives.

1.6 Creep Rate and Creep Curves

Usually where the effect of an oxidising atmosphere is to decrease rupture life there is a corresponding increase in creep rate and vice versa. The classic creep curve contains three regions where the creep rate has a different time dependence and evidence has been presented to show variance from this generalisation in at least one of these regions.

Sweetland and Parker⁽⁴⁾ showed that an air atmosphere and the resultant formation of an oxide film reduced the steady state creep rate of copper and aluminium. No correlation with rupture life was given. At low pressures Stegman et al⁽⁶⁾ showed creep rate to be dependent on oxygen pressure.

Steady state or minimum or secondary creep rate usually follows the inverse rule relative to rupture life and several investigations^(5 to 10,12 to 18,20) have given evidence showing this to be the case when creep properties are compared in oxidising versus non-oxidising atmospheres. Exceptions to this have been found. Sherman and Achter⁽¹⁰⁾ showed a curve for nickel where the secondary creep rate in air and vacuum was practically the same, but the vacuum tested specimen entered tertiary and failed before the air tested specimen. Bogacher et al⁽⁸⁾ found for cobalt that the primary and secondary creep rates were lower in air than vacuum, but the air tested specimen entered tertiary and failed prior to that in vacuum.

Shahinian and Achter⁽¹⁶⁾ found for nickel-chromium-aluminium alloy that the steady state creep rate was similar in air and vacuum, but the air test entered tertiary and failed first.

They^(9,15) also showed cases where air tested specimens exhibited a lower primary creep rate but higher secondary and

tertiary rates and earlier failure than vacuum tested specimens. Conversely, Duquette⁽¹³⁾ and Steele⁽¹⁴⁾ gave evidence of vacuum tested specimens with a lower primary creep rate but higher secondary and tertiary and earlier failure than air tests.

A comparison of creep behaviour in oxidising versus non-oxidising atmospheres can therefore show: (1) an overall difference in creep rates, Fig. 2a; (2) a difference in the creep rate of particular stages, Fig. 2b; (3) an alteration to the time at which the transition between stages occurs, Fig. 2c.

1.7 Creep Curve Form for Oxidation Strengthened Material

A creep curve of peculiar form has been reported^(9,11,12,14 to 17,21) for nickel and nickel base alloys when conditions are such to give oxidation strengthening. As shown in Fig. 3, creep behaviour initially passes through the three normal stages, but instead of failing in tertiary, the creep rate is drastically reduced and a "fourth stage of decelerating creep" is entered. Shahinian and Achter⁽¹⁶⁾ found that fracture occurred abruptly during this stage, but Widmer and Grant⁽¹⁷⁾ reported a fifth stage of accelerating creep, similar to the conventional tertiary stage, prior to fracture. Steele⁽¹⁴⁾ reported instances of multi stage creep where these fourth and fifth stages were repeated several times before fracture.

Reports of similar inflections in creep curves have been attributed to recrystallisation^(1,22,23), but there is strong evidence that it results from a different cause in oxidising atmospheres. It has only been reported where creep conditions have been in an oxidation strengthened region. The creep behaviour closely matched comparable vacuum tested specimens up to entry into the fourth stage^(11,12,15,16). The vacuum specimens

failed at this point. The phenomenon appears to be a consequence of highly effective oxidation strengthening in the tertiary stage coincident with extensive intergranular cracking, especially in materials with a high creep resistance^(12,15,16,17).

1.8 Ductility

Extension and reduction of area values are generally taken as a measurement of deformation prior to failure. In creep most metals fail by intercrystalline fracture and, strong creep resistant materials especially, do so while exhibiting very low ductility. Similarly, as rupture life increases so ductility decreases⁽¹⁷⁾.

Little specific attention has been given to the effect of an oxidising atmosphere on ductility. Several investigations^(3,5,6,7,9,10,11,12,15,18,25) have indicated reduced ductility, in terms of elongation or reduction of area, or both, in oxidising versus inert atmosphere. Pre-oxidation can also reduce ductility^(7,26). Those investigators^(10,18,25) who considered ductility as such, and found it to be reduced in an oxidising atmosphere, attributed this absorption of oxygen into the grain boundaries. Conversely, where pronounced oxidation strengthening was encountered, reduction of area and elongation were ^{increased} in the oxidising atmosphere^(10,11,12,15,16,17). In these cases this was not regarded as a true ductility effect due to the large volume of oxide formed in the grain boundaries.

Duquette⁽¹³⁾, however, reported increased ductility for a single crystal tested in an oxidising atmosphere.

Apart from the "false" increases in ductility, the most widely found effect is a lowering of ductility in oxidising versus inert atmospheres. This is probably a grain boundary

effect and is independent of the effect on rupture life. For single crystals, where rupture life increased in an oxidising atmosphere, the increased ductility may merely be a greater allowed deformation during the longer test time.

1.9 Crack Formation

The classic creep failure by intercrystalline cracking⁽²⁴⁾ is especially found at high temperature and low stress. At low temperature and high stress, failure is more likely to be transcrystalline. As stress decreases and rupture life increases this change in failure mode from trans to inter crystalline can give rise to a break in the plot of log stress versus log rupture life^(1,27,28), giving shorter than expected rupture lives from extrapolation of high stress results.

Environment only affects cracks formed at the surface of the material undergoing creep. Internal cracks are unaffected and are basically a function of strain^(6,18). Overwhelming evidence exists to show the extent of surface intergranular cracking is always greater in an oxidising relative to inert atmosphere. This is in terms of both crack initiation^(7,10,15,18) and propagation rate^(6,8,9,10,12,15) being greater. Evidence has also been presented to show a greater tendency for intergranular relative to transgranular cracking in an oxidising environment^(2,10,12,25,26). Effects on crack formation have not been found where conditions unequivocally cause transgranular cracking^(12,15).

Exceptions have been noted and Shahinian⁽⁵⁾ reported less surface cracking in an oxidising environment. Significantly, Duquette⁽¹³⁾ found less surface cracking in an oxidising atmosphere when testing single crystals.

Thus while an oxidising atmosphere may inhibit transgranular fracture, it certainly promotes intergranular fracture. This has also been reported for fatigue^(29,30,31,32).

1.10 Weakening Mechanisms

The most frequently advanced mechanism whereby creep resistance is lowered in an oxidising compared to inert atmosphere has been a grain boundary effect. Bleakney appears to have originated both theories, one of preferential grain boundary oxidation⁽¹⁾ and that of absorption of gas into the grain boundaries⁽²⁵⁾.

Preferential oxidation, the less popular theory, was first given a speculative mention^(1,8) but later investigations presented metallographic evidence in support^(14,18). Indeed Chaku and McMahon⁽¹⁸⁾ proffered a detailed case for the selective oxidation of grain boundaries forming massive oxide layers therein and the subsequent cracking and failure of these oxide wedges. McMahon and Coffin⁽³¹⁾ proposed a similar mechanism for failure under fatigue loading. Holmes and Pascoe⁽³³⁾ considered, but discounted, the possibility of a jacking displacement from such wedges opening cracks in the metal, but Hough and Rolls⁽⁷⁾ did suggest that stress intensification could result at the crack tip. Douglass⁽²⁶⁾, investigating pre-oxidation effects, suggested that grain boundary oxides would inhibit grain boundary sliding and provide a notch embrittling effect.

Greater credence is given to the gas absorption theory. Bleakney⁽²⁵⁾ suggested that oxygen absorbed into grain boundaries would act as an impurity leading to embrittlement and inter-crystalline failure. Shahinian and Achter⁽⁹⁾ proposed that absorption of gases onto the freshly exposed surface at the tip of a propagating crack would lower the surface energy and

facilitate crack propagation. This has been re-iterated in several investigations concerning creep^(6,7,10,12,14,15,16) and also fatigue^(29,30,32). Sherman and Achter⁽¹⁰⁾ further suggested that gas diffusion along the grain boundary could lower intergranular cohesion ahead of a crack. Stegman et al⁽⁶⁾ investigated the effect using various "vacuum" pressures of oxygen and successfully calculated a correlation of the results with the kinetic theory of gas.

Other, seemingly minor, effects have been suggested. Stresses set up at the metal/oxide interface could be responsible for an increased creep rate^(4,20,33). Cracks initiated within the surface oxide film, especially mechanically weaker thick films, could propagate across the interface into the metal^(7,33).

Rather more attention has been focused on the interaction between vacancy flow and formation of grain boundary voids due separately to creep and oxidation. This has been suggested as a cause of increased creep rate and intercrystalline cracking^(7,19,26,33).

Thus the gas absorption theory is well established as the major cause of the degradation of creep properties. Oxide formation within grain boundaries is a less certain cause of decreased creep resistance, especially in view of the fact that this same oxide formation is widely regarded as giving increased creep resistance. The theory of vacancy flow interaction has only received relatively recent consideration and may well prove to be of considerable importance.

1.11 Strengthening Mechanisms

The exposure of a metal to an oxidising environment results in the formation of a surface film or layer of oxide, the thick-

ness of which increases with time. Considering concurrent creep and oxidation, this surface layer will be present from the outset of creep and, therefore, has the potential to affect the creep process at all times. It has been suggested that such a surface layer can suppress dislocation generation and movement by acting as a barrier to their escape at the metal surface^(3,4,5,8,9,13,20,34). This suppresses slip processes which reduces the occurring deformation, lowering the creep rate. Originally, it was demonstrated⁽³⁴⁾ that the introduction of copper into the surface layer of a zinc single crystal could reduce the creep rate and alter its temperature dependence. It was then found that a similar effect was caused by the presence of an oxide film on a metal surface⁽⁴⁾. Subsequent investigations re-iterated and confirmed the effect, in some cases adding to the understanding of the mechanism^(8,13,20).

A hardening process in alloys resulting from internal oxidation was reported by Meijering and Druyvestyen⁽³⁵⁾. The mechanism, analogous to dispersion hardening, was a blocking of the glide planes by small oxide particles. Several investigators^(2,3,5,9,11,17,33) have suggested that during creep in an oxidising atmosphere this process would strengthen the material by increasing its resistance to deformation. Conversely Douglass⁽²⁶⁾ suggested that such a mechanism could serve to lower the creep resistance by embrittlement.

A third mechanism, responsible for spectacular increases in rupture life, comes into play during the latter stages of creep once crack formation has commenced. Most investigations have concerned polycrystalline material and therefore an intercrystalline crack mode, but this mechanism has been applied to single crystals⁽¹³⁾. It has been suggested, and in many cases backed

by metallographic evidence, that oxide forms inside cracks and blunts the crack tip reducing stress concentration and lowering the crack propagation rate^(5,9,12,14,16,17). Continued oxide formation can bridge or even completely fill the crack and this oxide may be able to sustain a tensile load^(3,11,12,14,16,17,21). Such mechanisms would not be applicable to all metals and alloys as it depends on the formation of a suitable oxide.

Thus increased creep resistance in an oxidising atmosphere is universally said to result from oxide formation. Interference with dislocation behaviour by a surface film would be applicable throughout the creep process and appears attractive, albeit arrived at by deduction rather than experimental proof, e.g. by electron microscope work on dislocation patterns. The hardening of metals by internal oxidation is open to interpretation as both a weakening and strengthening mechanism during creep. The original work⁽³⁵⁾ concerned alloys of silver, copper and nickel. The effect resulted from the oxidation of solute elements having a greater affinity for oxygen than the base metal. The work on nickel showed the hardening effect only with a relatively high concentration of aluminium. Most of the work on the effect of environment on creep has been carried out on nickel and nickel base alloys. Therefore in the majority of cases where the above mechanism has been cited, the original reference shows it to be inapplicable.

Much evidence has accumulated to support the mechanism of the formation of load bearing oxide within cracks. This would only be expected to occur in certain metals which form a suitable oxide. Although a great increase in rupture life can result, the metal has undergone such a drastic change, becoming a metal/metal

oxide composite, that it would then be unsuitable in many service applications.

1.12 Discussion of Weakening and Strengthening Mechanisms

The most obvious consideration is of the net result of simultaneously operating weakening and strengthening mechanisms. Much of the discussion on this topic has come from Shahinian and Achter^(9,10,12,15,16). It was suggested that strengthening being due to the formation of oxide and weakening being due to gas absorption would make conditions favouring appreciable oxidation favour increased creep resistance. Conditions of low stress and high temperature would, therefore, allow strengthening mechanisms to dominate while under conditions of high stress and low temperature, weakening mechanisms would dominate. This was borne out experimentally.

Even under conditions of extensive oxidation high strength alloys did not exhibit marked strengthening. This was attributed to the relative ineffectiveness of the oxide strength in relation to the metal strength⁽¹²⁾. This also indicates that under high stress conditions other strengthening mechanisms did not impart added creep resistance. Due to the relative absence of an atmosphere effect under such conditions, it was suggested that mechanisms acting both to increase and decrease creep resistance had cancelled each other out.

A distinct divergence of opinion exists as to whether grain boundary oxidation results in decreased or increased creep resistance. On the one hand Chaku and McMahon⁽¹⁸⁾ maintain that stress assisted preferential oxidation^{of} grain boundaries is followed by cracking of the oxide. The opposite school of thought led by Shahinian and Achter^(3,5,9 to 12, 14 to 17, 21) propound

the theory that intercrystalline cracking of the metal is followed by the formation of oxide within the cracks. The final structures would be similar and open to metallographic interpretation. Both theories referred to nickel base alloys, and nickel oxide is firmly adherent and load bearing. Metals which form mechanically weak, loosely adherent oxides, e.g. iron, would not be expected to exhibit oxide strengthening according to the load bearing oxide theory. The oxide formed on an alloy is not necessarily that of the base metal, especially in the region of grain boundaries where segregation may have occurred. This consideration may partly account for the disagreement over the effect of grain boundary oxidation. Chaku and McMahon⁽¹⁸⁾ found fine grained nickel alloy to be weakened but coarse grained to be strengthened, while Shahinian and Achter⁽⁹⁾ found that atmosphere effect on the creep of nickel to be independent of grain size. Therefore grain size may have a bearing on the effect.

Shahinian and Achter^(5,16) did not totally discount grain boundary oxidation ahead of a crack, but considered that the formation of oxide particles would inhibit grain boundary shear thus increasing creep resistance. Conversely, it could be argued that such particles would promote void formation⁽²⁴⁾ so decreasing creep resistance.

If stress assisted oxidation of grain boundaries does occur, it should be found over the entire gauge length of a stressed specimen but this has been found not to be the case⁽¹¹⁾.

Finally, there exists the apparent paradox that an oxidising atmosphere decreases creep resistance by promoting intercrystalline cracking, while this same cracking is essential to allow subsequent oxide formation therein, which imparts increased creep resistance.

Thus there are well formulated theories for weakening and strengthening mechanisms, which, when considered individually are quite logical, but attempts to reconcile the various theories leads to confusion and contradiction. Therefore further work is required to define the conditions under which mechanisms operate to cause increased or decreased creep resistance in oxidising atmospheres.

The general picture of the effect of atmosphere on creep has been outlined. As this present work concerns pure nickel, it is pertinent to turn in the next chapter to a specific review of the oxidation, creep and simultaneous creep and oxidation of nickel.

FIG. 1.

RELATIONSHIP BETWEEN APPLIED STRESS AND
CREEP RUPTURE LIFE.

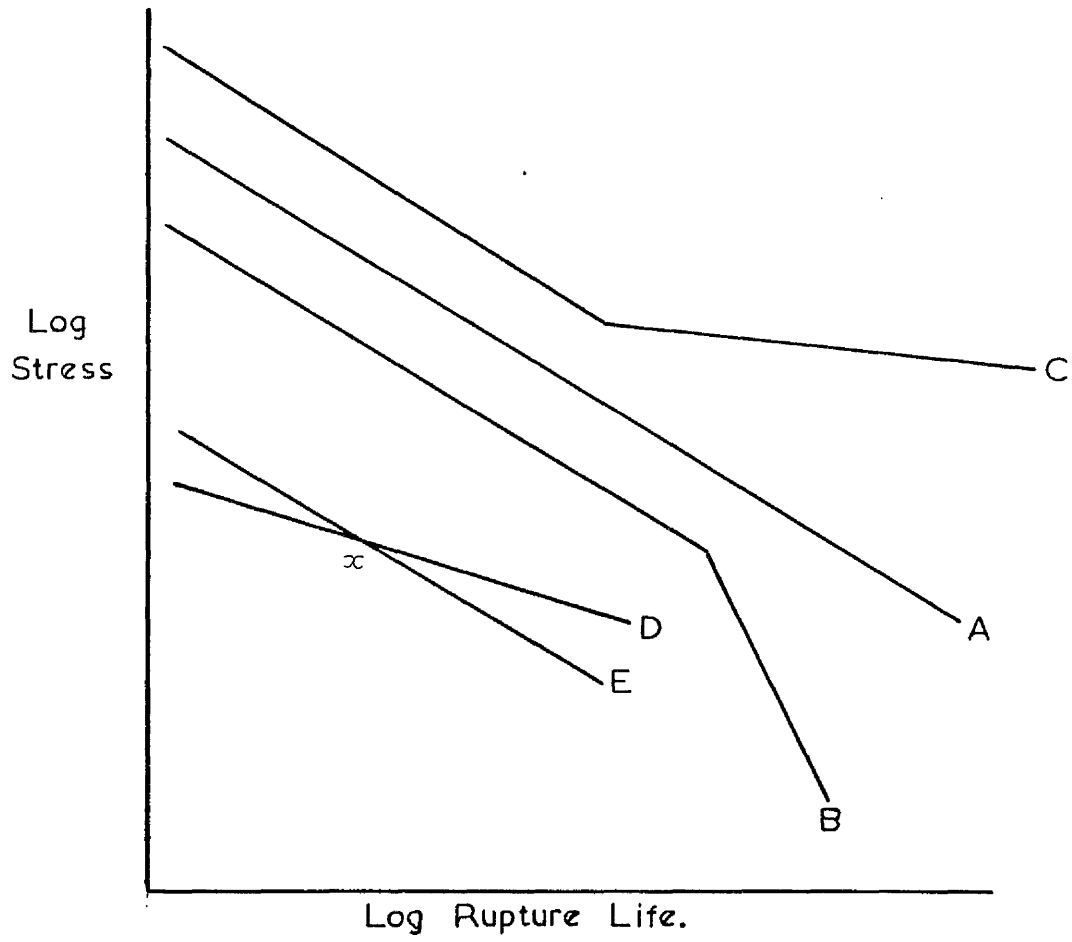


FIG. 2.

POTENTIAL DIFFERENCES BETWEEN CREEP CURVES
IN OXIDISING AND INERT ATMOSPHERES.

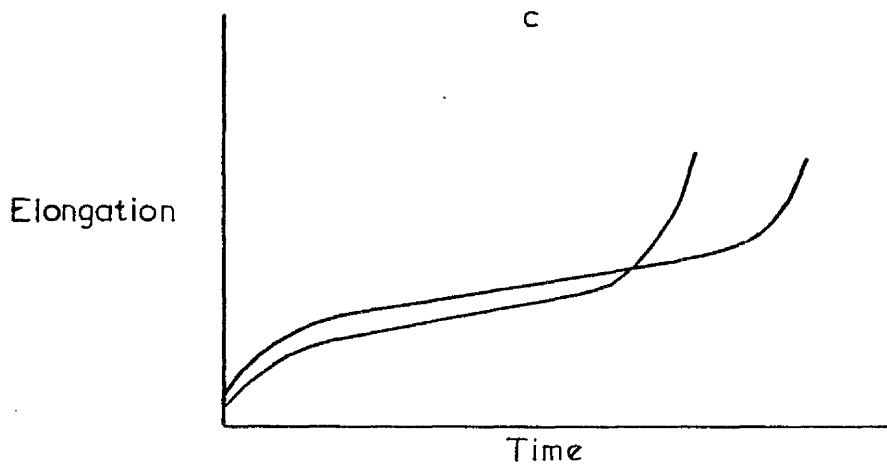
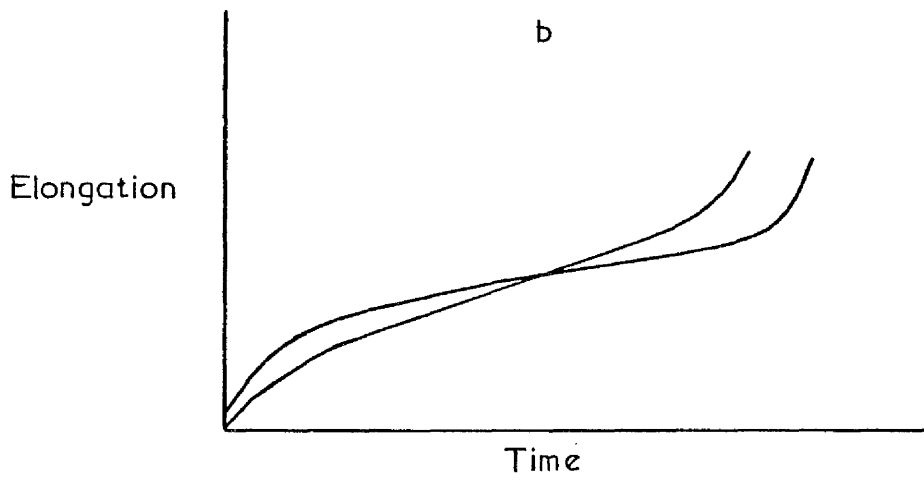
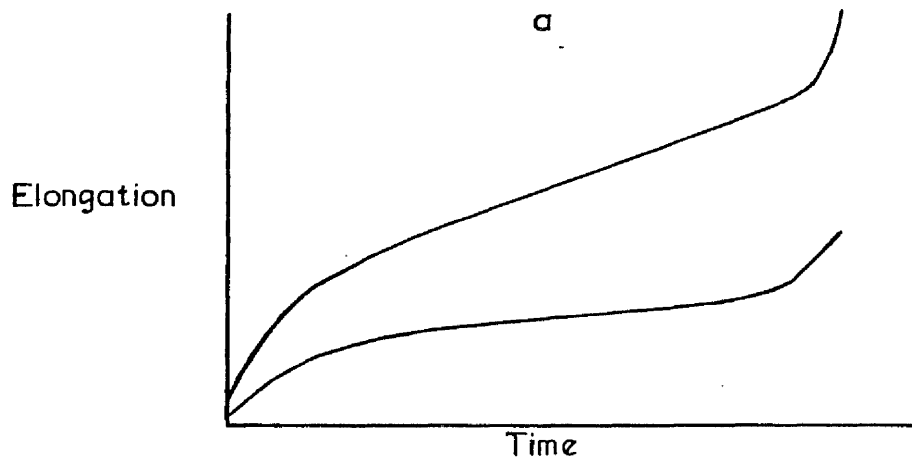
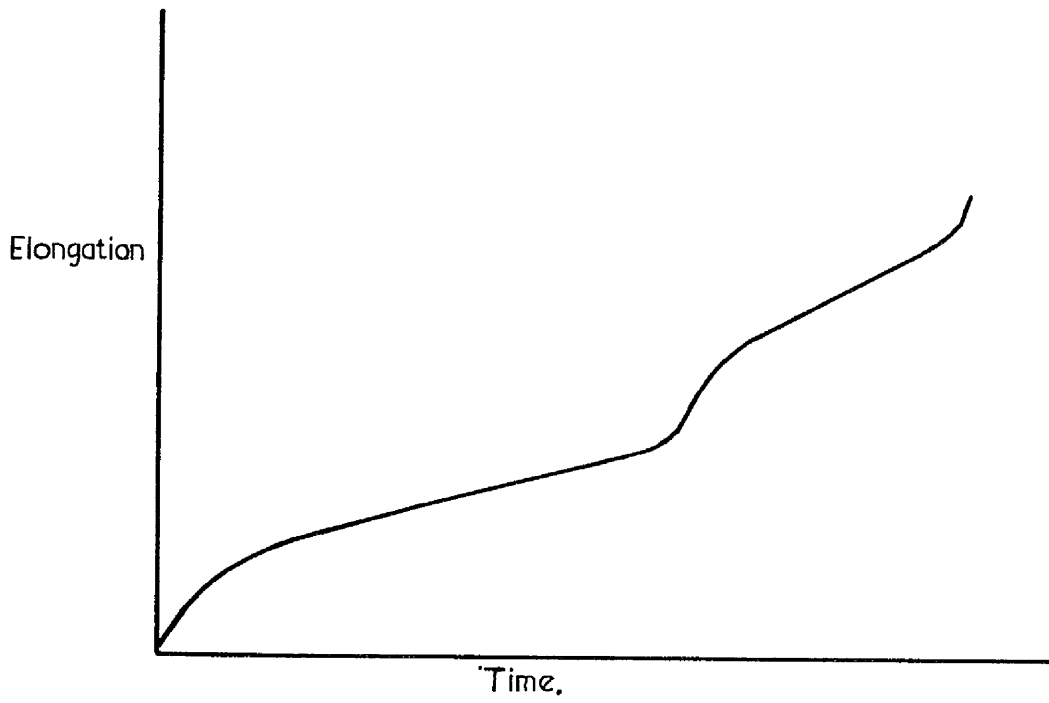


FIG. 3.

CREEP CURVE FOR OXIDATION STRENGTHENED NICKEL.



CHAPTER II

THE OXIDATION AND CREEP CHARACTERISTICS OF NICKEL

2.1 Introduction

In order to assess the effect of concurrent creep and oxidation, the separate mechanisms of creep and oxidation must first be considered. Potential interactions can then be postulated before examining the combined situation. In any case, a knowledge of these separate processes is essential when attempting to judge their effects on each other.

2.2 The High Temperature Oxidation of Nickel

Reviews by Seybolt⁽³⁶⁾ and Wood et al⁽³⁷⁾ give a fairly comprehensive description of the oxidation of nickel. A single oxide of nominal composition NiO is formed. This is a cation deficient p-type semi-conductor. The oxide, varying from a thin film at low temperatures (approximately 300°C) to a thick scale at 1400°C (melting point of nickel 1453°C), is formed by Wagner type mechanism with a parabolic rate at higher temperatures. Growth is controlled by the outward diffusion of Ni²⁺ ions through cation vacancies. This would indicate a one sixth power dependence of oxidation rate on oxygen pressure, but experimental evidence of a one fourth power dependence may suggest the ionization of only one electron hole per vacancy.

At temperatures above approximately 900°C, the scale, although of the single composition NiO, has a two layer structure and considerable discussion of this exists^(36 to 40). The most plausible theory of double layer formation is as follows. A

single layer scale grows, initially by the Wagner type mechanism, outward from the metal surface with a columnar grain structure. At some stage this adherent scale starts to lose contact with the underlying metal surface, generally agreed to be due to lack of plasticity in the growing oxide. Conditions in the so formed voidage or crack are such that NiO will dissociate, the nickel ions diffusing outward to the scale/oxidising atmosphere interface and the oxygen ions remaining to form fresh oxide at the metal surface. The inner layer is porous and allows dissociatively produced oxygen to reach the metal surface continuing the inward growth of the inner layer. The outer layer continues to grow by a Wagner mechanism, albeit by indirect nickel ion diffusion and its parabolic growth rate remains controlling.

Most workers agree the inner layer to be a light green colour with the outer layer being darker, descriptions varying from black through grey and blue to green. The ratio of thickness of the inner to outer layer changes from 0.5 at 1000°C to 0.2 at 1300°C. The extent of double layer formation decreases as nickel purity increases. Mrowec⁽³⁸⁾ detailed a mechanism of double layer formation based on oxide plasticity and specimen geometry in terms of the pinning influence of corners and small radii. Such a loss of contact at the scale/metal interface would agree with the observed temperature dependence.

A noteworthy comment by Wood et al^(37,39) was of the frequent occurrence of deep internal oxidation, even in high purity nickel, and it was suggested that this was due to a particularly high solubility of oxygen in the metal grain boundaries.

Hancock and Fletcher⁽¹⁹⁾ described the oxidation of high purity nickel in terms of vacancy concentration and void formation in the metal. They found that a high vacancy concentration or

supersaturation in thin metal specimens gave rise to a lower oxidation rate than in thicker specimens where the vacancy concentration was assumed to be lower. The number and penetration depth of grain boundary voids was found to increase as temperature and therefore extent of oxidation increased. In the thicker specimens (1.25 mm) at 1000°C voids formed within thirty minutes oxidation time and they penetrated the complete depth in four hours. Intergranular oxidation was observed above 900°C. Thin specimens (0.12 mm) essentially consisted of a string of single crystals, i.e. grain boundaries were nearly perpendicular to the main oxidising surface. Few grain boundary voids were found in these specimens. It was considered that effective vacancy sinks were only present on grain boundaries parallel to the metal surface. Therefore the relative absence of voids in the thin specimens compounded the vacancy concentration differential due to the size effect. In the thicker specimens void nucleation was said to occur heterogeneously at low vacancy supersaturations. The oxidation rate of the thick specimens eventually fell below that predicted by parabolic theory and it was postulated that this could be due to the attainment of some critical void size. The findings were concluded to be a possible explanation of discrepancies between various reported oxidation results.

Hales and Hill⁽⁴¹⁾ investigated the oxidation at 1100°C of nickel specimens of varying surface to volume ratio and surface geometry. Their findings were in broad agreement with the above theories of double layer formation and vacancy injection. On rod specimens grain boundary voids formed more readily as surface to volume ratio increased. Sheet specimens of equivalent surface to volume ratio had a lesser tendency to form grain boundary

voids than did rods. This was explained in terms of a greater stress in the oxide layer of the rod configuration giving rise to separation or void formation at the metal/oxide interface. Oxidation rate apparently increased with surface to volume ratio.

A high surface to volume ratio would be expected to result in a high vacancy concentration in the metal. Thus the latter is seemingly in contradiction to the results of Hancock and Fletcher⁽¹⁹⁾, but void formation would lower vacancy concentration and massive intrusion of oxide into the metal grain boundaries found by Hales and Hill⁽⁴¹⁾ for rods of high surface to volume ratio would have nullified the quoted weight gain per unit area figures.

Harris⁽⁴²⁾ considered that the above evidence could equally apply to a mechanism whereby voids formed as a result of Hull Rimmer diffusion type creep caused by stresses set up in the metal and that vacancy injection did not necessarily occur.

Gibbs and Hales⁽⁴³⁾ related proof of vacancy injection during oxidation to breakdown of the initial scale and the subsequent formation of a double layer oxide.

A considerable amount of recent work has investigated the stress set up in growing oxide layers and the effect of this stress on the scale structure and oxidation characteristics. Hales⁽⁴⁴⁾ found from electron microscopy that nickel oxide has a dislocation structure typical of materials which have undergone recovery creep. This deformation was said to assist scale/metal adhesion and further that preferred slip systems contributed to the relatively large columnar grained structure of the scale.

This recovery creep mode of deformation contradicts the work of Strafford and Smith⁽⁴⁵⁾ who found for sintered bulk nickel oxide that the creep parameters indicated a deformation mode of

stress directed vacancy diffusion. Applied stresses were within the range expected to occur in growing oxide film.

Hales⁽⁴⁴⁾, among others^(46,47), found evidence of a stress gradient or stratification within the scale, where the highest stresses acted at the metal/oxide interface and the lowest at the oxide/atmosphere interface.

A mechanism for the generation of a compressive stress within the growing oxide scale has featured in the literature. The classic Wagner theory of oxidation for an infinite plane metal surface does not allow the development of a compressive stress parallel to the metal surface. As suggested by Mrowec⁽³⁸⁾ the geometry and surface irregularity of finite, real metal samples would enable such stresses to be generated. While accepting this and various other mechanisms of stress generation, Rhines and co-workers^(47,48) have postulated an alteration to the classic theory of oxidation for nickel which allows for a compressive stress in the scale parallel to the metal surface. It was suggested that nickel diffuses outward through the columnar oxide grains and oxygen diffuses inward along the oxide grain boundaries, neither process interfering with the other. The meeting of the reactants in the grain boundaries generates fresh oxide there, giving a three dimensional swelling of the scale. A residual stress component would therefore exist parallel to the metal surface. This causes deformation of the oxide producing grain growth and grain boundary migration which was said to distribute fresh oxide throughout the whole volume of the scale. Stress generation and grain growth were said to be essential to scale growth and differences in the oxidation rates of convex versus concave surfaces were explained by differences in stress state.

Although attractive in some ways, the theory contains several discrepancies. The deformation due to residual stress in the scale was said to cause grain refinement necessary to form the inner oxide layer and, conversely, to cause grain growth necessary for scale growth. Cases of apparently equal merit were presented for increased and decreased stresses in scales on convex relative to concave surfaces. It is, therefore, difficult to see the justification for the assertion that increased stress and deformation gave a higher oxidation rate when a tube bore was compared to a tube outer surface. In any case, the difference in scale thickness can be explained in terms of the different geometric configurations alone. It was further stated that scale thickening stopped if grain growth due to scale deformation was prevented, but the method used to prevent grain growth was the removal of the oxidising atmosphere. While this theory of oxide formation in the grain boundaries may seem plausible, it has since been totally rejected by Harris^(42,49).

It is pertinent to note that Rhines and Wolf⁽⁴⁷⁾ claimed that stresses in the region of 10 N/mm^2 could be generated in the oxide layer and that at this stress level the creep rates of nickel and nickel oxide were within an order of magnitude of each other. Also claimed was that increased stress in the scale due to convexity of surface gave an increased tendency to double layer formation.

The generation of stresses within and deformation of a growing oxide scale are accepted facts. Uncertainty still surrounds the exact mechanisms of both. Holmes and Whitlow⁽⁵⁰⁾ in a conference review listed dislocation glide and climb Herring-Nabarro stress assisted diffusion creep and grain boundary

sliding as likely modes of deformation. Hancock^(51,52) carried out work to determine the mechanical properties of growing oxide layers. This is necessary to relate the mechanical behaviour of the oxide to tendency to double layer formation, spalling, and oxidation rate. A specific instance is the excellent adherence of nickel oxide to nickel due both to the closeness of coefficient of thermal expansion of metal and oxide and the oxide's relatively high plasticity^(46,50,51).

Thus due to the potential effect of generated stress and oxide deformation, it would be expected that a superimposed stress on a nickel undergoing oxidation could alter the normal oxidation behaviour. Evidence has been presented to show that imposition of a tensile stress reduced the oxidation rate⁽⁴⁷⁾.

2.3 The Creep of Nickel

In common with many other metals, nickel creeps by one of three mechanisms according to temperature range. Below $0.3 T_M$ (245°C) deformation occurs as a logarithmic function of time. As deformation proceeds, work hardening strengthens the material, no recovery takes place and very quickly creep virtually ceases.

Above $0.9 T_M$ (1282°C) the self diffusion rate is sufficiently high to allow, in the presence of a small applied stress, transfer of atoms from longitudinal interfaces or grain boundaries to transverse ones. Here the creep rate is a linear function of time.

The most studied and practically important creep mechanism is that occurring in the temperature range 0.3 to $0.9 T_M$. Considered simply, the deformation due to an applied stress results from the relatively high temperatures supplying sufficient energy to allow dislocation movement. This creep range can be

sub-divided, the break occurring at approximately $0.5 T_M$ (590°C). Below this temperature it is generally believed that full recovery does not occur as the creep rate always declines with time⁽²⁴⁾. Thus only in the temperature range 0.5 to $0.9 T_M$ does the classic creep curve, including a steady state region, exist. It is this creep mechanism which is of direct relevance to the present study.

McLean⁽²⁴⁾ gives a comprehensive description of this creep mechanism. The strain versus time curve shows three distinct stages; primary creep, where the creep rate falls with time, leading into secondary or steady state creep, where the creep rate is constant, and the tertiary stage, where the creep rate increases with time. The tertiary stage is essentially concerned with fracture.

The creep mechanism during secondary creep has been most studied and the theory is based on this stage. Two approaches have been made. One is a consideration of slip or dislocation movement in relation to reaction rate theory where an activation energy is overcome by the applied stress in order to cause deformation. The other is that continued deformation occurs due to concurrent work hardening, resulting from strain caused by the applied stress, and recovery or softening caused by the annealing action of high temperature. The approaches should be regarded as aspects of the same theory, as they can be simply linked by considering the activation energy to be governed by the relative effects of work hardening and annealing^(24,53).

Deformation occurs by slip or dislocation movement. The dislocations are distributed through the metal grains in a three dimensional grid. As motion occurs the total dislocation length increases and the mesh size decreases due to intersection

of dislocations. This of course is the accepted mechanism of work hardening. At the same time recovery takes place giving an opposite increase in mesh size. During primary creep, work hardening dominates, the metal is strengthened and the creep rate falls. The steady state condition is reached when work hardening and recovery balance each other and the creep rate becomes constant.

Consideration of the internal grain structure shows that the dislocation grid is not necessarily homogeneous, rather it consists of areas of relatively low dislocation density surrounded by bands of high dislocation density or tangles⁽⁵³⁾. This is in effect the so called sub-grain structure. The increase in dislocation density and reduction in sub-grain size during primary creep, as well as the constant structure during steady state creep, may be a cyclic rather than uniform effect^(24,53,54). The sub-grain boundaries can act both as barriers to and sources of dislocations during this cyclic behaviour. During the steady state stage the movement of jogged screw dislocations appears to be rate controlling^(23,53).

The decrease of work hardening rate to a level matching the recovery rate, due to an increase in the work hardening coefficient^(55,56), suggests that primary and secondary creep are closely related. Several investigations have confirmed this by fitting these two stages to a single creep strain equation^(55,57).

Recovery seems to depend on a dislocation climb mechanism^(58, 59) which in turn depends on diffusion and it is accepted that the temperature dependence of steady state creep, i.e. activation energy, is the same as that for self diffusion (approximately 65,000 K cal/mol for nickel)^(24,58,60). The steady state creep rate depends on stress with an exponent of approximately 5^{(24,58,}

60) and this is due mainly to the stress dependence of the recovery rate^(32,56,61).

At the extremes of the main temperature range deviations from the above creep behaviour have been reported, diffusion creep, grain boundary diffusion creep and dislocation pipe diffusion being suggested mechanisms^(54,60,62). One last comment worthy of note is the marked effect of small variations in the impurity content on creep behaviour which has been reported for nickel⁽⁶³⁾.

Attention can now be given to tertiary creep which is in effect a consideration of fracture. McLean's description⁽²⁴⁾ must again lay the foundation. At high temperatures creep fracture is of a brittle or intergranular nature. During creep, possibly as early as the primary stage and certainly from the start of the secondary stage^(64 to 69), voids are nucleated in the grain boundaries. These steadily grow and coalesce eventually leading to separation of the grain boundaries. The rapid increase in creep rate during the tertiary stage of the strain/time curve is manifestation of this failure⁽⁵⁷⁾. It has been suggested⁽⁶⁴⁾ that void formation or failure strain, especially under low stress conditions, represents a significant proportion of the total creep strain.

The most significant feature of the fracture process is that it is governed by the rate of deformation, probably due to the importance of grain boundary sliding in the mechanism^(32,57,68,69). In a polycrystalline metal internal dislocation movement deforms individual grains causing the grains to move relative to each other. In other words the grain boundaries act as glide planes and movement across them is termed grain boundary sliding. The nucleation of voids is now accepted as taking place at obstacles in the grain boundaries such as ledges, triple points,

corners and foreign particles^(24,67 to 72).

Void nucleation is proportional to strain^(65,66), the rate showing a similar relationship with time as that of overall strain rate^(64,68,69), i.e. decreasing during primary creep, constant during secondary creep and increasing during tertiary creep. Both grain boundary sliding^(65,66) and intragranular deformation^(68,69) have been cited as being responsible for nucleation. A stress dependence of nucleation has also been indicated⁽⁶⁸⁾.

Uncertainty also surrounds the mechanism of grain boundary void growth. A simple explanation would be growth by absorption of excess vacancies. A stress dependence of void growth suggesting stress induced vacancy diffusion⁽⁶⁸⁾ does not explain the relation between growth and deformation rate^(24,66,67,69,73). Some connection between void growth and grain boundary sliding must be sought^(24,57,69). A mechanism involving the motion of dislocations along the grain boundary has been offered as part solution^(69,74). Vacancies are emitted during the non-conservative motion of dislocations in the boundary⁽⁷⁴⁾ and are directed to voids by stress induced vacancy flow^(68,69). Supporting this is the fact that void growth can be more closely related to the grain boundary self diffusion coefficient than to the lattice self diffusion coefficient^(24,64). It has also been shown⁽⁶⁸⁾ that initially void growth occurs in three dimensions with a similar dependence on stress and time in each dimension. This gives an approximately constant void shape suggesting a crystallographic influence. After the initial stages of creep, growth continues only in the two dimensions within the plane of the grain boundary said to be due to stress concentrations setting up directional vacancy fluxes.

In contrast to the above, it has been shown that voids become thermodynamically stable at the start of tertiary creep in that only after this do they readily absorb vacancies⁽⁷⁵⁾. This and the fact that grain boundary voids formed during tensile creep are not sintered out under subsequent compressive stressing⁽⁷¹⁾ indicates that simple vacancy diffusion is not a major factor in growth.

Although attempts have been made to relate the extent of void formation to a particular point in the creep life^(64,66,69) this appears to be invalid due to the complexity of the process. Void coalescence cannot be accounted for in simple terms and fracture does not take place at some particular level of voidage⁽⁶¹⁾. A low applied stress appears to allow a greater extent of void formation before fracture than does a high stress⁽⁶¹⁾. It would seem more logical to assume that fracture would occur when some critical area of the grain boundaries was occupied by voids⁽⁶⁹⁾. However, localised stress concentrations⁽⁶⁸⁾ and void spacing⁽⁶⁴⁾ may play a part. Some reconciliation is possible if it is considered that an individual grain boundary will fail when some critical condition of stress and void area and spacing is fulfilled. However, void formation throughout an entire specimen is not necessarily homogeneous and this may mask the effect.

Grain size affects the final stages of fracture in that crack propagation is more difficult along a boundary at a low angle to the applied stress where there is less void formation. In a fine grained specimen there is a greater length of low angle boundary and a higher likelihood of propagation having to occur along such a low angle boundary^(24,57,76).

2.4 Potential Interference of the Creep and Oxidation Mechanisms of Nickel

Both oxidation and creep are temperature dependent - the higher the temperature the greater the effect. Both are cumulative in relation to time. Therefore any interference should be greatest under conditions of high temperature and long exposure. To some extent temperature and time are synonymous in that increased temperature increases the rate of both processes. This simplification is made with the realisation that the temperature dependence or activation energy of the two is different. It merely allows a simple time based comparison of the mechanisms to be made. Stress level would have a time equivalence for creep alone.

If oxidation is regarded as a single time related process, it can be considered superimposed on the three stage time related process of creep. Oxidation occurs at the free surface while creep affects the entire specimen. Basically, oxidation forms a layer of oxide on the metal surface and may cause stresses to be set up in the metal substrate and may inject vacancies into the metal. During primary creep the major happening is an increase in dislocation density. It is difficult to visualise any great interference of the mechanisms at this stage.

During secondary creep the increase due to slip and the decrease due to recovery, cancel, allowing dislocation density to remain constant. Diffusion undoubtedly plays a part in this process and a vacancy flux into the metal, increasing vacancy concentration, may well have some effect. Facilitation of dislocation movement could occur by the annihilation of excess lattice vacancies. An increased vacancy concentration may also increase recovery rate by increasing the opportunity for dislocation

climb. These would tend to increase the steady state creep rate. The possibility that the oxide film would have pile up repercussions inhibiting dislocation movement has already been noted. It would be expected that such an effect would be highly dependent on specimen geometry and grain size due to a variation in the ratio of free surface area to grain boundary area. In any case, creep theory does not place great importance on the egress of dislocations at the free surface although single crystals may be the exception. Thus such a potential decrease in creep rate would not be universally important and, further, would depend on the nature of the oxide layer. Specimen geometry or surface to volume ratio will of course always have an overall influence on the relative contributions of creep and oxidation to mechanism interference.

Void nucleation and growth occurs during secondary creep. Although current creep theory regards these processes as being intimately connected with grain boundary sliding and leaves little room for a vacancy condensation mechanism, grain boundary voids are heterogeneously nucleated during oxidation alone. It must therefore be expected that void formation will be enhanced during simultaneous creep and oxidation.

With increasing time, grain boundaries become the focal point of the creep mechanism and the fracture process of void coalescence and crack propagation develops. Similarly at long oxidation times, void formation occurs and oxide penetration into the grain boundaries takes place. Here then is a situation where direct impingement of the processes must occur and it is to be expected that the clearest manifestation of an interrelation between creep and oxidation will be during creep fracture.

The consideration of the interference of creep and oxidation mechanisms cannot be left without taking the opposite viewpoint.

An assessment of the effect of creep on oxidation must be made. Two effects would appear possible. Firstly, void formation and vacancy concentration, modified by creep, may alter the oxidation rate. Secondly, deformation of the underlying metal due to an independent applied stress would be expected to markedly affect the stress state of the growing oxide layer. This in turn may modify the double layer structure of nickel oxide.

2.5 The Simultaneous Creep and Oxidation of Nickel - A Survey of Prior Work

Table 1 provides a summary of the published results in this field. It can be seen that the creep properties in an oxidising atmosphere, relative to an inert atmosphere, are apparently impaired at low temperatures and improved at high temperatures. The high temperature improvement was first noted by Weertman and Shahinian⁽⁵⁶⁾ and the mainstream of subsequent papers has come from Shahinian and his colleagues.

McHenry and Probst⁽³⁾ next encountered this strengthening effect in air atmospheres. Tube and bar specimens of nickel were tested in atmospheres of air and argon and, in the case of tubes, with air outside and argon inside. At low stresses bar and tube specimens tested wholly in air gave considerably longer rupture lives than did tubes tested wholly in argon. Tubes tested in the dual atmosphere showed an intermediate effect. The fracture mode was ductile at high stresses ($> 34 \text{ N/mm}^2$) and intergranular at low stresses. Severe embrittlement of specimens tested in air was observed. At low stress the grain boundaries perpendicular to the axis of stress showed void formation and cracking in the argon atmosphere, and in an air atmosphere exhibited oxidation or partly and fully oxide filled cracks. The strengthening effect was, in

the main, considered to have resulted from the formation of oxide in the grain boundaries and that the oxide was able to withstand a tensile load. A surface to volume ratio effect was found in that bar specimens were not air strengthened to the same extent as tube specimens. Where only the external tube surface was in an air atmosphere, which gave a similar oxidised surface to volume ratio to bar specimens, the tube rupture life was shorter, said to be due to the internal free surface allowing dislocation escape.

Shahinian and Achter⁽⁹⁾ compared the creep rupture of cylindrical specimens in air and vacuum. They found that nickel had a longer rupture life in air at low stresses, the reverse being true at high stresses. At low stresses the creep rate was always lower in air but at high stresses, while the primary creep rate in air was lower, the secondary creep rate was greater than in vacuum. The atmosphere effect was enhanced in notched specimens. An explanation by way of the simultaneous operation of competing processes was suggested. Absorption of gases lowered surface energy and facilitated crack propagation. Strengthening resulted from the oxide layer blocking dislocation escape, internal oxidation and oxide formation in cracks blunting the crack tip thereby lowering the propagation rate. At the higher temperature the strengthening effect occurred at shorter times in agreement with the greater oxidation rate. The weakening mechanism was said to be dominant at high creep rates due to the small effect of diffusion controlled oxidation in such circumstances.

Sherman and Achter⁽¹⁰⁾ conducted interrupted creep tests on cylindrical specimens in a temperature/stress regime where the rupture lives were approximately equal in air and vacuum. Crack

initiation and propagation were compared. Intergranular cracking always appeared earlier and occurred to a greater extent in air. At a higher stress this was reflected in a greater creep rate in air. At a lower stress the creep rate in air and vacuum was approximately the same, but the rupture life was greater in air. Surface absorption of gas was suggested as the reason for the increased cracking tendency in air and, at lower stresses, strengthening mechanisms were able to balance this effect giving a slightly greater rupture life in air.

Reuther, Shahinian and Achter⁽¹¹⁾ crept tapered cylindrical nickel (99.8% pure) specimens and found that fracture did not necessarily occur at the minimum diameter. Tests were also conducted on parallel specimens of the minimum and maximum diameters of the taper. As the stress was lowered and the rupture life increased, the fracture position was displaced further from the minimum diameter. Under such conditions the rupture life was greater in air than in vacuum. Metallography showed that intergranular cracking first occurred at the surface at the minimum diameter followed by internal intergranular cracking at this point. At higher stresses failure ensued at this position. At lower stresses the surface cracks and subsequently the internal cracks filled with oxide. This cracking and oxidation pattern progressively spread along the gauge length until, at some stress dependent position, failure took place. There were few surface cracks and no internal cracks beyond the failure. The quantity of oxide in the internal cracks decreased as the diameter increased and these cracks were oxide free at the fracture position. The small diameter parallel specimen gave greater oxidation strengthening. This was said to prevent failure in the smaller diameter

section of the tapered specimens. As section size increased the ratio of oxide filled surface cracks to clean internal cracks decreased, until at some point fracture occurred. The strengthening mechanisms were concluded to be as stated previously^(3,9).

Cass and Achter⁽²¹⁾ measured the rupture strength of bonded nickel/nickel oxide layers. Nickel specimens were oxidised and sintered together under a compressive load at 817°C, the same temperature as subsequent tensile testing. Rupture strength of the oxide layer was independent of sintering stress and showed an asymptotic increase with sintering time up to approximately 28 N/mm². There was a metallographic similarity between the bonded oxide layers and oxide filled cracks found in crept nickel specimens. This was seen as confirmation of the strengthening mechanism whereby the oxide in intergranular cracks could support a tensile load in excess of the applied stress.

Shahinian⁽¹²⁾ investigated the effect of a notch on the environment effect. The notch was found to enhance oxidation strengthening. At low temperatures and high stresses, weakening in air occurred, and at high temperatures and low stresses strengthening occurred. When transgranular fracture took place little atmosphere effect was observed. The same mechanisms as before were suggested and unnotched specimens again showed fourth stage creep⁽¹¹⁾. Elongations were generally higher in air than in vacuum, but exceptionally high elongations recorded in cases of pronounced oxidation strengthening were said to be due to the large volume of oxide formed in grain boundary cracks.

Stegman, Shahinian and Achter⁽⁶⁾ presented convincing support for the surface absorption of gas theory of weakening. Rupture life decreased with increasing oxygen pressure from 10⁻⁷ to 10⁻³

torr thereafter remaining constant. At low pressures an increase in pressure during a test was found to increase the creep rate. The results were correlated with a mathematical model based on the kinetic theory of gas.

Bogachev, Veksler and Sorokin⁽⁸⁾ found the creep resistance of nickel to be higher in air than vacuum for the early stages of creep at 650°C. The results were explained in terms of interaction of the oxide film with dislocation movement. Denisenko and Skorokhod⁽²⁰⁾ also explained their findings of reduced creep deformation in porous nickel compacts, due to oxidation, by an interaction of the oxide film and dislocation movement.

Steele⁽¹⁴⁾ presented evidence of pronounced oxidation strengthening. As would be expected, rupture life was found to be considerably greater under constant stress conditions compared to constant load. Both loading conditions showed not merely fourth stage creep, but multi stage creep where the creep rate increased and decreased several times during the rupture life with abrupt changes of slope. Strengthening was said to result from the previously advanced mechanisms. Multi stage creep was tentatively explained by successive tertiary type crack propagation followed by a rapid build up of load bearing oxide in the surface linked cracks causing stress reduction in that region. This continued in various parts of the nickel until a crack propagation rate, too great for oxide formation to halt, resulted in failure.

Some investigations have concerned the creep testing of pre-oxidised nickel. Douglass⁽²⁶⁾ preoxidised specimens of two purities at 1200°C, where oxidation strengthening occurs, and subsequently creep tested at 600°C where no effect or a weakening effect is found. The high purity nickel suffered severe deterior-

ation of creep resistance which lessened as the preoxidation time increased. The results were discussed in terms of internal grain boundary oxidation and void formation, but several discrepancies meant that a convincing explanation was not given.

Hancock and Fletcher⁽¹⁹⁾ preoxidised high purity nickel at 1000°C and creep tested at 725°C. Their explanation, also supported by Hales and Hill⁽⁴¹⁾, of deterioration in creep resistance was in terms of pre-existing grain boundary voids.

2.6 Literature Review Summary

A general criticism of the published work, evident from Table 1, is the lack of corroborative experimental evidence. Individual investigations show similar trends, but there is a wide variation in creep parameters for different work performed under ostensibly similar conditions. In many cases the paucity of data means that its statistical significance could be questioned.

The weakening effects due to an oxidising atmosphere, e.g. increased crack initiation and propagation, seem well established. Although the strengthening effect also appears to be an established fact, the preoxidation work and some work not on nickel cast some doubts. Certainly the mechanisms of strengthening have not been adequately defined or proved. The phenomenon of fourth or multi stage creep can be considered an extension of strengthening and requires investigation. There is apparently no published work concerning the effect of simultaneous creep on the oxidation process, possibly due to the experimental difficulties involved.

2.7 Aims of the Investigation

The previous section highlighted areas in which further work would be desirable. It was therefore the purpose of this investigation to:

- (a) compare the creep properties of nickel in oxidising and non-oxidising atmospheres under equivalent conditions of stress and temperature.
- (b) obtain sufficient results to make the above comparison meaningful.
- (c) seek an explanation of the strengthening mechanisms due to an oxidising atmosphere and, in particular, the operation of these which results in fourth or multi stage creep.
- (d) take into consideration any effect of creep on the mechanism of oxidation.

TABLE I

LIST OF PUBLISHED CREEP DATA FOR NICKEL

Temp °C	TM*	Atmosphere	Nickel Purity Wt %	Stress N/mm ²	Rupture Life Hrs.	Secondary Creep Rate % per Hr.	Grain Size mm	Spec Dia mm	Ref
510	.45	O ₂	99.8	117.2	150	.024	-	4.58	6
"	"	Vac	"	"	190	.013	-	"	"
600	.51	O ₂	"	58.6	120	.064	-	"	"
"	"	Vac	"	"	240	.044	-	"	"
"	"	Air	99.75	21	767	8.4 x 10 ⁻⁵	0.33	6.36	58
"	"	"	"	63	323	2.9 x 10 ⁻⁴	"	"	"
"	"	"	"	84	16.2	.006	"	"	"
"	"	"	"	140	.18	.41	"	"	"
"	"	"	"	175	.04	3.72	"	"	"
648	.53	"	99.8	31	807	.0072	.14 to .29	"	9
"	"	Vac	"	31	767	.0066	"	"	"
"	"	Air	"	41.4	180	.035	"	"	"
"	"	Vac	"	"	197	.030	"	"	"
"	"	Air	"	62	19.3	.48	"	"	"
"	"	Vac	"	"	29.5	.33	"	"	"
"	"	Air	"	"	57	.27	.07	"	10
"	"	Vac	"	"	50	.28	"	"	"
"	"	Air	"	69	42.7	.35	-	6.41	12
"	"	Vac	"	"	53.8	.23	-	"	"
"	"	"	"	"	68.1	.20	-	"	"
"	"	Air	"	"	60.7	.31	-	"	"
"	"	Vac	"	"	114	.15	-	"	"
"	"	Air	"	"	63.1	.23	-	9.07	"
"	"	Vac	"	"	83.9	.17	-	"	"
"	"	Air	"	"	68.1	.26	-	"	"
"	"	Vac	"	"	99.4	.13	-	"	"
"	"	Air	"	83	3	3	.14 to .29	6.36	9
"	"	Vac	"	"	6.2	1.9	"	"	"
"	"	Air	"	"	12.8	1.6	.07	"	10
"	"	Vac	"	"	14.2	1.4	"	"	"
800	.62	Air	99.75	10.5	-	5.3 x 10 ⁻⁵	.33	"	58
"	"	"	"	21	24.4	7.8 x 10 ⁻⁴	"	"	"
"	"	"	"	"	160.9	1.4 x 10 ⁻⁴	"	"	"
"	"	"	"	28	23.6	2.8 x 10 ⁻³	"	"	"
"	"	"	"	49	.83	.072	"	"	"
"	"	"	"	70	.11	.9	"	"	"
"	"	"	"	105	.02	13.4	"	"	"

*Temperature as fraction of melting point.

TABLE I

(Cont'd)

Temp °C	TM	Atmos phere	Nickel Purity Wt %	Stress N/mm ²	Rupture Life Hrs.	Secondary Creep Rate % per Hr.	Grain Size mm	Spec Dia mm	Ref
816	.63	Air	99.8	55.2	1.5	9.7	-	9.07	12
"	"	Vac	"	"	"	10.6	-	"	"
"	"	Air	99.3	48.2	< .5	-	.09	6.36	3
"	"	"	"	41.2	1.5	-	"	"	"
"	"	"	"	34.5	4.4	-	"	"	"
"	"	"	99.8	"	3.2	1.9	.14 to .29	"	9
"	"	"	99.3	27.6	30	-	.09	"	3
"	"	"	99.8	"	28.3	.34	-	9.07	12
"	"	Vac	"	"	14.1	.65	-	"	"
"	"	"	"	"	23.5	.32	-	"	"
"	"	Air	"	"	27.6	.31	-	6.41	"
"	"	Vac	"	"	19.1	.35	-	"	"
"	"	Air	"	"	7.3	.83	.14 to .29	6.36	9
"	"	Vac	"	"	9.5	.58	"	"	"
"	"	Air	"	"	1.9	2.16	.63	"	"
"	"	Vac	"	"	2.8	1.6	"	"	"
"	"	Air	99.3	"	24.3	-	.09	"	3
"	"	"	"	24.1	78	-	.09	"	"
"	"	"	99.8	"	73.5	.091	-	9.07	12
"	"	Vac	"	"	36.4	.22	-	"	12
"	"	Air	"	"	20.3	.24	.14 to .29	6.36	9
"	"	"	99.3	20.7	680.9	-	.09	"	3
"	"	"	99.8	"	59.3	.087	.1	"	11
"	"	"	"	"	47	.106	"	9.07	"
"	"	"	"	"	869	.0046	-	"	12
"	"	Vac	"	"	113.5	.067	-	"	"
"	"	Air	"	"	946.3	.0042	-	6.41	"
"	"	Vac	"	"	138.4	.051	-	"	"
"	"	Air	"	"	53.9	.12	.14 to .29	6.36	9
"	"	Vac	"	"	23.5	.18	"	"	"
"	"	Air	"	"	8.1	.33	.63	"	"
"	"	Vac	"	"	13.5	"	"	"	"
"	"	Air	"	19.3	76.8	.053	.10	"	11
"	"	"	"	"	61.6	.078	"	9.07	"
"	"	"	99.3	19.0	847	-	.09	6.36	3
"	"	"	99.8	18.6	126	.032	.10	"	11
"	"	"	"	17.9	> 2560	-	"	"	"
"	"	"	"	"	75	.055	"	9.07	"
"	"	"	"	17.58	123	.029	"	"	"
"	"	"	"	17.23	> 2460	-	"	"	"
"	"	"	99.3	17.23	1154	-	.09	6.36	3

TABLE I

(Cont'd)

Temp °C	TM	Atmos phere	Nickel Purity Wt %	Stress N/mm ²	Rupture Life Hrs.	Secondary Creep Rate % per Hr.	Grain Size mm	Spec Dia mm	Ref
816	.63	Air	99.8	17.23	> 4000	.0003	.14 to .29	6.36	9
"	"	Vac	"	"	48.5	.061	"	"	"
"	"	Air	"	"	62.1	.10	.63	"	"
"	"	Vac	"	"	19.5	.16	"	"	"
"	"	Air	"	13.78	> 3000	.0005	.14 to .29	"	"
"	"	Vac	"	"	112	.025	"	"	"
"	"	Air	"	"	> 3817	.0007	.63	"	"
"	"	Vac	"	"	39.5	.041	"	"	"
900	.68	Air	99.75	14	119	4.8 x 10 ⁻⁴	.33	"	58
"	"	He	"	17.5	10.9	5.6 x 10 ⁻³	"	"	"
"	"	Air	"	21	7.8	.0072	"	"	"
"	"	He	"	21	5.6	.0132	"	"	"
"	"	"	"	35	.45	.162	"	"	"
"	"	Air	"	42	.25	.318	"	"	"
"	"	"	"	49	.10	1.02	"	"	"
950	.71	"	99.997	14.62	8.5	-	-	7.14	14
"	"	"	"	"	27	-	-	"	"
"	"	Vac	"	"	4.2	-	-	"	"
1100	.79	Air	99.75	35	.017	9	.33	6.36	58
"	"	"	"	28	.055	2.58	"	"	"
"	"	He	"	"	.009	24.6	"	"	"
"	"	"	"	21	.15	.84	"	"	"
"	"	Air	"	14	5.2	.035	"	"	"
"	"	He	"	"	1	.123	"	"	"
"	"	"	"	21	.275	.474	"	"	"
"	"	"	"	10.5	8.2	.039	"	"	"
"	"	Air	"	9	.33	.408	"	"	"
"	"	He	"	7	8.3	.017	"	"	"

CHAPTER III

APPARATUS AND EXPERIMENTAL

3.1 Introduction

The bulk of the experimental work consisted of a series of constant stress creep tests on high purity nickel in atmospheres of oxygen and vacuum. Oxidation experiments on unstressed and stressed specimens were also carried out. All specimens were subsequently subjected to metallographic examination.

3.2 Constant Stress Creep Testing Apparatus

The apparatus used was designed and built by Fletcher⁽⁷⁷⁾ and the principle and mode of stress conditions are fully explained therein.

Fig. 4 shows a schematic diagram of the apparatus. Port A leads from the vacuum pump system into the closed chamber consisting of a steel base plate B, body C, roof D and recrystallised alumina closed end tube E. The specimen F is subjected to a load exerted by springs G. Up to five springs could be accommodated in the assembly. The springs react against the chamber body C, transmitting the load to the moving platform H. The load is in turn transmitted to the specimen through the compression rods I (four of), crossed knife edge assembly J and upper tension shackle K. The specimen load is reacted through the lower shackle L, tension member M, single knife edge N, plate O and compression rods P (four of) against the adjustable clamps Q. The partly threaded pull rod R is moved up or down by an electric motor, the rotation of shaft T being converted to linear motion through the threaded worm gear

assembly S. The load bearing members in the hot zone were made in Nimonic 105 alloy, the remainder from stub steel.

Fig. 5 is a simplified diagram of the apparatus showing the location of the ancillary equipment. The specimen F was heated by an annular three zone resistance wound furnace a, suspended around the ceramic tube E. Specimen temperature was monitored by two chromal alumel thermocouples b fixed at either end of the gauge length. The temperature was continuously recorded on chart and accurate spot readings were made using a potentiometer/galvanometer arrangement. Temperature was controlled using a platinum resistance thermometer placed in the furnace insulation. The winding current was supplied from a saturable core reactor. The voltage across each of the three furnace windings was variable by means of a Variac autotransformer. This arrangement allowed a constant temperature zone to be imposed over the entire length of the specimen.

The specimen extensometry system consisted of a linear transducer c mounted on platform H which contacted the probe of a barrel micrometer d mounted in the roof of the chamber. The transducer signal was fed to a matched potentiometer, whose output was continuously monitored by a pen chart recorder. The lower end of the specimen was fixed. Specimen extension therefore resulted in relative movement of the upper end only. The extension of the rods I and M and dimensional changes in the shackles and knife edge assembly were negligible as they were of greater modulus and cross sectional area than the specimen. The design of the apparatus inherently compensated for thermal expansion. Thus upward displacement of platform H was directly equivalent to specimen extension. During test the barrel micrometer d could be backed

off to maintain the highest accuracy of the extensometry system.

A trigger e fixed to pull rod R operated a microswitch f mounted on platform H. This controlled the electric motor driving R, through a relay circuit. A second microswitch g mounted on platform H was operated by a barrel micrometer h. This overriding microswitch stopped the test at any predetermined extension. All electrical connections were made into the chamber via vacuum lead through i and j.

Fig. 6 shows the vacuum and gas admittance system servicing the test chamber. The vacuum pressure was monitored by a diaphragm pressure gauge v graduated from 0 to 760 torr. The vacuum could be broken by means of an air admittance valve u. A blank connection w was available for accurate pressure determination using a Pirani vacuum gauge or for the connection of leak testing equipment. Valve x was connected to a bottled gas supply, in this case oxygen. A solenoid operated valve y was interposed between the test chamber and vacuum pump. Both manual switching and automatic switching by microswitch g was available. Vacuum was established and held by a rotary pump z. Originally the apparatus had in addition been serviced by an oil diffusion pump but the rig design throttled access to the test chamber and low pressure was not established at the specimen. The rig was only used for testing in oxygen or vacuum levels of 10^{-1} torr.

The standard testing procedure on the rig was as follows:

With the springs G fully relaxed, i.e. pull rod R free of platform H, the specimen F was assembled into the shackles K and L. Thermocouples b were attached to either end of the specimen gauge length. In most tests an unstressed dummy nickel specimen was attached to one

of the compression rods I, exactly opposite specimen F, for oxidation study comparison. The chamber roof assembly was lowered and secured. The extensometry system was zeroed by adjusting micrometer d. Pull rod R was driven downward, drawing platform H down to compress the springs G. The required spring compression was established precisely by advancing the micrometer the corresponding distance and re-zeroing the extensometry system. A trial application of the load could be carried out at this stage to ensure that the loading system was free from backlash. If so the spring compression was reset and the chamber evacuated by opening valve y. The furnace was then lowered around the ceramic tube and switched on. A heat up period of twenty-four hours was taken to establish the hot zone. The clamps Q were then secured on the compression rods P. Micrometer h was adjusted to the required clearance from microswitch g, either to allow rupture or stop the test at a chosen extension. The test atmosphere was then established, either remaining under vacuum or closing valve y and admitting oxygen. Pre-oxidation could be effected at this stage by delaying the application of load for the desired period.

Stress was applied by advancing pull rod R at a rate greater than the specimen initial creep rate. At a fixed clearance above platform H, the microswitch f was contacted, cutting out the drive motor. As the specimen extended, allowing platform H to move upwards under the action of the springs, the microswitch arrangement auto-

matically cut the motor in and out to maintain the clearance. On specimen rupture, platform H contacted pull rod R, the motor cut in and upward movement was controlled until micrometer h triggered microswitch g. Through a relay circuit this stopped the motor, switched off the furnace and in oxygen tests opened valve y to evacuate the chamber. Thus damage to the rig and/or specimen and post rupture oxidation were prevented. The facility obviously existed for the test atmosphere to be changed from oxygen to vacuum or vice versa during the test.

A second, improved, version of the apparatus was built to the basic design⁽⁷⁷⁾ by Fletcher in collaboration with the author. This was specifically designed for testing in vacuum of better than 10^{-6} torr and included a simplification of the mechanical arrangement and a highly efficient heating configuration. Fig. 7 shows a schematic drawing of this apparatus. The vacuum system consisted of an oil diffusion pump backed by a matched rotary pump. The vacuum level was measured by a Pirani gauge and a Penning ionisation gauge mounted adjacent to the specially wide port A which led into the test chamber. The closed chamber consisted of body B, roof C and closed end ceramic tube D. The specimen E is subjected to a load exerted by springs F (up to five). The load is reacted against the chamber roof C and transmitted through the moving platform G. The compression member is a ceramic tube H, the load in turn passing through the double knife edge assembly I and shackle J. The specimen load is reacted through shackle K, tension member L, universal joint M and tension member N. This tension member N is driven, along with pull rods O,

by an electric motor via a gear train and threaded worm drive assemblies P which run between thrust bearings Q held in position by plate R. To apply load to the specimen the pull rods O are driven upwards in unison with tension member N. When the desired spring compression has been set the gear train is disconnected from the central worm drive, in effect tension member N. To apply this load, determined by the spring compression, the pull rods O are driven down at a rate faster than the specimen initial extension. The central worm drive acts as a clamp reacting the load in tension member N. Fig. 7 also shows the heater arrangement which consists of a resistance winding S direct onto ceramic tube H. It is therefore entirely contained within the vacuum chamber and is sited at the closest possible point to the specimen to give optimum temperature control. The outer ceramic tube is surrounded by insulation T. The overriding test termination microswitch U is mounted outwith the chamber. The remaining ancillary equipment is similar to the original apparatus.

Specimen extensometry is by a transducer mounted on platform G and activated by striking the core of a barrel micrometer protruding through the chamber roof C. During test the clearance between platform G and pull rods O is controlled by a microswitch arrangement. All electrical connections into the chamber are made via vacuum lead throughs. Thermocouples are fixed at either end of the specimen gauge length. This second apparatus was not completed in time to embark on a test programme and commissioning tests only were carried out.

3.3 Constant Stress Loading Theory

As discussed previously^(14,77) the apparatus eliminated loading errors associated with other methods of applying constant stress

within a sealed chamber^(78 to 83). This was an important requirement in the present work as relatively low loads with small differences between loads were used.

The error analysis for the constant stress condition of the apparatus has also been discussed previously^(14,77).

The constant stress condition invoking the constant volume criterion is:

$$\frac{P_d}{P_o} = \frac{A_d}{A_o} = \frac{l_o}{l_o + \Delta l_o}$$

where P_o is the initial specimen load, A_o is the initial specimen cross sectional area and l_o is the initial specimen length. P_d and A_d are the load and cross sectional area at creep strain Δ .

For the apparatus the change in load developed by the spring cage is related to the specimen strain by

$$\frac{P_d}{P_o} = 1 - \frac{k \Delta l_o}{P_o}$$

where k is the overall stiffness of the spring cage.

The dimensionless parameter

$$\gamma = \frac{k l_o}{P_o}$$

is found to be important in the error analysis. Variation of the value of γ determines the closeness of approximation to constant stress conditions up to a particular value of creep strain. Fig. 8 shows that the values of γ between 0.85 and 0.95 give the best approximation to constant stress over the widest creep strain range for various creep exponents where

$$\dot{\Sigma}_d = B \sigma_d^n$$

and $\dot{\Sigma}_A$, B, σ_A and n are the linear creep rate, constant, stress and stress exponent respectively.

Thus in order to optimise the value of γ , certain experimental conditions must be carefully chosen. For a given stress range and specimen cross sectional area, in this case 40 mm^2 , the total loads required can be calculated. A spring cage stiffness can then be selected to provide these loads allowing for spring compression which can be accommodated in the rig. Specimen gauge length, l_0 , is therefore taken as a variable used to optimise the value of γ . The actual parameters used in the experimental work are listed in Table II.

Both spring cage stiffnesses were obtained using a set of four springs. The spring cages were calibrated on a Hounsfield Tensometer and checked periodically to ensure no deviation during the course of the test programme. The accuracy of measurement in the calibration was $\pm 0.01 \text{ N/mm}$. In both cases the stiffness was reproducible to within $\pm 0.1 \text{ N/mm}$.

3.4 Oxidation Apparatus

A simple dead load apparatus was constructed for the oxidation of stressed specimens. Fig. 9 shows a schematic diagram of this apparatus. A mullite tube A was closed using the end seal devices B. The specimen C was subjected to a load exerted by the load pan D. The load was reacted on the base plate E through supports F and top sealing cap. The heater was a resistance wound furnace G. Ports H and I were the gas inlet and outlet respectively. During specimen heat up an argon flow was maintained through the chamber. On commencement of a run the load pan was weighted and the gas flow switched to oxygen. Both gases were passed through a drying tower of magnesium perchlorate prior to entering the

chamber and a flowmeter monitored the throughput. An unstressed specimen was normally mounted alongside the stressed specimen in the rig.

3.5 Other Apparatus and Facilities

A small closed chamber furnace was available for vacuum annealing and unstressed oxidation experiments.

Comprehensive machine shop facilities were available for such as specimen manufacture and post test specimen sectioning. The usual grinding, polishing and etching facilities for metallographic preparation were available.

Optical microscopy was carried out using sophisticated Reichert bench microscopes. The scanning electron microscope used was a Cambridge Instruments Stereoscan S-600.

3.6 Specimen Preparation

Specimens were machined from 13 mm diameter wrought bar of Nickel 270 supplied by Henry Wiggin and Company Ltd. The impurity analysis of the material is shown in Table III. By difference the material is 99.973 per cent pure nickel.

Specimen geometry is shown in Fig. 10. The gauge length portions of all specimens were of 7.14 mm diameter although the shackling arrangements were different in the creep rig and stressed oxidation rig. Also shown are the unstressed specimens which were positioned in the test chambers in most tests. The specimens for the constant stress creep rig were made in various gauge lengths.

After machining, specimens were degreased and annealed in batches of three for twenty-four hours at 1050°C in a vacuum of better than 10^{-5} torr. The specimens then exhibited a mirror finish with no trace of tarnish. The specimens were stored in a dessicator until required. Prior to testing specimens were again

cleaned in an ultrasonic bath of acetone. The grain size of the wrought nickel bar was variable and even after annealing the grain size was not uniform, varying between 0.1 mm and 0.2 mm. The annealing treatment was therefore primarily designed to give a grain configuration which would be stable during subsequent testing. After testing, specimens were mounted in Araldite and sectioned longitudinally for optical microscopy. Certain fracture surfaces were mounted for scanning electron microscopy.

3.7 Test Conditions

All stressed oxidation tests were carried out at $950^{\circ}\text{C} \pm 10^{\circ}\text{C}$ and a nominal stress of 5.0 N/mm^2 . The duration of these tests was from 26 to 164 hours. All specimens were unbroken at the conclusion.

Constant stress tests were carried out at two temperatures, the majority at 950°C and some at 700°C . Temperature control was $\pm 2^{\circ}\text{C}$ in all cases. At 700°C the applied stress ranged from 23 N/mm^2 to 32 N/mm^2 . At 950°C the applied stress ranged from 8.0 N/mm^2 to 12.0 N/mm^2 . Test atmospheres were either a vacuum from air of 10^{-1} torr or oxygen at a pressure of 400 torr. During certain tests the atmosphere was altered from one to the other.

The micrometer which activated the extensometry transducer could be read to $\pm 0.01 \text{ mm}$ and the extensometry system itself was accurate to $\pm 0.01 \text{ mm}$. Therefore the total error in stress setting by combining these errors with errors in spring stiffness measurement was $\pm 0.09 \text{ N/mm}^2$ for the low stress tests and $\pm 0.10 \text{ N/mm}^2$ for the high stress tests.

The constant stress condition for the apparatus is based on the constant volume criterion assuming no significant necking or internal cracking and void formation. Due to the extensive void

formation and crack formation found, especially in longer time tests in oxygen, the specimen was probably not subjected to a true constant stress state. However this did not detract from the benefit of using this particular apparatus in this investigation. As the specimen extends the load is automatically shed. This therefore extends the rupture life beyond that found in constant load tests and exaggerates the oxidation strengthening effect. The apparatus was therefore ideal for a detailed study of this effect.

TABLE II

LOADING PARAMETERS FOR CONSTANT STRESS CREEP TESTS

Spring Compression mm	Spring Cage Stiffness N/mm	Total Load on Specimen N	Specimen Stress N/mm ²	Specimen Gauge Length mm	δ
22.300	14.35	320	8.0	20.0	0.897
27.875	"	400	10.0	24.0	0.861
29.268	"	420	10.5	25.0	0.854
30.662	"	440	11.0	26.0	0.848
32.056	"	460	11.5	27.0	0.842
33.449	"	480	12.0	28.0	0.837
23.428	39.27	920	23.0	20.0	0.854
25.465	"	1000	25.0	22.0	0.864
27.502	"	1080	27.0	24.0	0.873
30.558	"	1200	30.0	26.0	0.851
32.595	"	1280	32.0	28.0	0.859

TABLE III

ANALYSIS OF NICKEL 270 (WEIGHT PER CENT)

Element	Fe	C	S	Pb	Mn	Si	Ag	Sn
Content	.020	.005	.001	.0001	.0001	.0001	.0001	.0001
Element	Al	Ca	Cr	Cu	Mg			
Content	<.0001	<.0001	<.0001	<.0001	<.0001			

FIG. 4.
SCHEMATIC VIEW OF CONSTANT STRESS APPARATUS.

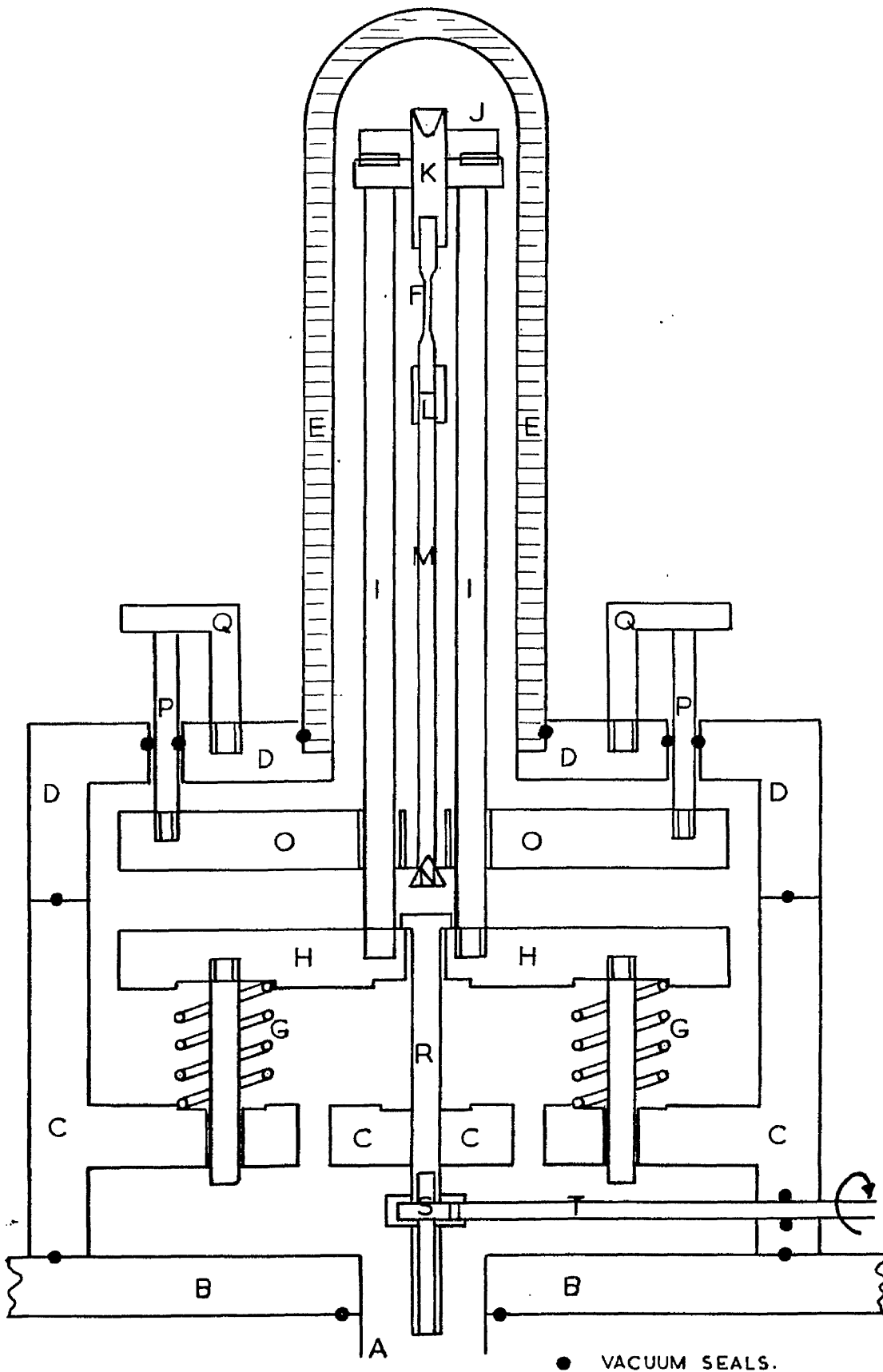


FIG. 5.
SIMPLIFIED VIEW OF CONSTANT STRESS APPARATUS
SHOWING ANCILLIARY EQUIPMENT.

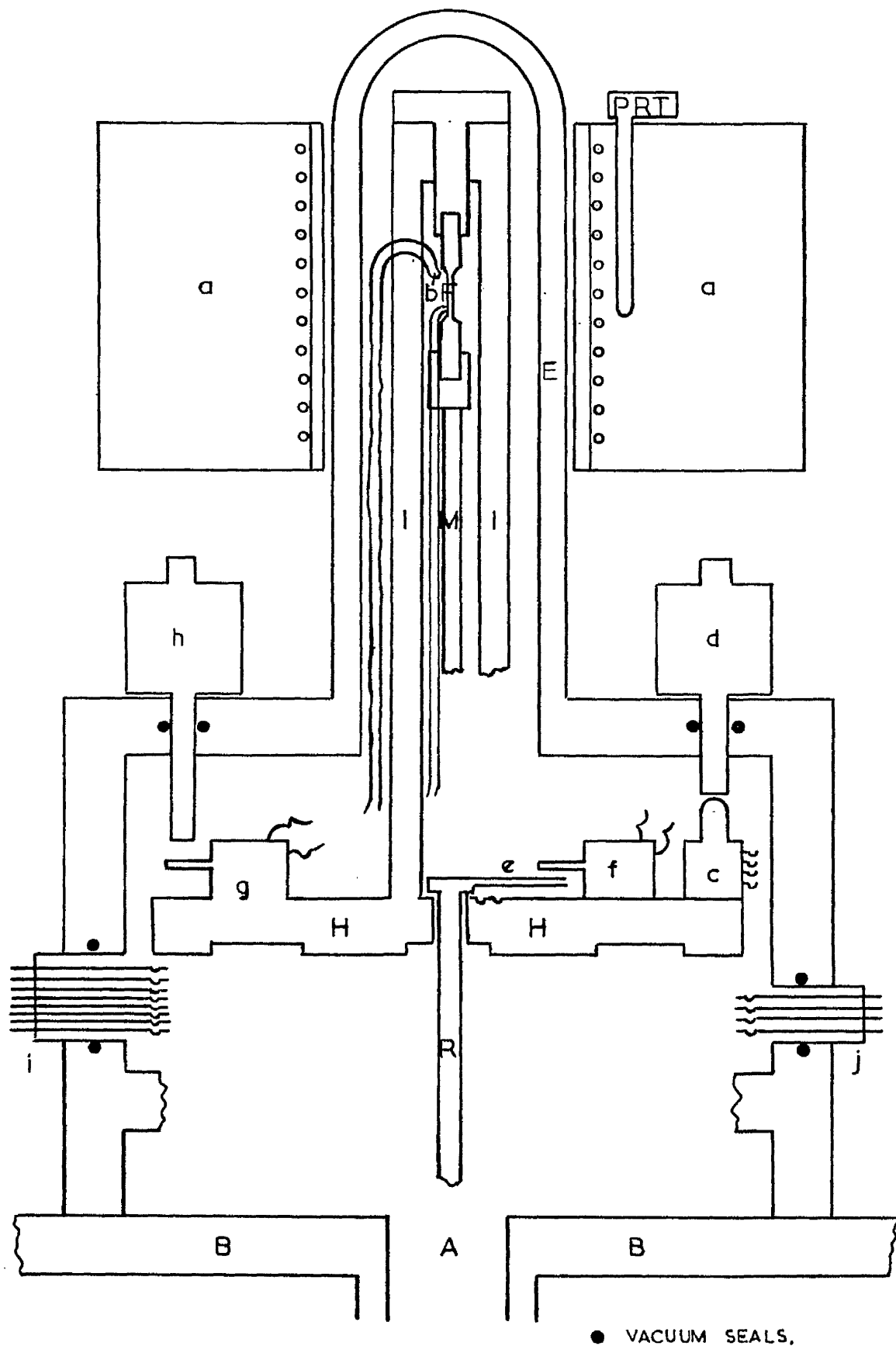
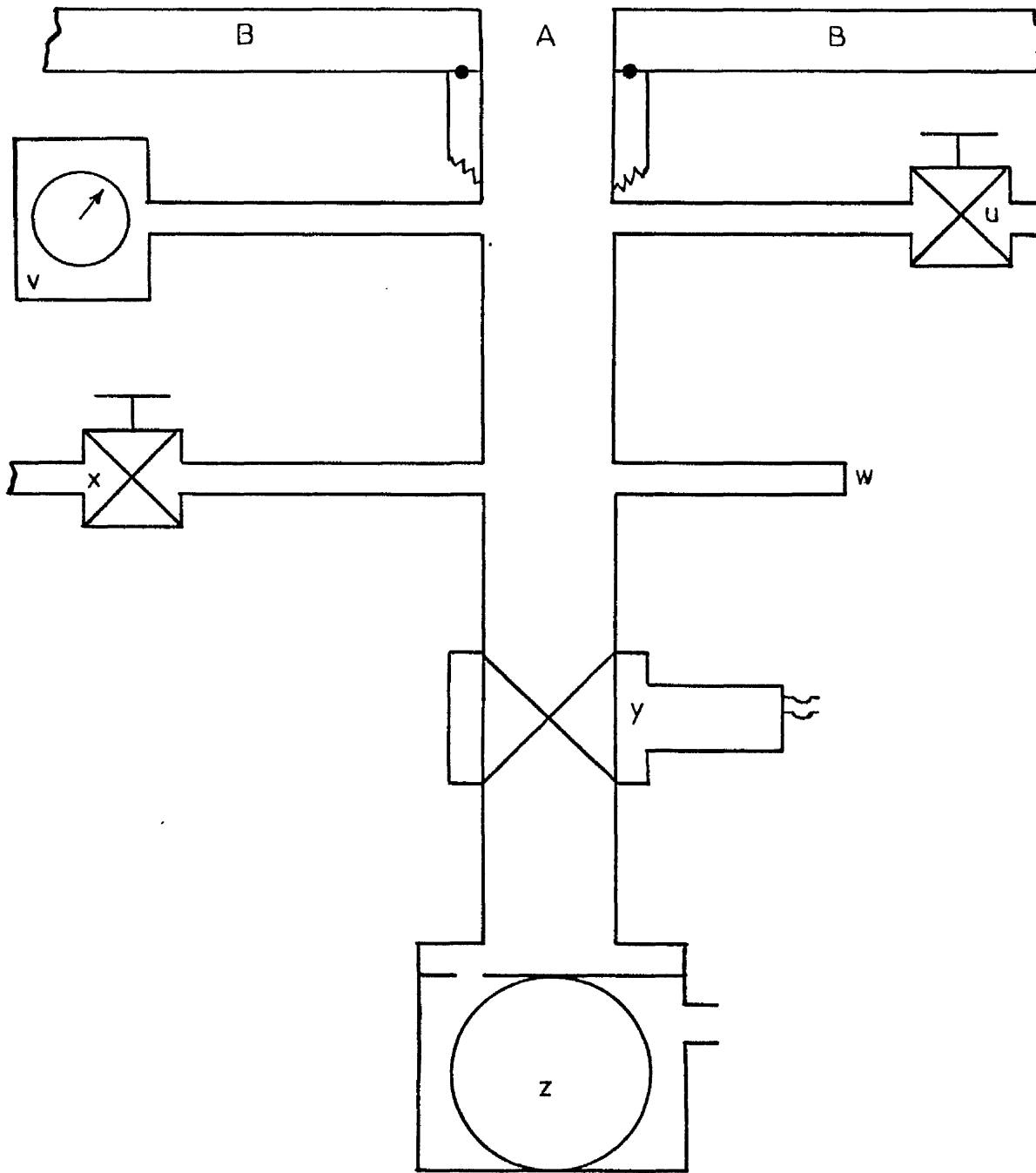
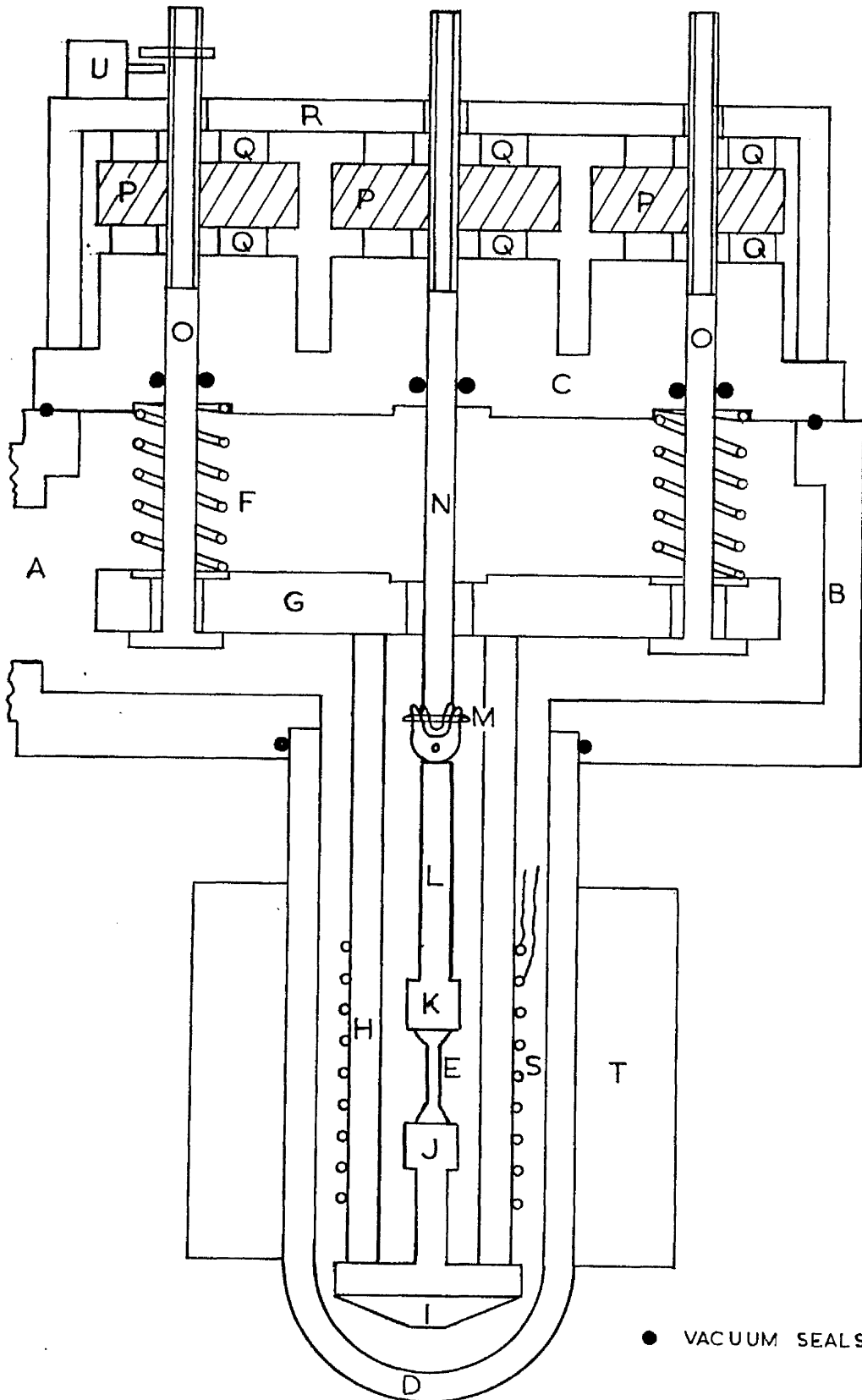


FIG. 6.
VACUUM EQUIPMENT FOR CONSTANT STRESS APPARATUS.



● VACUUM SEALS.

FIG. 7.
IMPROVED VERSION OF CONSTANT STRESS
CREEP APPARATUS.



● VACUUM SEALS

π, γ CHARACTERISTICS FOR MAXIMUM STRAIN
RATE ERROR OF $\pm 5\%$.

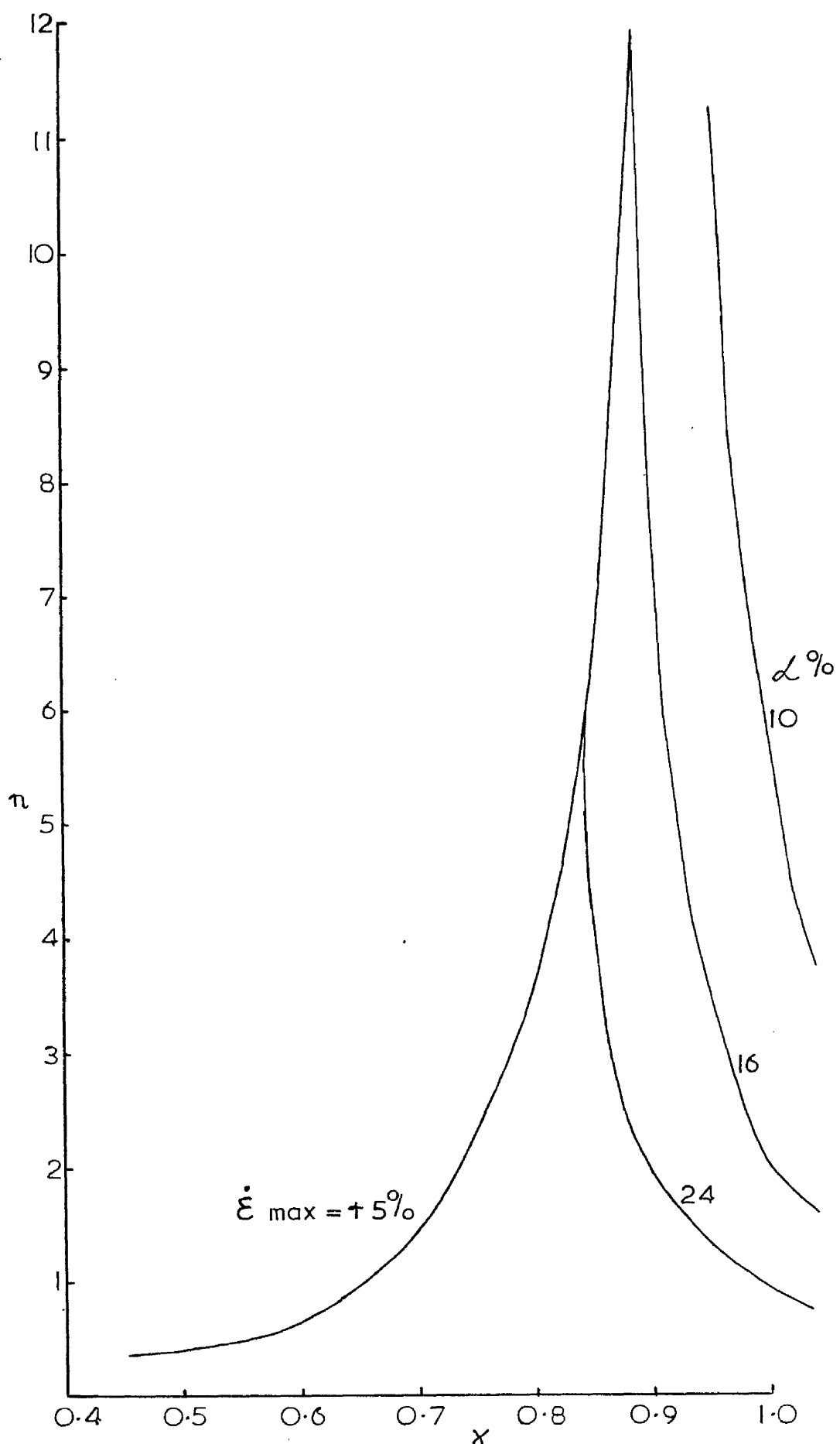
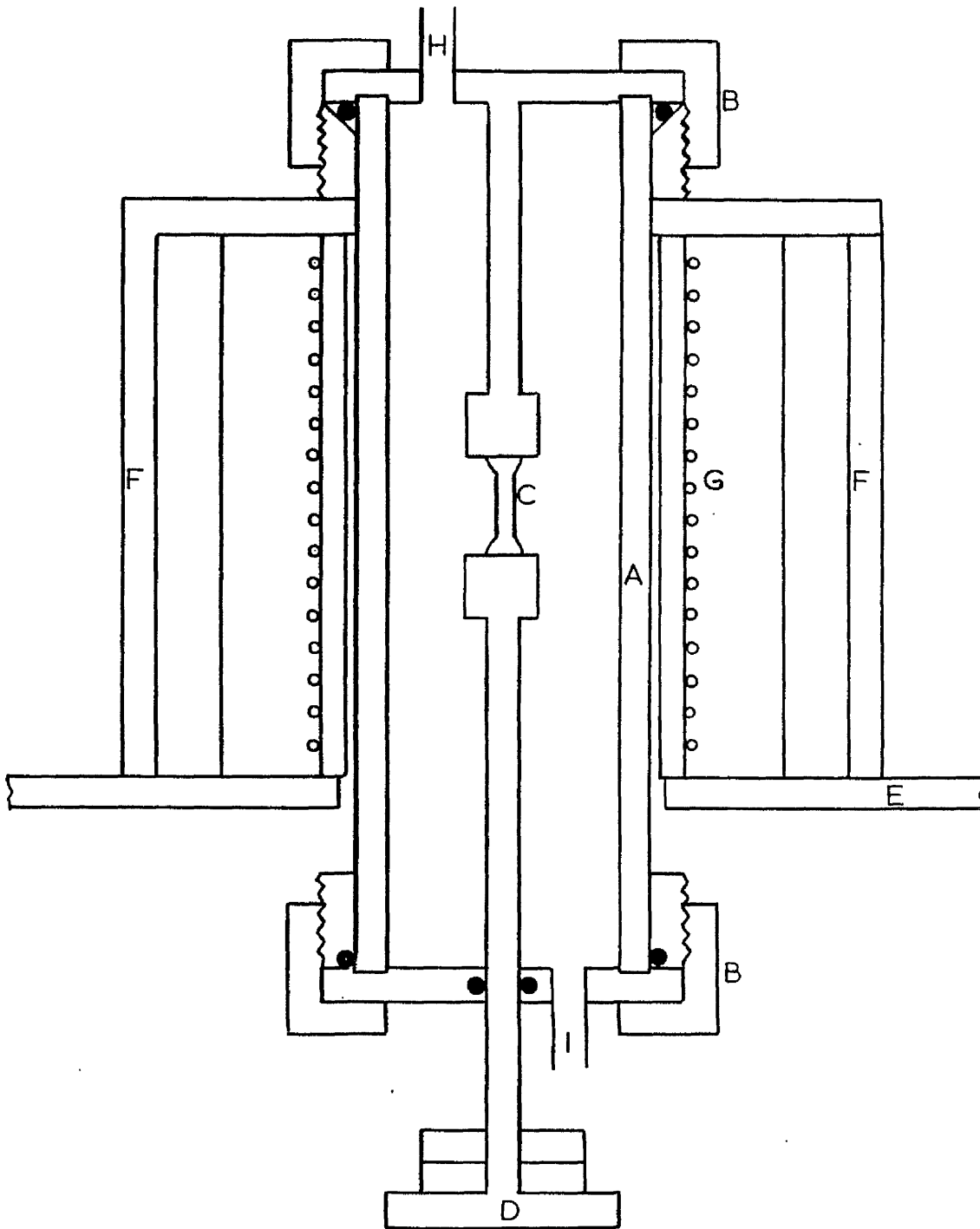


FIG. 9.
APPARATUS FOR THE OXIDATION
OF STRESSED SPECIMENS.



● HIGH TEMPERATURE
'O' RINGS.

FIG. 10.
NICKEL SPECIMENS

Constant stress creep rig specimens.

Stressed.

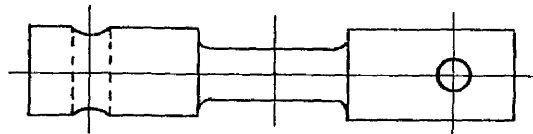


Unstressed.

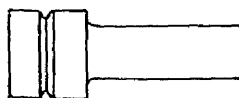


Oxidation rig specimens.

Stressed.



Unstressed.



APPROX FULL SIZE.

CHAPTER IV

RESULTS AND METALLOGRAPHY

4.1 Introduction

A series of creep rupture tests was carried out at 950°C in oxygen or vacuum to provide basic creep data for the batch of nickel used. A shorter series of tests was carried out at 700°C to provide a comparison of creep behaviour in oxygen or vacuum at a lower temperature.

A small number of tests were conducted at 950°C, changing the atmosphere from oxygen to vacuum or vice versa, to explore the roles of oxygen and vacuum in affecting creep behaviour. Also at 950°C, pre oxidised specimens were tested to further examine the effect of oxidation on the creep process.

The creep data in terms of rupture life, secondary creep rate, elongation and reduction in area are presented and discussed. The form of the creep curves is also examined.

The results of metallographic examination of the specimens are presented and discussed. In addition results of metallography on pairs of stressed and unstressed oxidation specimens and unstressed sintered nickel discs are given.

The creep results for oxygen tested specimens at 950°C are initially interpreted in terms of the conventional three stage creep behaviour. As will later become clear this approach is not strictly applicable but serves as a useful introduction to the results.

4.2 Creep Rupture Tests at 950°C

Tables IV and V present the data for these tests including some values for specimens not taken to rupture. Some scatter is evident in the results but on the whole, rupture life decreases and secondary creep rate increases as the stress is increased. Elongation increases as rupture life increases. Reduction of area values from the vacuum tests are presented but it was not possible to obtain meaningful values from tests in oxygen due to the heavy surface scaling.

In most cases rupture life in oxygen is significantly greater than that in vacuum at the same stress. The difference narrows as stress increases. Elongation values are greater for tests in oxygen. This could be solely a function of increased rupture life but the tests at 12.0 N/mm² stress in oxygen indicate larger elongations than tests of similar duration in vacuum. The product of secondary creep rate and rupture life gives a further comparison of the creep processes in oxygen and vacuum. Much higher values are found for tests in oxygen. This immediately indicates that nickel, crept in oxygen, can tolerate a higher level of deformation or damage prior to fracture, than in vacuum.

Fig. 11 further illustrates this point. The plot of log rupture life versus log secondary creep rate has a slope of unity for vacuum tests showing a direct relationship between these parameters, i.e. Rupture Life \propto (Secondary Creep Rate)⁻¹. For oxygen tests the slope is not unity and over the range considered the secondary creep rate values are displaced to longer rupture lives, i.e. Rupture Life \propto (Secondary Creep Rate)^{-1.25}. Alternatively it can be said that for a given rupture life the secondary creep rate is greater in oxygen than in vacuum.

Fig. 12 shows the plot of log rupture life versus log stress. Although no well established correlation emerges, it is evident that a different relationship holds for creep in oxygen than for creep in vacuum. At equivalent stress, rupture life in oxygen is greater than that in vacuum and the dependence of rupture life on stress is much more sensitive in oxygen.

A similar lack of correlation exists in Fig. 13 where log secondary creep rate is plotted against log stress. At the same stress the creep rate is greater in vacuum than in oxygen. The sensitivity of creep rate to stress is much greater in oxygen. The exponents indicated by the graph give the following relationships:

$$\begin{aligned} \text{In vacuum, Secondary Creep Rate} &\propto (\text{Stress})^9 \\ \text{In oxygen, Secondary Creep Rate} &\propto (\text{Stress})^{22} \end{aligned}$$

There is no abrupt change in slope in either Figs. 12 or 13, indicating that the effect of atmosphere is operative over the entire stress range considered.

If some inconsistencies are accepted as being due to experimental scatter, these results show a marked difference in creep behaviour between tests carried out in oxygen and vacuum.

4.3 Creep Rupture Tests at 700°C

Table VI shows the creep data for these tests. Again allowing for some experimental scatter the trends are as would be expected. In this case there appears to be no significant difference between creep in oxygen or vacuum. The rupture lives and secondary creep rates are within the ranges encountered in the tests at 950°C and so the absence of an atmosphere effect must be due to the altered temperature or stress.

Fig. 14 shows that in the plot of log secondary creep rate versus log rupture life, points for both oxygen and vacuum tests

fall on the same line which has a slope of unity. Comparison with Fig. 11 indicates that for a given creep rate, rupture life at 700°C is longer than in vacuum at 950°C but shorter than in oxygen at 950°C. This confirms the absence of an atmosphere effect at 700°C but shows nickel to be more resistant to fracture at the lower temperature.

Figs. 15 and 16 again show data for both oxygen and vacuum tests to lie on single lines. From Fig. 16 the stress exponent of secondary creep rate is approximately 4 which, although slightly low, is in reasonable agreement with literature values.

These results would indicate that atmosphere does not play a marked role in the creep of nickel at 700°C.

4.4 Strain/Time Creep Curves

Particular attention was paid to the form of the creep curves as one object of the work was to investigate the so called fourth stage creep. None of the oxygen tested specimens gave spectacular examples with abrupt changes of slope. In nearly all cases at 950°C however, there were inflections in the curves during the secondary stage and the quoted creep rates have been taken as the overall average rate during such periods. All other specimens exhibited normal three stage creep.

Fig. 17 shows representative curves for nickel crept at 700°C. These curves, over the stress range 23 to 32 N/mm², are fairly consistent showing an increase in secondary creep rate and primary extension as the stress is raised. Tertiary extension is variable and no trend is evident. There is no discernible difference between the form of the curve in a test atmosphere of oxygen or vacuum.

Fig. 18 shows the strain/time curves for specimens tested in vacuum at 950°C at stresses between 8.0 and 10.5 N/mm².

Correlation is reasonable and the curves give an indication of the experimental scatter involved with regard to stress level, e.g. variation in the extent of primary extension. There is a smooth transition into a well defined steady state region and then an abrupt transition into tertiary creep. The amount of tertiary extension is relatively large.

Fig. 19 shows creep in oxygen under the same conditions of stress and temperature as Fig. 18. None of these tests was taken to rupture. There is good agreement between the curves with some variation in primary extension. This variation is to some extent anomalous in that the highest stress level gives the smallest extension. Some experimental scatter in primary extension would be expected as most creep rigs impart some variation due to take up in the load application system. The curves show a normal decreasing creep rate during the primary stage. The curves of Fig. 19 now reveal the problem of explaining the creep behaviour of nickel, in oxygen at 950°C , in terms of three conventional stages. The creep rate continues to decline but does not enter a true steady state region. In the apparent secondary stage, the creep rate, while showing slight perturbations, continues to decline up to the point of interruption. Ignoring the inflections the entire creep curves are reasonable approximations to Andrade's time law of creep, i.e. $\Sigma = \beta t^{\frac{1}{3}}$.

Fig. 20 shows the creep curves at 950°C in vacuum for a stress level of 11.0 N/mm^2 . Apart from the time of entry to tertiary creep there is remarkably close agreement. There is a similar extent of primary extension then a smooth transition into steady state creep. Although the creep rates vary somewhat the curves lie very close to one another. As at lower stress (Fig. 18) there is a sharply defined entry into a relatively large tertiary

extension. The curve for the test conducted in a vacuum of 10^{-6} torr, as opposed to 10^{-1} torr, lies slightly apart from the others. As only one test was conducted under this condition it is difficult to say whether this is a real effect due to different vacuum or possibly a consequence of being tested in a different rig. In any case the variation is marginal and within the experimental error band encountered on a single rig.

Fig. 21 shows the strain/time curves at 950°C in oxygen at the same stress of 11.0 N/mm^2 . Again the curves show remarkable correlation. There is slight variation in the extent of primary creep with a smooth transition into a secondary stage. As at lower stress the secondary stage is not steady state but instead the creep rate varies about an average. The transition into tertiary creep is very gradual and it is difficult to pin-point a precise entry time.

Fig. 22 shows creep curves for tests in vacuum at 950°C and 12.0 N/mm^2 . As at lower stress these curves are representative of classic three stage creep.

Fig. 23 shows strain/time curves for tests in oxygen at 950°C and 12.0 N/mm^2 . They show reasonable agreement, the greatest scatter being in the extent of primary creep. The two specimens with the shortest rupture lives exhibited normal three stage behaviour with a rather more gradual entry into tertiary than was found for vacuum tests. Once again longer time tests shows the variable secondary creep rate which is characteristic of the creep of nickel in oxygen at this temperature. A tertiary region is almost impossible to define for these curves. Although there is an increase in creep rate close to fracture, it is not much greater than the secondary creep rate.

Fig. 24 shows the one exception to the pattern of creep at 12.0 N/mm^2 and indeed all creep in oxygen. There is a normal primary stage, creep rate continues to decline during secondary and fracture occurs with virtually no tertiary extension at an extremely long rupture life.

4.5 Comparison of Strain/Time Curves in Vacuum and Oxygen at 950°C

Figs. 25, 26 and 27 show the early stages of the creep curves for oxygen tested specimens plotted on the same scale as the entire curves for vacuum tested specimens. These plots present together representative curves from Figs. 18 to 24. Fig. 28 shows a comparison of the curves for other tests not taken to rupture.

The most striking aspect of the comparisons given by these graphs is the similarity of the early stages of creep in oxygen to creep in vacuum at the same stress. There does, however, appear to be some difference at the primary stage. In the majority of cases the creep rate in oxygen decreases faster than the creep rate in vacuum. This results in less primary extension in oxygen tested specimens. Although there may be some error arising from the load take up factor there is a consistent trend in the results. It is therefore difficult to dismiss this feature as being entirely due to experimental uncertainty.

Reference to Table VII sheds some further light on this question. The creep strain after 0.5 hours under stress was measured on the extension/time trace for all tests conducted on annealed specimens. The data were pooled irrespective of stress level. Table VII shows that the average stress for vacuum tests was slightly lower than that for oxygen tests. It would therefore be reasonable to expect the mean creep strain at 0.5 hours of vacuum tests to be slightly lower. This is not the case. Standard deviation shows the variation in creep strain to be similar for both test atmospheres.

Application of the 't' test on the statistical parameters reveals that the difference in mean creep strain is significant at the 98% confidence level. This would indicate that there is a real difference between primary creep behaviour in oxygen and that in vacuum.

Fig. 28 shows curves for specimens where creep was interrupted for metallographic purposes. The early stages of creep in vacuum and oxygen are practically identical. In view of the described differences in primary creep and overall scatter in the results, the close similarity in the 1.5 and 3.0 hour comparisons, respectively, appears to be somewhat fortuitous. Scatter is amply illustrated by the fifth (upper) curve. This specimen was interrupted in tertiary, not having reached the desired comparison time. However, the similarity of these curves is a highly effective demonstration of the indication from Figs. 25 to 27 that the creep rate in oxygen is little different from the steady state creep rate in vacuum, compared over the equivalent time interval.

Close examination of the creep rate in these early stages of oxygen tested specimens shows no steady state region. The creep rate always declines with time. This continuously declining creep rate is even shown in tests over hundreds of hours, as in Figs. 19 and 24. Indeed none of the oxygen creep curves show much evidence of a period of steady state creep. Instead they show, from the start of creep, a continuously declining creep rate well beyond the point where the establishment of steady state would be expected. Creep then enters directly into that period where the creep rate cycles. The final stage of accelerating creep rate prior to fracture (tertiary) in most cases occurs over a much extended period, as in Figs. 21 and 23.

The difficulty of explaining the creep of nickel in oxygen at 950°C in terms of conventional three stage behaviour is now explained. The definition of a secondary stage is somewhat academic but could be done by firstly defining the limits of the primary and tertiary stages and terming the remainder secondary. However this does not ascribe a specific creep condition to the secondary stage. A single creep equation can describe both conventional primary and secondary creep^(55,57).

It therefore appears more likely that secondary creep in oxygen is included in the period of declining creep rate and some factor has prevented the achievement of the steady state balance. The period of cycling creep rate is then included into the tertiary stage. This last statement is supported by the fact that in several curves in Figs. 21 and 23 the fluctuations in creep rate occur within an overall trend of increasing creep rate.

4.6 Creep of Pre Oxidised Specimens

Six specimens were pre oxidised for 24 hours at 950°C and immediately creep tested at the same temperature at a stress of 12.0 N/mm². Three specimens were creep tested in oxygen and vacuum respectively. Table VIII lists the creep data and Figs. 29 and 30 are plots of the strain/time curves. The same two curves for oxygen tests appear in both graphs. In spite of the scatter the data indicates some trends. Rupture life in oxygen is much greater than that in vacuum. The rupture life of pre oxidised specimens is in general greater than that of annealed specimens, both tested in oxygen. There would appear to be some reduction in the rupture lives of vacuum tested specimens.

There is little difference between the primary stages of the creep curves for tests in oxygen or vacuum. The extent of primary

creep is comparable to that found for annealed specimens tested in oxygen. Of the creep curves for pre oxidised nickel, the two vacuum tests and the short rupture life oxygen test show conventional three stage behaviour. The longer term oxygen tests show the typical features as found in other creep tests in oxygen at 950°C.

Thus pre oxidation would appear to reduce the extent of primary creep. Other generalisations are difficult due to the scatter in the results but there may be a weakening effect as evidenced by the vacuum tests. Alternatively the oxygen tests show a possible magnification of the effect of simultaneous oxidation.

4.7 Effect of Atmosphere Change During a Creep Test

Six tests were conducted where the atmosphere was altered from vacuum to oxygen or vice versa during "secondary" creep at 950°C. Two tests of each type were carried out at a stress of 10.0 N/mm² and a single test of each type at a stress of 11.0 N/mm².

Tables IX and X summarise the results of these tests. Figs. 31 and 32 show the strain/time curves for tests at 10.0 N/mm² in oxygen/vacuum and vacuum/oxygen respectively. Fig. 33 shows the strain/time curves for tests at 11.0 N/mm².

Appraisal of Tables IX and X along with IV and V enables some generalisations to be made. The introduction of oxygen during a test extends the rupture life over tests conducted entirely in vacuum but probably not to the values reached in tests entirely in oxygen. Tests started in oxygen and continued in vacuum appear to give similar or slightly greater rupture lives compared to tests conducted wholly in vacuum.

The creep curves shown in Figs. 31 to 33 provide the best insight into the effect of an atmosphere change. The most striking

feature is the sudden change in creep rate, amounting to a second primary stage, when oxygen is introduced. There is no such abrupt change in creep rate when vacuum is introduced. After the introduction of oxygen there is virtually a complete oxygen type pattern of creep behaviour. After the introduction of vacuum, steady state conditions are immediately established in place of the continuously declining creep rate in oxygen. The exact point in late primary or secondary creep at which the atmosphere is altered does not appear to be of major consequence. The overall creep behaviour approximates to that typical in the atmosphere which has been introduced.

4.8 External Appearance of Specimens

After vacuum annealing, all test pieces had a mirror like surface finish. This condition was maintained by storing in an evacuated dessicator until required for testing.

The only occasion on which the surface was in a similar condition after testing was the single test in a vacuum of 10^{-6} torr. All other tests whether carried out in oxygen at 400 torr or vacuum at 10^{-1} torr allowed some surface oxidation to occur.

There was little difference between specimens tested either in oxygen or vacuum at 700°C . All had what could best be described as a tarnished appearance. At 950°C there was an obvious difference between specimens tested in oxygen or vacuum. Those tested in vacuum exhibited a surface oxide film. Those tested in oxygen showed variation from a similar film, in very short time tests, to a heavily scaled surface as test time increased. In nearly all cases these scales were firmly adherent, as in Fig. 34. The exceptions were pre oxidised specimens, where the oxide film was blistered and flaking, even where the creep test was in oxygen, as in Fig. 35.

Surface cracks could be clearly seen on many specimens apart from some of those tested in oxygen for long periods of time, where the surface was heavily scaled. Some oxygen tested specimens were extensively cracked along the gauge length and near failure at several points was found in some cases. Fig. 36 shows an extreme example, still in test position in the constant stress creep rig. Heavily cracked oxygen tested specimens were found to be brittle and several broke during removal from the shackles.

4.9 Metallography of Specimens Creep Tested at 700°C

All specimens had the typical structures of crept material. No significant difference could be seen between specimens tested in oxygen or vacuum, apart from a slightly greater thickness of oxide on oxygen tested specimens. The surface oxide films were only just visible at high magnification and there was virtually no oxide penetration into grain boundaries.

The extent of grain boundary void formation was variable. The only relationship between this and test conditions was a tendency for the number, size and coalescence of voids to increase as rupture life increased. Voids were concentrated on grain boundaries approximately perpendicular to the axis of stress. The void formation was not uniformly distributed along the gauge length, but invariably the greatest concentration of voids occurred adjacent to the fracture surface.

Distribution of voids, across specimens, was fairly consistent with a tendency for greater occurrence in the centre. Relatively few cracks or void chains emanated from the surface. There were some examples of surface steps at grain boundaries, indicative of grain boundary sliding. Grain size was variable even within single specimens. Void formation was greater in fine grained areas.

Figs. 37 and 38 depict typical structures of oxygen tested specimens, illustrating the above points, and Figs. 39 to 41 similarly show vacuum tested specimens.

4.10 Metallography of Specimens Creep Tested in Vacuum at 950°C

In general the microstructures of these specimens were similar to those of specimens tested at 700°C. Grain boundary void formation, void coalescence and resultant intergranular cracking were clearly present. The incidence of void formation was relatively low, again tending to occur in bands and not uniformly along the entire gauge length. Individual voids were relatively small and mostly occurred in chains along grain boundaries at high angles to the axis of stress.

Fig. 42 illustrates that voids could form within a short time of the application of stress. A void chain, typical of those found in vacuum tested specimens, is shown in a specimen which failed after only six minutes. Although widespread, void coalescence was not extensive and actual cracks were limited in number. Fig. 43 shows a rare example of advanced void coalescence which is at the stage of developing into a propagating crack.

The process of void coalescence/crack formation was always furthest advanced, close to the fracture surface. Void formation tended to be concentrated in the specimen interior away from the surface. Crack faces and fracture surfaces showed clear serrations or indentations resulting from the original void formation, as shown in Figs. 44 and 45 respectively.

Specimen surfaces had a light oxide film and the few cracks which connected to specimen surfaces showed slight signs of oxidation, near to the surface.

4.11 Metallography of Specimens Creep Tested in Oxygen at 950°C

The microstructures of these specimens were similar to those already described and typical of crept material. However, there were marked differences especially in the level and extent of void formation, coalescence and crack formation. The differences became more pronounced as test time increased.

Void formation was more uniform along the specimen gauge length and did not occur in bands to the same extent. Void coalescence and crack formation were more common, being furthest advanced close to the fracture surface. The positional balance of void formation was altered in that there was a relatively greater occurrence near to and connecting with the specimen surface. Noticeably larger voids were found than in vacuum tested specimens. However, comparison of specimens tested in oxygen and vacuum where creep was interrupted after the same duration showed a similar extent and size of voidage.

The surface oxide was clearly visible, thickness depending on test time. There was extensive oxidation of crack faces, in many cases extending completely through the specimen thickness. The extent of oxide penetration into grain boundary damage varied but in general increased with increasing rupture life. Specific features of the specimen structures are depicted in photomicrographs.

Fig. 46 shows early void formation. Grain boundary sliding is indicated by the clearly visible surface steps. Voids close to the specimen surface, at such an early stage in the creep life, is a clear sign of the increased tendency for void formation in this region. Fig. 47 also shows considerable void formation close to the free surface in a specimen of relatively short rupture life. Fig. 48 shows a marked example of preferential void formation near the specimen surface. The rupture life was still relatively short

at 13 hours. Figs. 49 and 50 reveal that at a rupture life of 100 hours the level of void formation in the specimen interior increases to match that at the surface.

Figs. 49 and 50 also show the large size of individual voids in oxygen tested specimens at 950°C . In addition the voids grow to a greater size prior to coalescence than either in vacuum at 950°C or either atmosphere at 700°C . The lengths of void coalescence, especially in relation to their width, are less in oxygen tested specimens at 950°C .

Crack development can now be considered. Fig. 51 shows the propagation of a crack from the specimen surface, along a voided grain boundary. It can be seen that the crack faces are subsequently oxidised as the oxygen atmosphere penetrates the crack.

With increasing rupture life, extensive continuous crack networks develop, far in excess of anything encountered in vacuum tested specimens. Figs. 52 and 53 show such networks, near the specimen surface and in the interior, respectively. This specimen was perhaps one of the most spectacular examples of the effect of an oxygen atmosphere. Heavy oxide scale can be seen on the crack faces and rupture had not occurred after 24.1 hours with an elongation of 25 per cent. Figs. 54 and 55 show crack networks in specimens which had rupture lives of around 100 hours with elongations of over 10 per cent. Fig. 54 shows an area remote from the fracture surface and Fig. 55 shows an actual fracture surface. The oxide layer on the crack faces is clearly visible and the fracture surface has a continuous oxide layer which was typical of all fracture surfaces on specimens tested in oxygen at 950°C .

Although damage was always furthest advanced close to the fracture surface, Figs. 52, 53 and 54 show that extensive damage commonly occurred in regions remote from the fracture surface.

Figs. 51 to 55 also reveal that the cracks were not fully oxide filled but rather bridged by oxide at many points.

In common with literature reports, cracks emanating from the specimen surface occurred much more in oxygen tested specimens relative to vacuum tested specimens. In many cases these surface cracks were relatively short and filled with oxide. Figs. 56 to 58 show examples of such features and in addition Fig. 58 shows the formation of a crack in the oxide. This may be an indication of the eventual failure mode, i.e. by crack propagation through the nickel oxide within intergranular cracks in the nickel. It may also be noteworthy that the crack in the oxide has a relatively large ratio of width to length.

Having considered the typical sequence of events leading from void formation to fracture, it is of interest to turn to the unusual structures shown in Figs. 59 and 60. These are photomicrographs of two of the longest lived specimens. The rupture lives are unknown since the tests were stopped with the specimens unbroken after 332 hours and 530 hours respectively. Only in the 530 hour test were some actual cracks formed. Void formation is extensive, the voids are large and considerable coalescence of limited length has occurred. There was only limited oxide penetration into short surface openings. This emphatically confirms the indications from other specimens that void coalescence and crack formation in the bulk of the specimen can be inhibited in oxygen. The elongation values for both specimens were greater than those for any vacuum tested specimen.

4.12 Metallography of Unstressed Specimens

This section deals with those specimens which were mounted alongside the stressed specimens in the creep rig in order to

provide a comparison of the effect of oxidation alone on the nickel structure. It should be noted that absolutely no evidence of voids was found in the as received and vacuum annealed structures of the nickel.

There was little or no effect on the structure of unstressed specimens when tested in a vacuum of 10^{-1} torr, either at 700°C or 950°C . The majority of these specimens had a void free structure similar to the vacuum annealed state. In a few instances, at longer times at 950°C , there was a very slight degree of void formation close to the specimen surface. Specimens tested in oxygen at 700°C showed only a light degree of void formation adjacent to the free surface.

Those specimens tested in oxygen at 950°C showed clear evidence of grain boundary void formation. This occurred within a short time as evidenced by Fig. 61. Voids increased in size, number and depth of penetration as oxidation time increased. This is demonstrated in Figs. 61, 62 and 63. The voids are formed primarily on grain boundaries parallel to the specimen surface although there were instances of void chains penetrating into the specimen interior along boundaries at high angles to the specimen surface. Such penetration was found at longer oxidation times and there was also a sparse random distribution of voids on interior grain boundaries as shown in Figs. 64 and 65. Long oxidation times caused some void coalescence close to the specimen surface and slight oxide penetration into this voidage. Fig. 66 shows an extreme example of this.

Voids in the unstressed specimens were invariably smaller, less in number and showed less coalescence than in the corresponding stressed specimens.

4.13 Metallographic Comparison of Stressed and Unstressed Oxidation

Specimens

Figs. 67 to 74 show the typical structures of a series of tests exposing one stressed and one unstressed specimen to oxidation in the same chamber. The applied stress of approximately 5.0 N/mm^2 was effected by a dead load. The temperature was approximately 950°C and the oxidising atmosphere produced by an oxygen flow of 150 ml/min through the chamber.

Figs. 67 and 68 show the structures of a pair of specimens after 49 hours. In Fig. 67 grain boundary voids are widespread throughout the specimen on boundaries at high angles to the axis of stress. Voidage decreases slightly towards the specimen centre. In Fig. 68 the voids are heavily concentrated close to the specimen surface on boundaries approximately parallel to the surface. Only a few isolated voids exist in the interior.

Figs. 69 and 70 show structures after 120 hours oxidation. The stressed specimen in Fig. 69 shows an anomalous structure for this series of tests. There is advanced creep damage consisting of an extensive oxide filled crack network. However this specimen was approximately half the diameter of the others and this effect of advanced damage in small sections has been reported previously (11). The unstressed specimen in Fig. 70 shows a heavy concentration of voids on grain boundaries close to and parallel to the specimen surface. The greater oxidation time has allowed void penetration into the specimen interior, but these central void chains do not show the same preference for a particular grain boundary orientation.

After 144 hours oxidation Fig. 71 shows that, in the stressed specimen, creep damage had reached the stage of extensive void coalescence and even crack propagation. The damage is predominantly on high angle grain boundaries. The unstressed specimen in Fig. 72

again has voids concentrated on boundaries close to and parallel to the specimen surface. After this time, void size had increased, coalescence in the surface region was extensive and penetration into the interior was considerable.

Figs. 73 and 74 show, that, after 164 hours oxidation, there appears to be little difference between the structures of the stressed and unstressed specimens. The damage in the stressed specimen is not noticeably greater than that after 144 hours. In the unstressed specimen a concentration of voids on the parallel grain boundaries close to the specimen surface was still evident. But penetration of voids into the interior is more marked and coalescence has occurred even near the centre. However, true cracks had not formed and, as in all unstress specimens, void coalescence was of a strictly limited length.

4.14 Metallographic Illustration of Oxide Growth in a Simulated Crack

In this exercise, pairs of thin nickel discs were bound together with nichrome wire and oxidised at 950°C for various times in air. This was in effect an "oxidation sintering" treatment in the virtual absence of a compressive stress. The slight gap between the discs at their edges formed the simulated crack.

Figs. 75 to 78 show the progressive build up of the surface oxide layer on the two discs. By the time oxidation had been in progress for 48 hours, the oxide had filled the gap between the discs and the separate oxide layers on each disc had fused together to form a single oxide mass within the simulated crack. It is of interest to directly compare Figs. 75 to 78 with Figs. 54, 55 and 58, and in particular, the relative crack widths and oxide thicknesses. The appearance of the oxide filled simulated crack is very similar to cracks found in specimens which had undergone creep in oxygen.

4.15 Metallography of the Oxide Layer

After long polishing times, some structure was visible in the oxide layers. Even though extreme care was taken in the mounting of specimens, the oxide was still susceptible to considerable polishing damage. This resulted in partial detachment and occasionally fracture of the oxide layer. Such damage was quite definitely due to polishing and the oxide layer was tightly adherent to the metal, apart from on those specimens which had been pre oxidised and then subjected to creep.

Figs. 79 to 84 show typical oxide structures of creep rig specimens, both stressed and unstressed, for long test times. Other examples of the oxide layer can be seen in previous photomicrographs.

For short oxidation times the oxide was single layered with a columnar grain structure. For times of 100 hours and more, a distinct double layer structure was found. The outer layer was of a columnar nature and the inner layer appeared to be equiaxed. The oxides, especially after long oxidation times, contained considerable porosity. In many cases there was a distinct concentration along the junction of the two layers.

Comparison of oxide thicknesses was difficult, due to the use of cylindrical specimens. Some doubt must exist as to whether the plane of the photomicrographs are precisely on a diameter and therefore perpendicular to the specimen surface. However it was consistently found that the oxide layer on unstressed specimens was thicker than that on corresponding stressed specimens. The difference was most marked after long oxidation times. While the above considerations make exact quantitative assessment of low significance, the differences found were between 10 and 40 per cent.

Comparisons should be made between Figs. 79 and 80 and between Figs. 83 and 84.

The oxide formation within cracks in stressed specimens was difficult to categorise. Both equiaxed and columnar grain oxide were found, rarely together. The uncertainty in knowing precisely where the metallographic plane cuts the crack makes it difficult to say whether any real difference exists between oxide formed on the outer surface and on crack faces.

4.16 Scanning Electron Microscopy

This technique particularly enabled examination of fracture surfaces to be carried out and also gave information on oxide formation.

Fig. 85 shows a general view of a portion of heavily cracked gauge length of an oxygen tested specimen. The fracture surface is at the top of the photograph. The cracking in this region is sufficiently severe to have broken through the scale. This clearly illustrates the extensive crack systems found in many specimens tested for long times in oxygen.

Figs. 86 to 92 show views of the fracture surfaces of specimens tested in oxygen. In Figs. 86 and 88, at lower magnification, the nickel grains are clearly visible. Fig. 86 shows an intergranular crack leading off the fracture surface. In Fig. 88, depressions on the grain surfaces can be seen particularly clearly. These are evidence of grain boundary voids. Figs. 87 and 89 are higher magnification views from Figs. 86 and 88 respectively. While heavier oxide deposits can be seen in Figs. 86 and 88, the peculiar form of the oxide layer which covered the majority of the surface can be seen in Figs. 87 and 89. Figs. 90 and 91 show this thin, "frothy" network of oxide even more clearly. Such a structure has

been said to be typical of oxide which had undergone plastic deformation^(48,84). Fig. 92 shows a nickel protrusion, partially free from "frothy" oxide. There are obvious void depressions on the uncovered surface. It is conceivable that this was one of the final points to part on fracture and therefore remained unoxidised.

Figs. 93 to 95 show the early columnar growth of the oxide on the original specimen surface. The whisker or needle like growths are shown at three magnifications. Under optical microscopy this appeared as a film and contrasts starkly with the thin "frothy" oxide found on the fracture surfaces.

Figs. 96 to 99 show views of the two layer scale formed at long oxidation times. Fig. 96 shows the typical faceted grains of the surface of the columnar outer layer. Figs. 97 to 99 show views through the oxide where it had fractured above crack mouths in the nickel. The columnar nature of the outer layer and the equiaxed nature of the inner layer are clearly visible. The oxide porosity, seen under optical microscopy, was not evident under scanning electron microscopy.

TABLE IV

CREEP DATA FOR ANNEALED SPECIMENS

TESTED AT 950°C IN VACUUM (10^{-1} torr)

Stress	Rupture Life	Secondary Creep Rate	Elongation	Reduction of Area	Rupture Life X Secondary Creep Rate
N/mm ²	Hrs	% per Hr	%	%	%
8.0	17.5	0.08	4.34	2.37	1.40
10.0	7.3	0.23	3.79	2.78	1.68
10.0	17.4	0.08	3.98	1.00	1.39
10.5	29.3	0.08	5.69	-	2.34
10.5	21.5	0.14	5.91	-	3.01
10.5	1.4	1.15	3.15	-	1.61
11.0	6.3	0.20	4.32	2.23	1.26
11.0	4.7	0.27	3.75	-	1.27
11.0*	3.5	0.41	4.26	2.06	1.44
11.0	2.1	0.63	4.33	1.26	1.32
11.0	1.5	0.98	3.34	1.52	1.47
11.0	1.1	1.28	3.07	1.66	1.41
11.0	0.1	-	0.19	0.28	-
12.0	1.78	1.05	3.81	2.53	1.87
12.0	1.65	0.99	3.98	-	1.63

* 10^{-6} torr

TABLE V

CREEP DATA FOR ANNEALED SPECIMENS

TESTED AT 950°C IN OXYGEN (400 torr)

Stress	Rupture Life	Secondary Creep Rate	Elongation	Rupture Life X Secondary Creep Rate
N/mm ²	Hrs	% per Hr	%	%
9.0	> 240	0.001	7.33	> 0.24
10.5	> 530	0.006	9.04	> 3.18
10.5	> 332	0.005	6.42	> 1.66
10.0	> 310	0.010	11.73	> 3.10
10.0	> 308	0.008	8.65	> 2.46
11.0	169	0.032	10.59	5.41
11.0	122	0.063	14.21	7.69
11.0	101	0.069	13.65	6.97
11.0	100	0.065	11.29	6.50
11.5	0.90	1.90	3.64	1.71
12.0	173	0.010	6.64	1.73
12.0	> 24.1	-	25.0	-
12.0	14.8	0.35	9.39	5.18
12.0	13.0	0.36	8.09	4.55
12.0	10.0	0.46	7.69	4.60
12.0	5.6	0.48	4.74	2.69
12.0	4.2	0.38	4.38	1.60

TABLE VI

CREEP DATA FOR ANNEALED SPECIMENS TESTED AT 700°C

Atmosphere	Stress N/mm ²	Rupture Life Hrs.	Secondary Creep Rate % per Hr.	Elongation %	Reduction of Area %	Rupture Life X Secondary Creep Rate %
Vacuum (10 ⁻¹ torr)	23.0	25.5	0.12	5.98	3.48	3.06
Vacuum (10 ⁻¹ torr)	25.0	4.5	0.47	5.86	3.06	2.12
Vacuum (10 ⁻¹ torr)	25.0	8.9	0.22	4.92	2.37	1.96
Vacuum (10 ⁻¹ torr)	27.0	10.8	0.19	5.33	4.15	2.05
Vacuum (10 ⁻¹ torr)	32.0	8.0	0.44	6.97	3.61	3.52
Vacuum (10 ⁻¹ torr)	32.0	5.6	0.38	6.15	3.06	2.13
Oxygen (400 torr)	23.0	13.7	0.11	4.44	3.07	1.51
Oxygen (400 torr)	25.0	18.3	0.14	5.47	3.34	2.56
Oxygen (400 torr)	30.0	8.7	0.28	5.36	2.09	2.44
Oxygen (400 torr)	32.0	5.5	0.45	7.41	4.99	2.48

TABLE VIISTATISTICAL DATA OF CREEP STRAIN (%) AFTER 0.5 HRS AT 950°C

Atmosphere	Average Stress N/mm ²	Number of Tests	Mean Creep Strain %	Standard Deviation %
Vacuum (10 ⁻¹ torr)	10.63	20	1.316	0.435
Oxygen (400 torr)	11.22	18	0.913	0.490

TABLE VIIICREEP DATA FOR PRE OXIDISED SPECIMENS AT 950°C

Atmosphere	Stress N/mm ²	Rupture Life Hrs.	Secondary Creep Rate % per Hr.	Elongation %	Rupture Life X Secondary Creep Rate %
Vacuum (10 ⁻¹ torr)	12.0	7.0	0.35	5.30	2.45
Vacuum (10 ⁻¹ torr)	12.0	0.60	2.10	3.40	1.26
Vacuum (10 ⁻¹ torr)	12.0	Instant Failure	-	-	-
Oxygen (400 torr)	12.0	137.90	0.022	9.27	3.03
Oxygen (400 torr)	12.0	>127.50	0.022	6.87	> 2.81
Oxygen (400 torr)	12.0	3.70	0.54	4.46	2.0

TABLE IX

CREEP DATA FOR TESTS AT 950°C

STARTED IN VACUUM AND CONTINUED IN OXYGEN

Time in Vacuum Hrs.	Stress N/mm ²	Rupture Life Hrs.	Secondary Creep Rate % per Hr.	Elongation %	Rupture Life X Secondary Creep Rate %
4.5	10.0	>33.7	0.13	6.98	> 4.38
6.5	10.0	>54.0	0.03	4.93	> 1.62
1.5	11.0	9.95	0.24	6.47	2.39

TABLE X

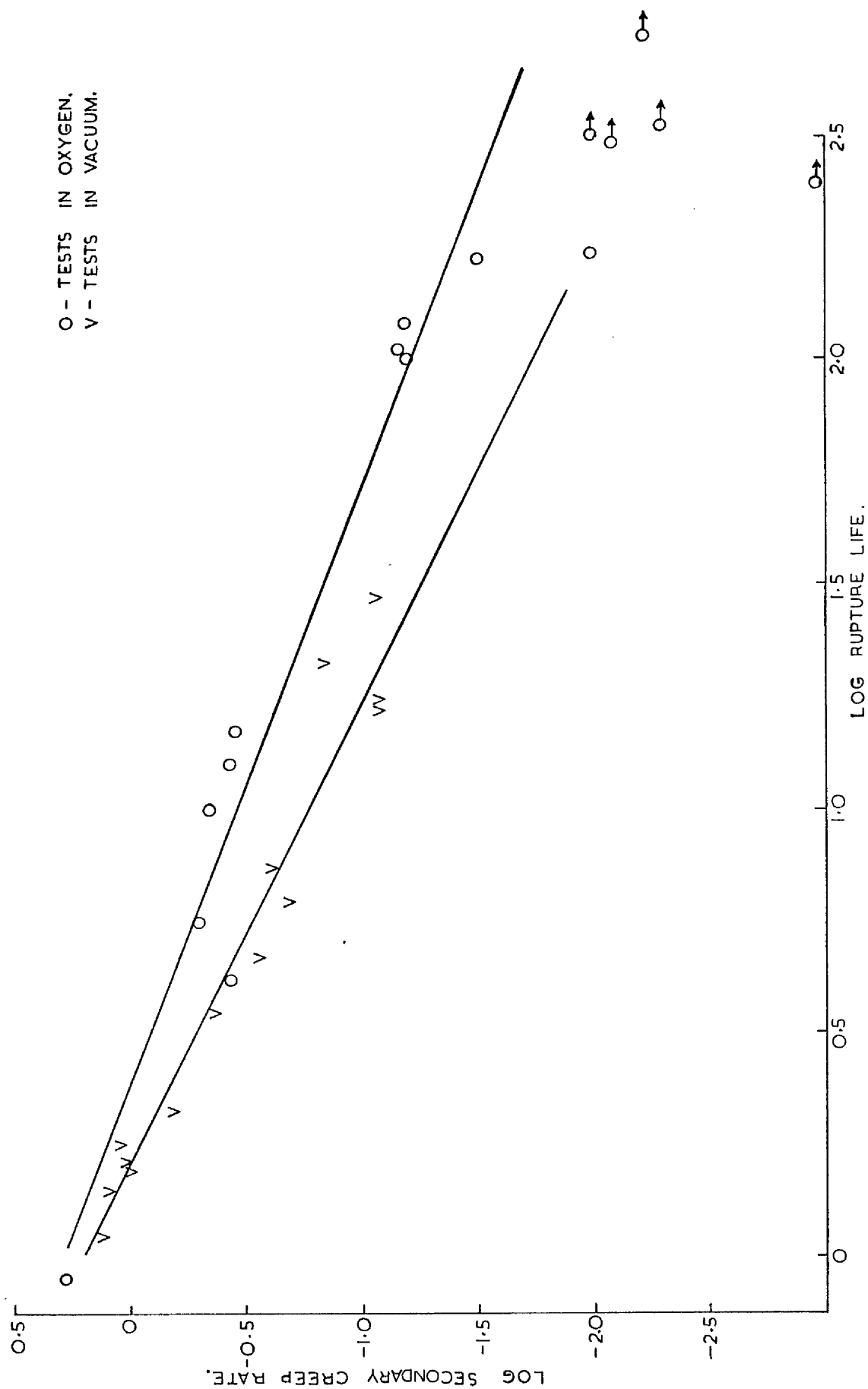
CREEP DATA FOR TESTS AT 950°C

STARTED IN OXYGEN AND CONTINUED IN VACUUM

Time in Oxygen Hrs.	Stress N/mm ²	Rupture Life Hrs.	Secondary Creep Rate % per Hr.	Elongation %	Reduction of Area %	Rupture Life X Secondary Creep Rate %
2.0	10.0	> 21.4	0.10	3.96	2.09	> 2.14
18.0	10.0	31.2	0.06	6.12	1.26	1.87
1.5	11.0	3.54	0.19	1.85	0.28	0.67

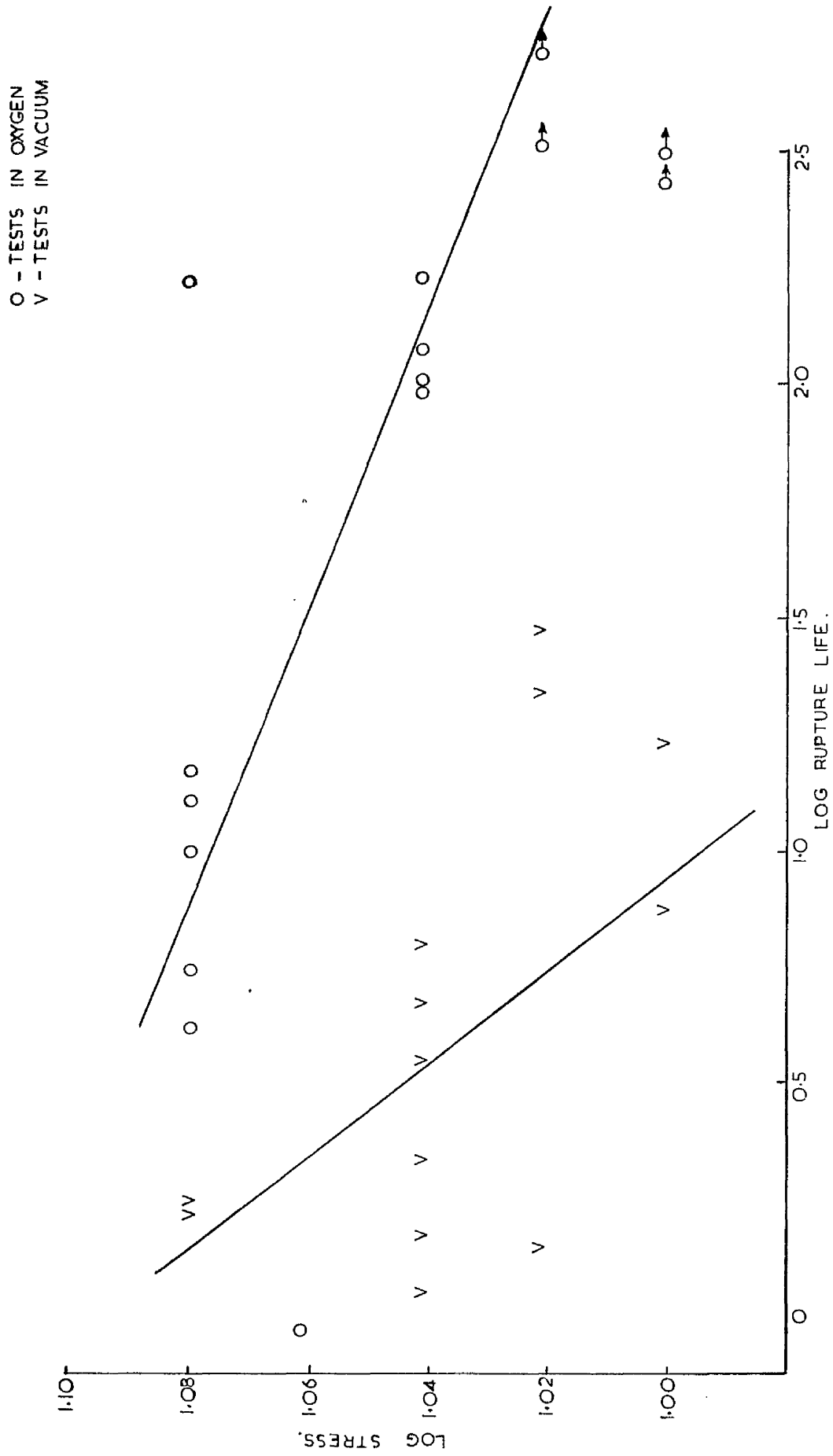
Relationship Between Secondary Creep Rate and Rupture Life at 950°C.

Fig. 11.



Relationship Between Stress
and Rupture Life at 950°C

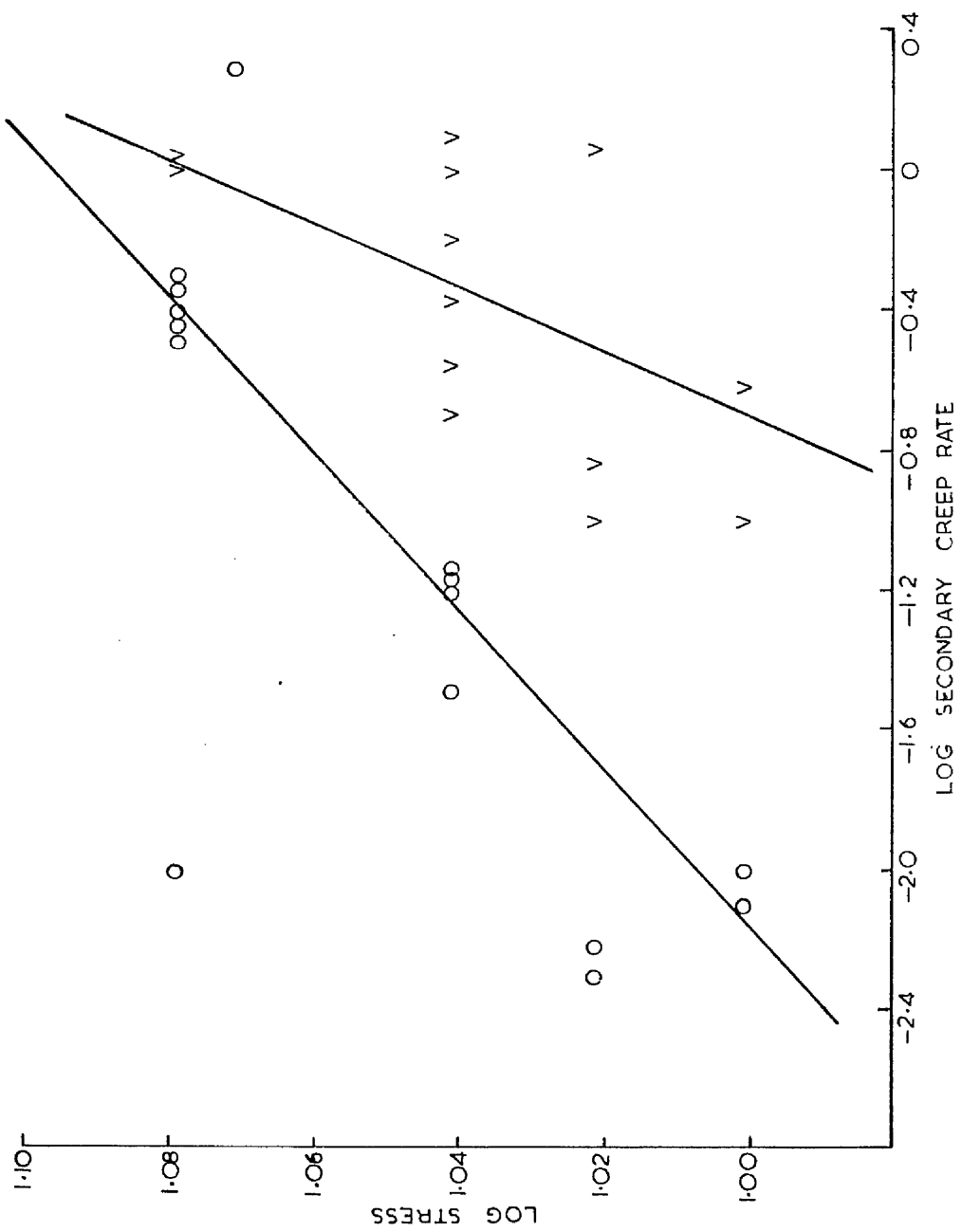
Fig.12.



Relationship Between Stress and Secondary Creep Rate at 950° C.

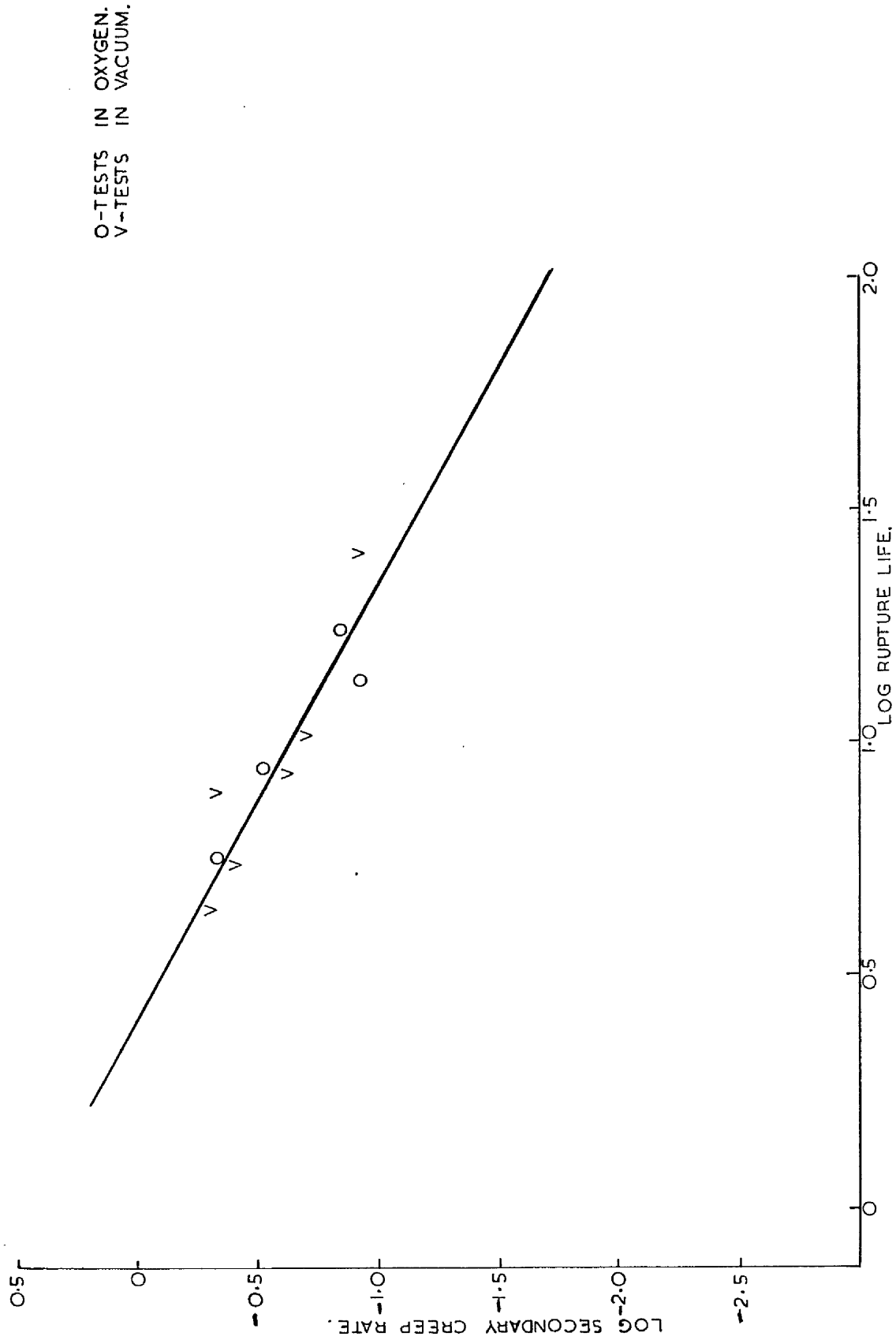
Fig.13.

O - TESTS IN OXYGEN
V - TESTS IN VACUUM



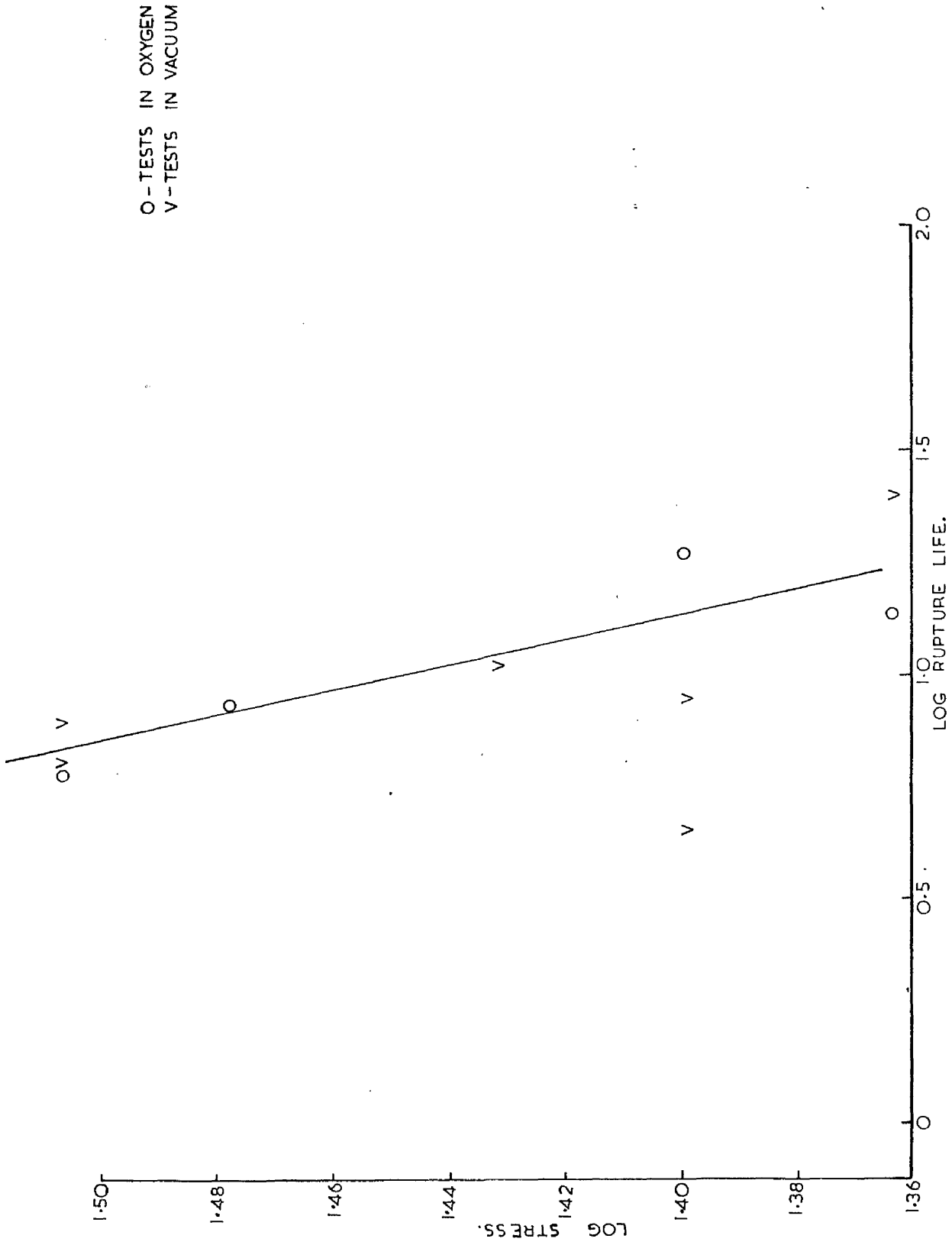
Relationship Between Secondary Creep Rate
and Rupture Life at 700°C

Fig.14.



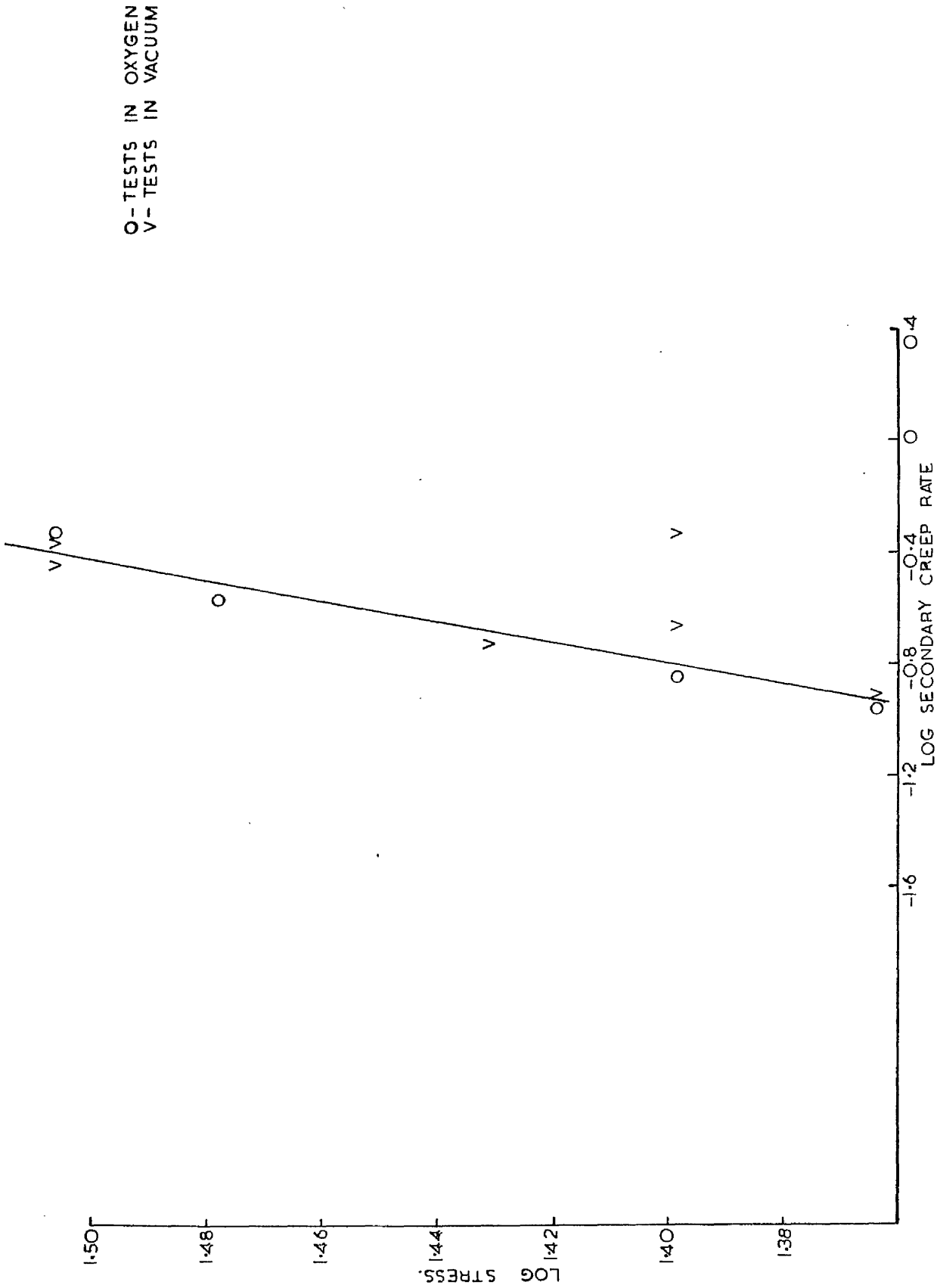
Relationship Between Stress and Rupture Life at 700°C.

Fig. 15.



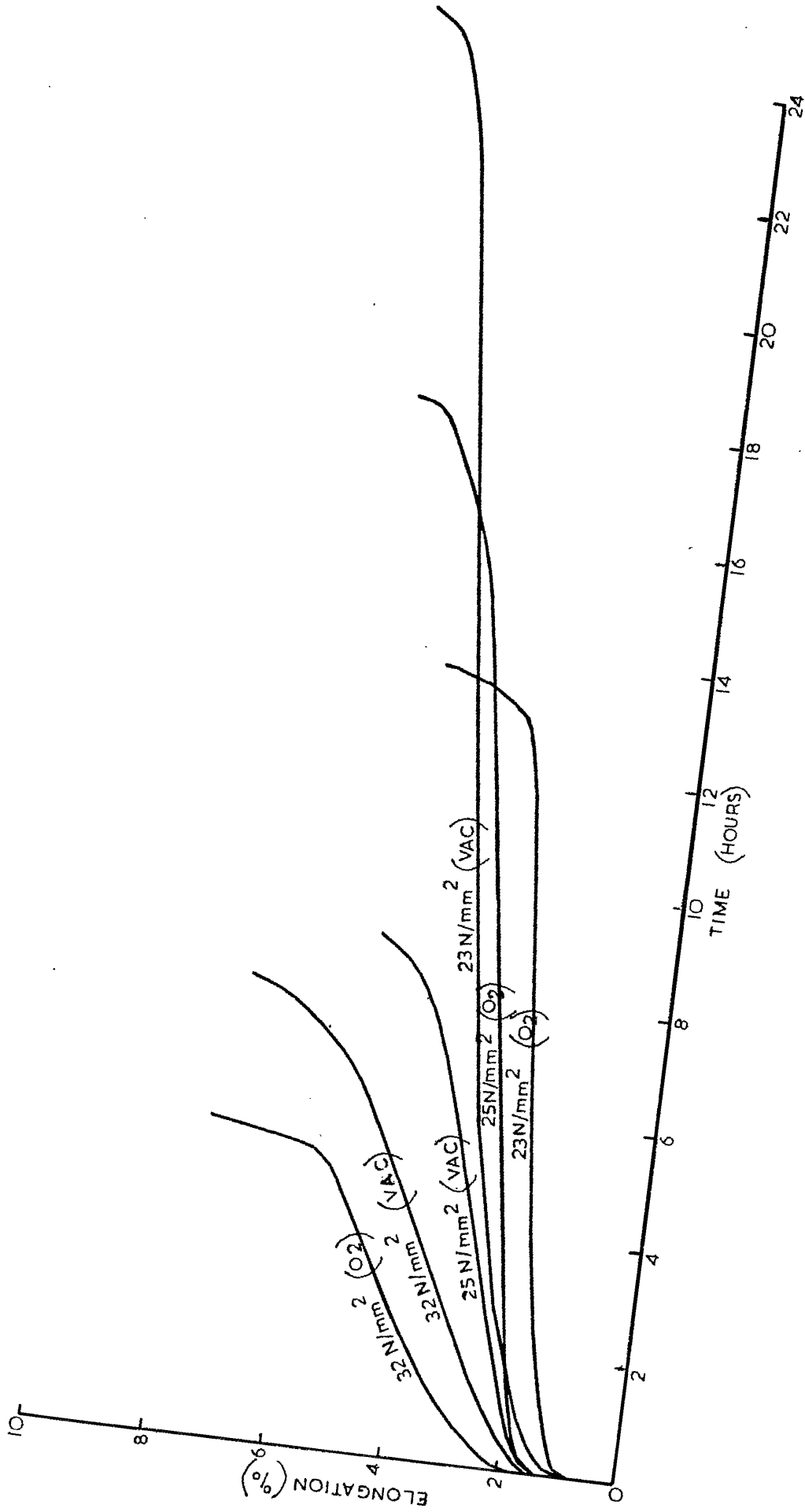
Relationship Between Stress and
Secondary Creep Rate at 700° C

Fig.16



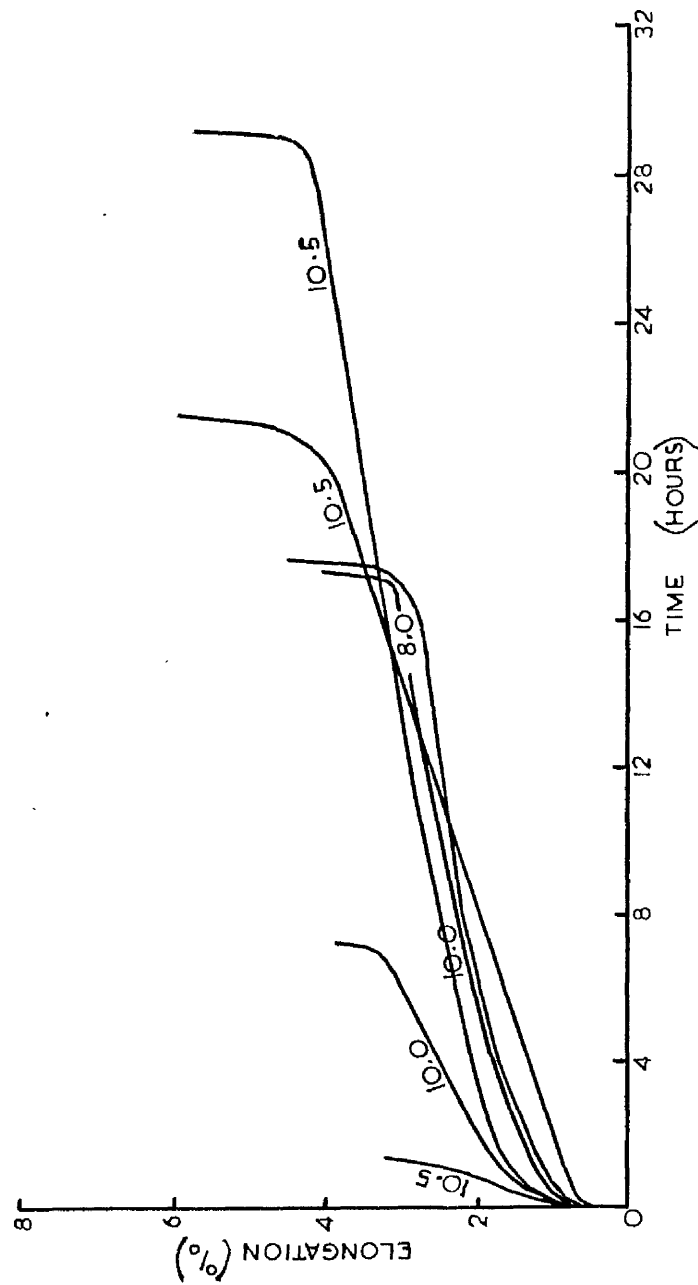
Creep Curves at 700°C.

Fig. 17

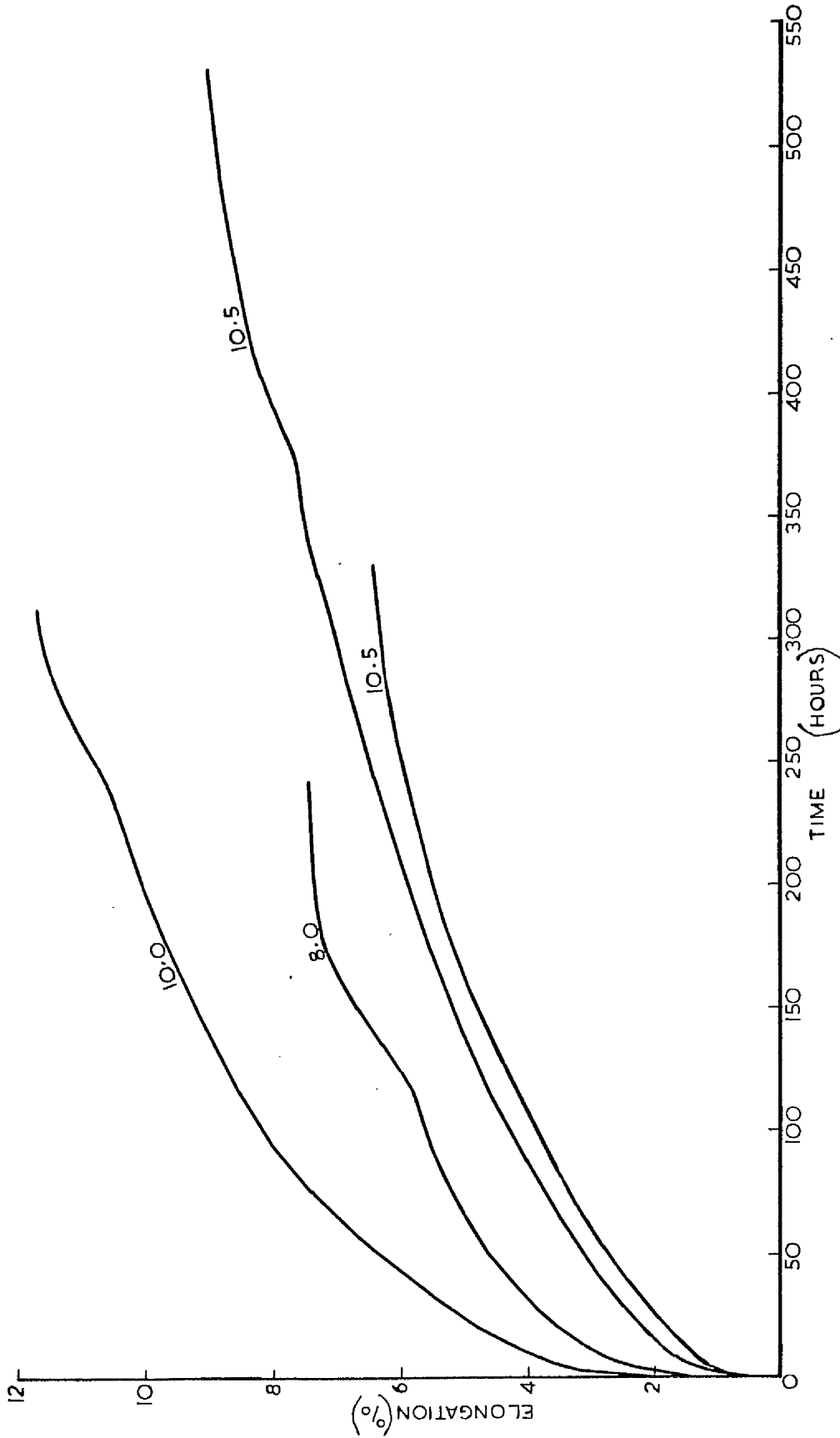


Creep Curves at 950°C and Low Stress in Vacuum. Fig.18

STRESS IN N/mm² MARKED ABOVE EACH CURVE.

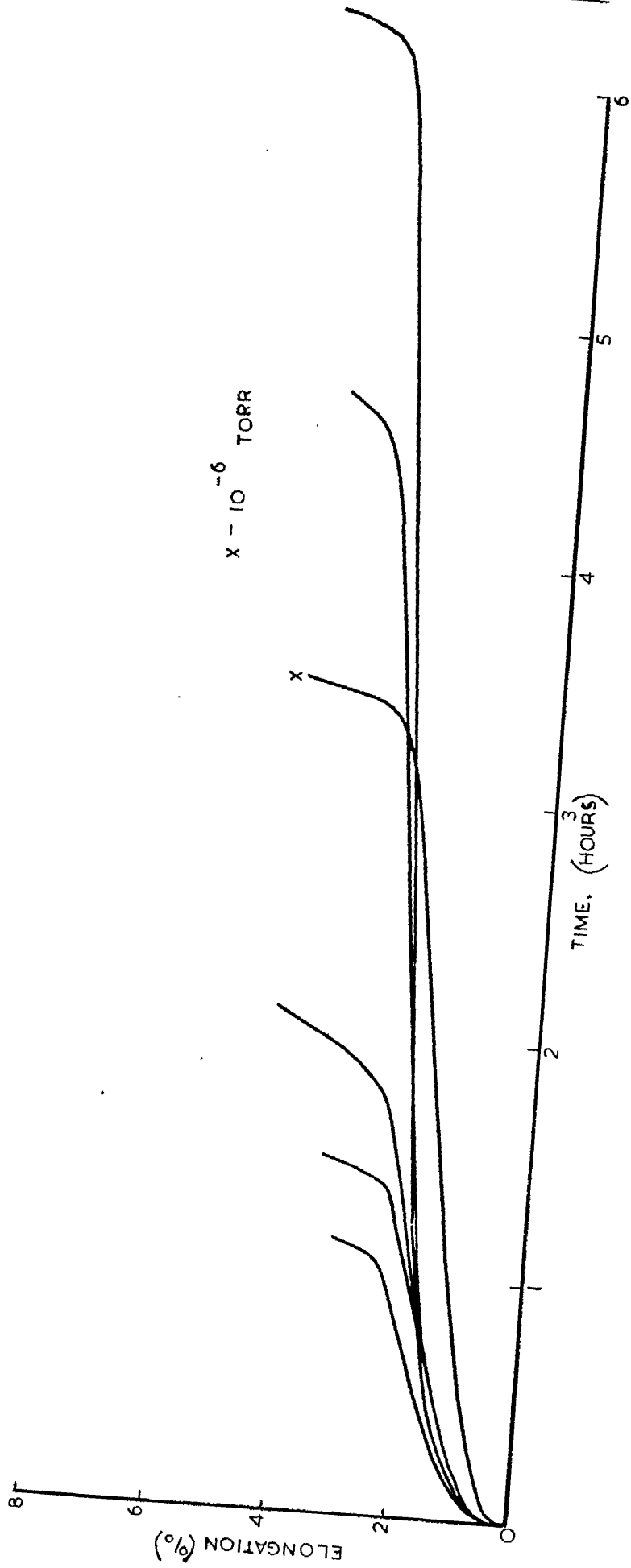


STRESS IN N/mm² MARKED ABOVE EACH CURVE.

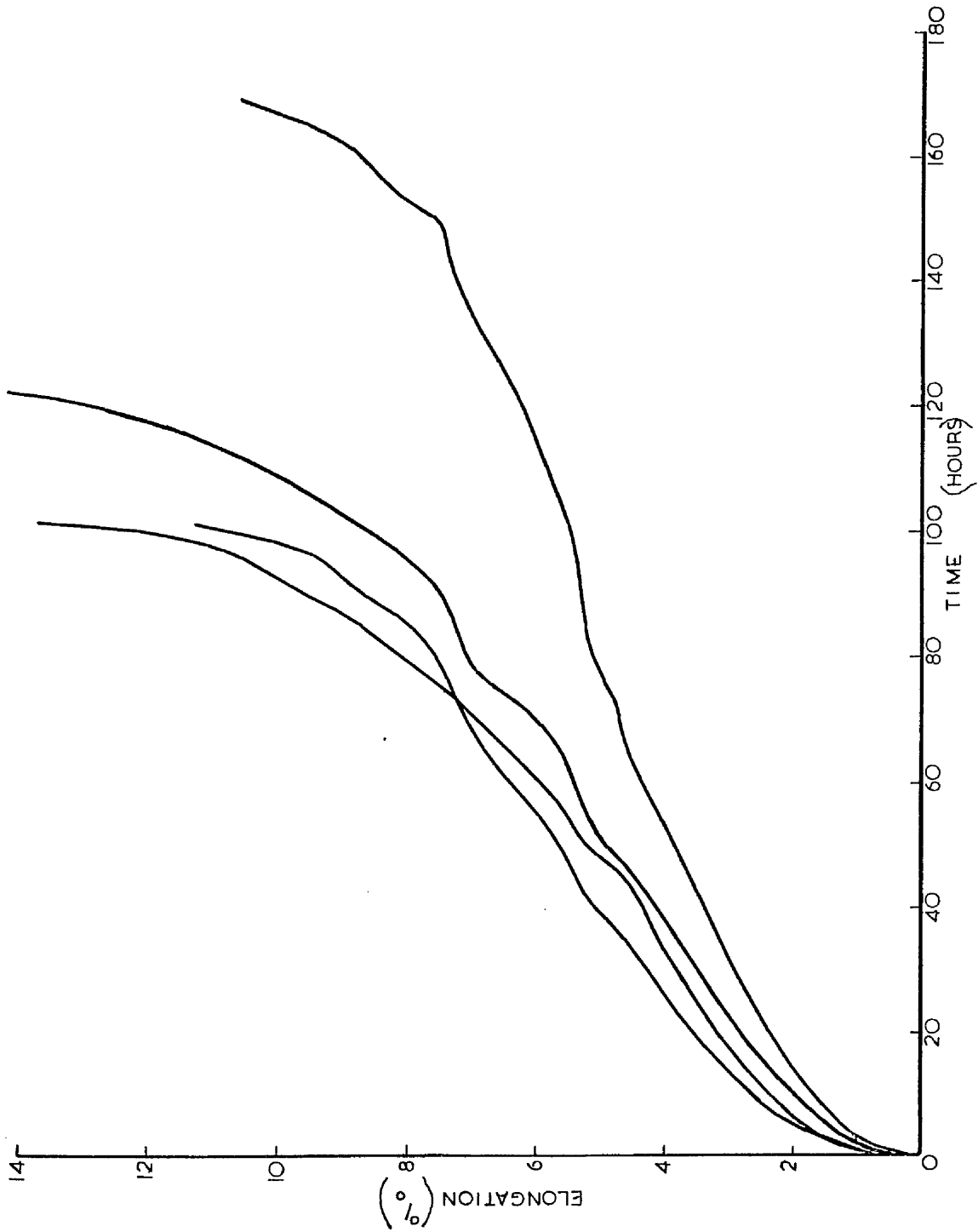


Creep Curves at 950°C and 11.0N/mm² in Vacuum.

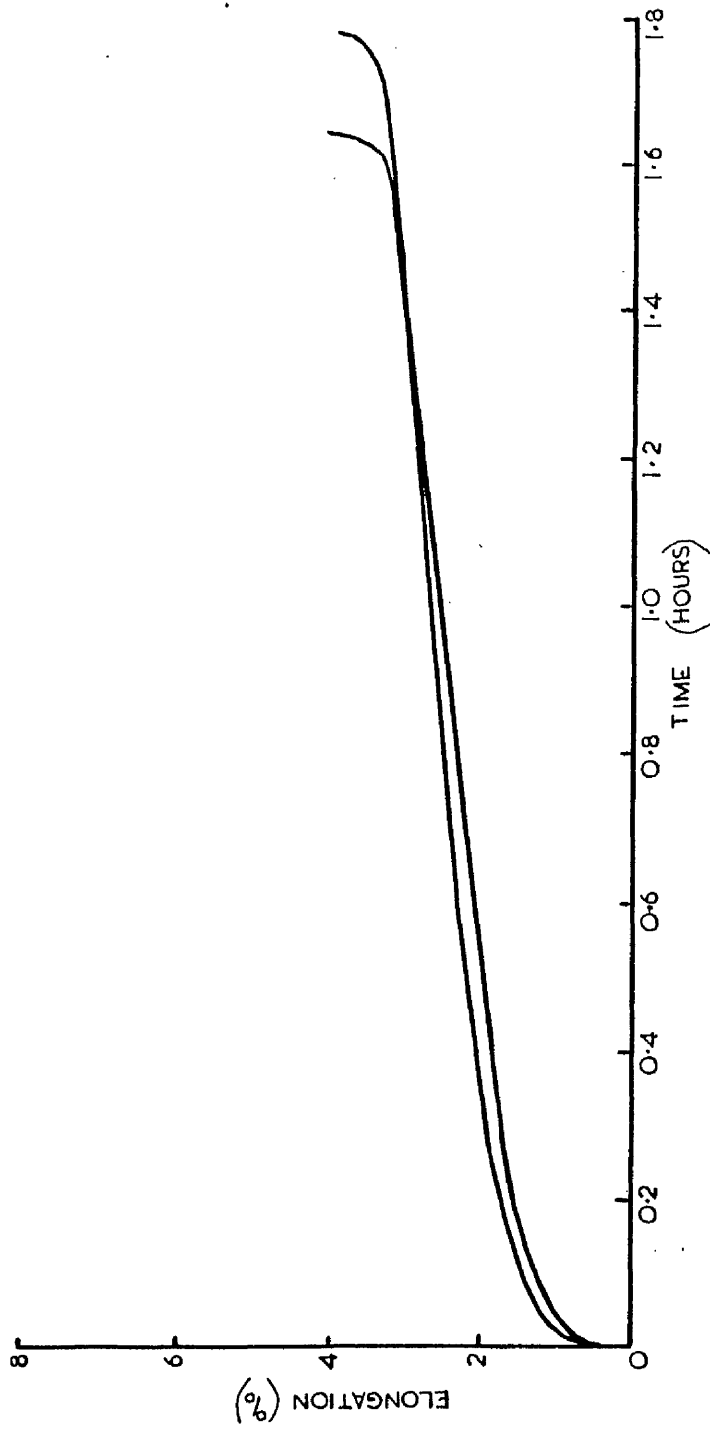
Fig.20



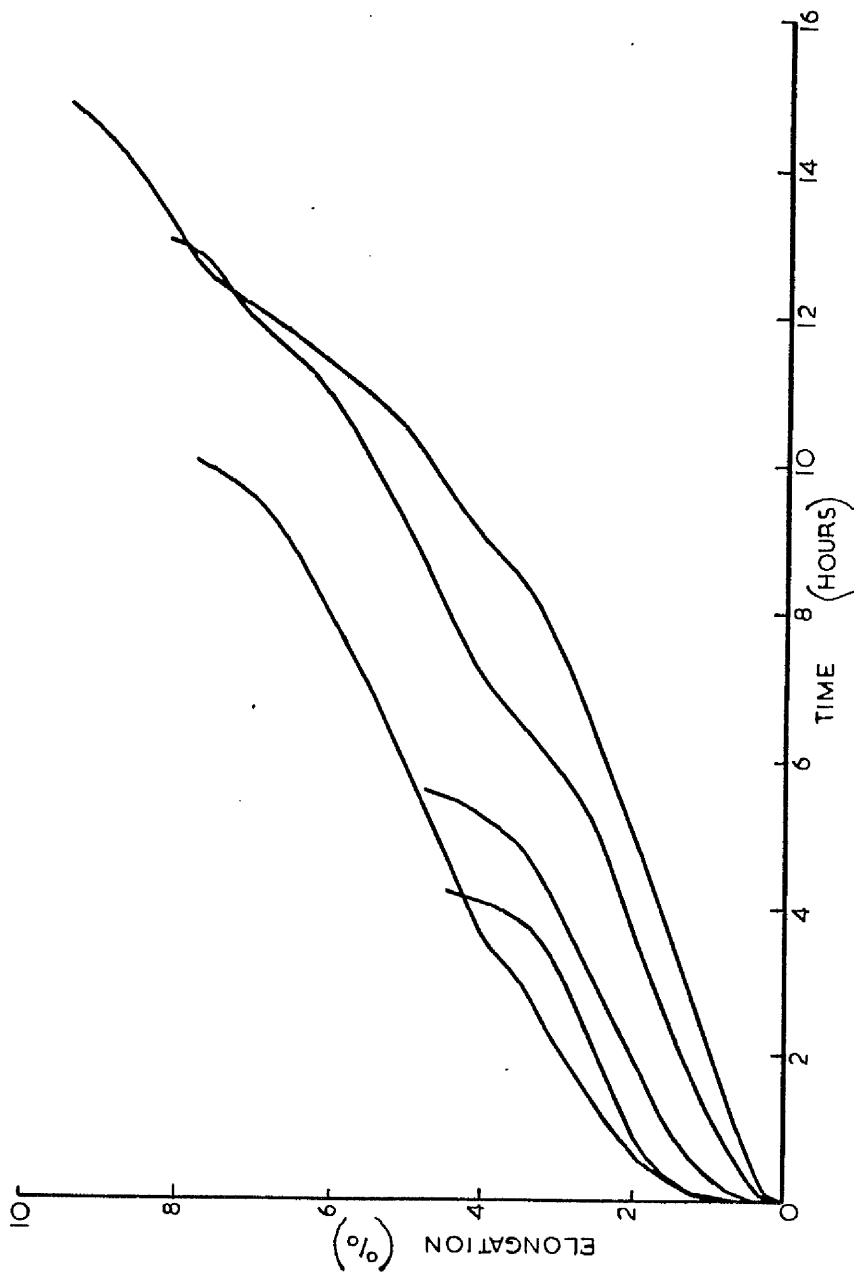
Creep Curves at 950°C and 11.0N/mm² in Oxygen. Fig. 21.



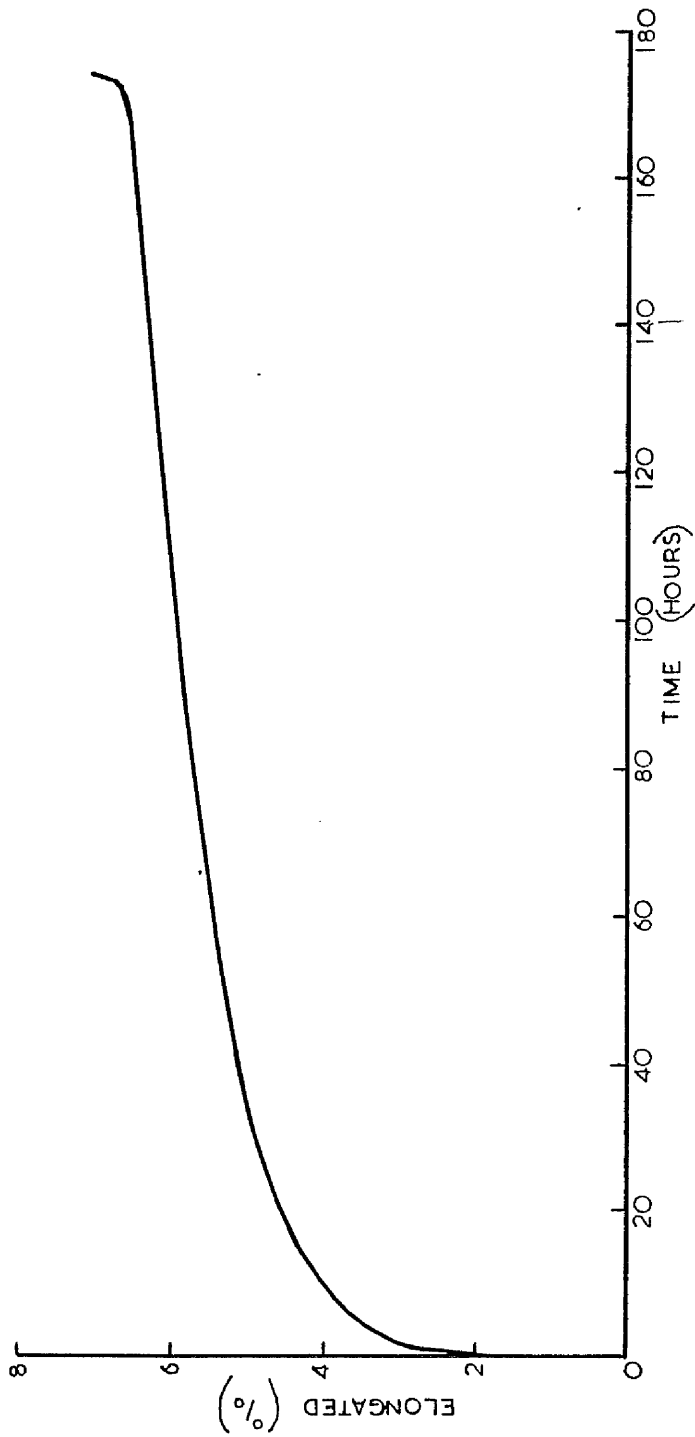
Creep Curves at 950°C and 12.0 N/mm² in Vacuum. Fig. 22.

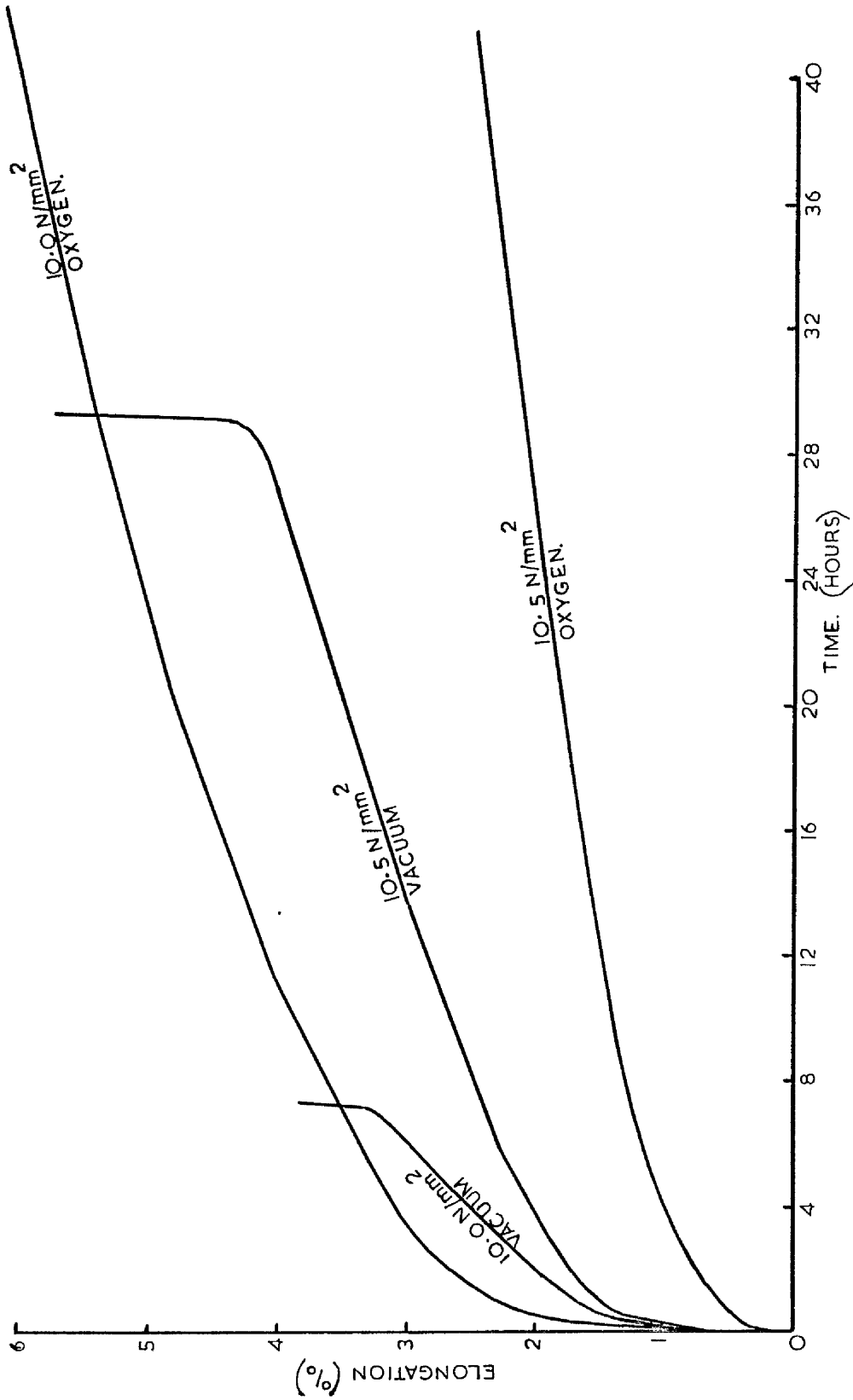


Creep Curves at 950°C and 12.0 N/mm² in Oxygen. Fig. 23.

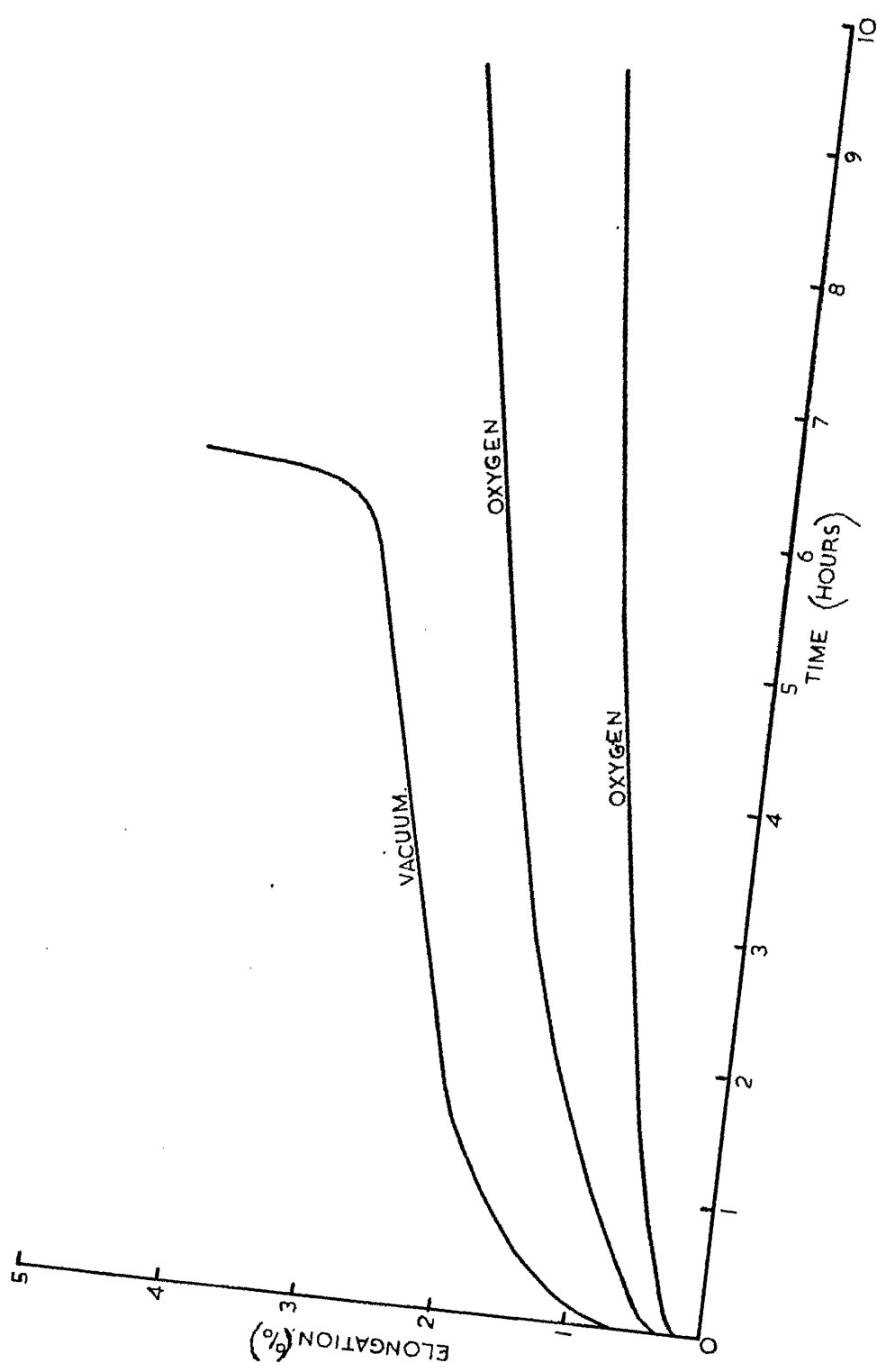


Creep Curve at 950°C and 12.0N/mm² in Oxygen. Fig. 24.

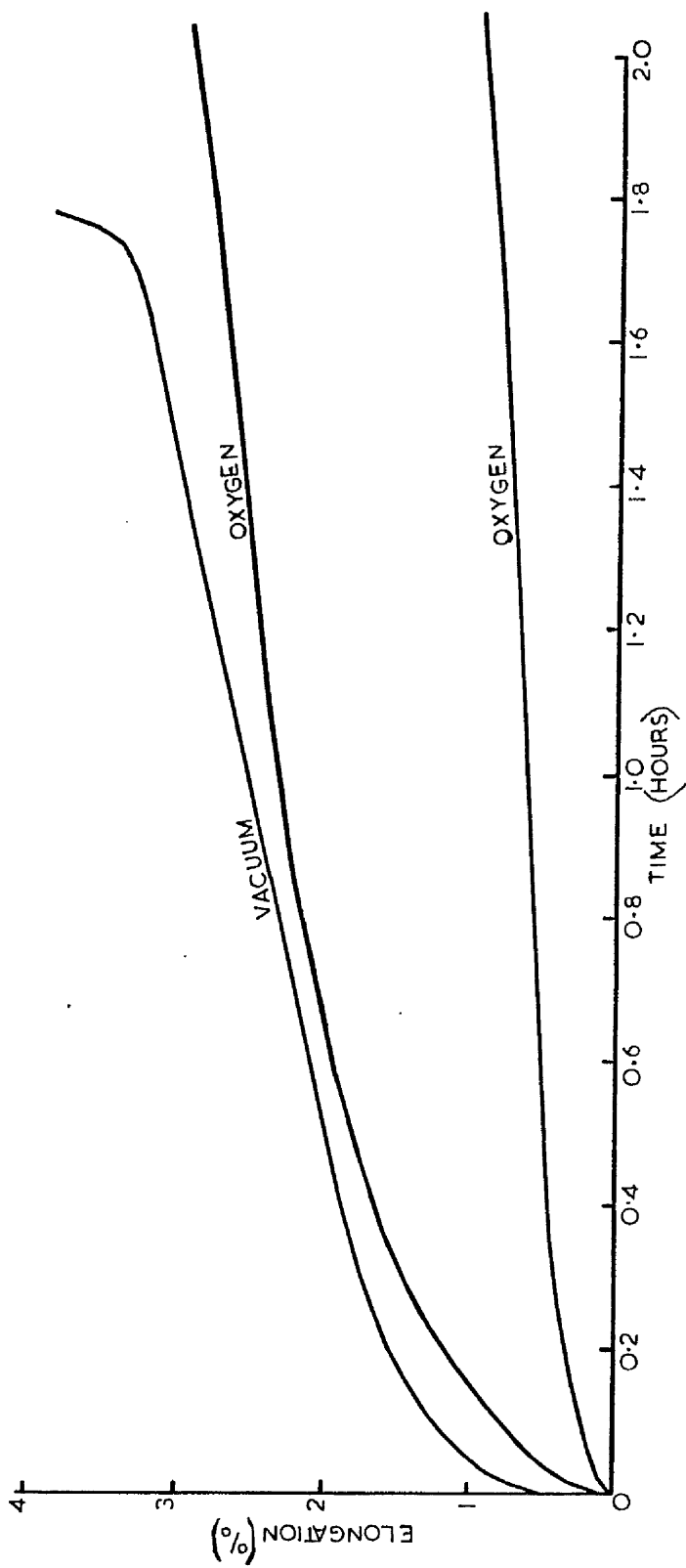




Early Stages of Creep at 950°C and 11.0 N/mm² Fig.26

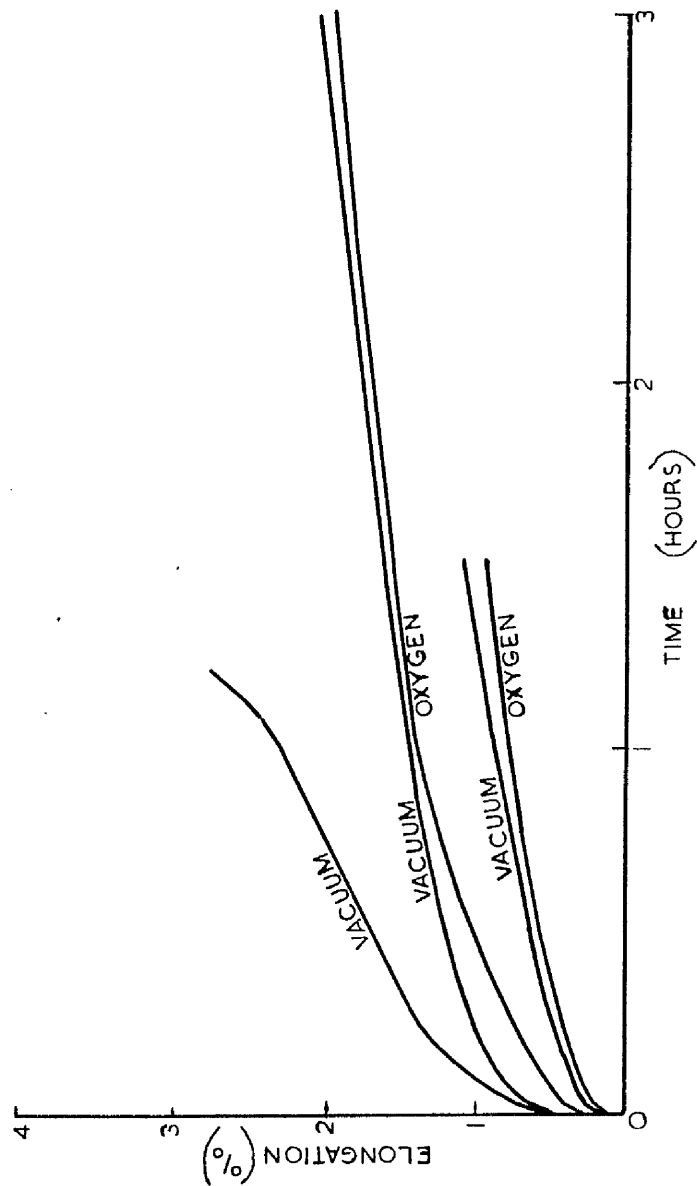


Early Stages of Creep at 950°C and 12.0 N/mm². Fig.27



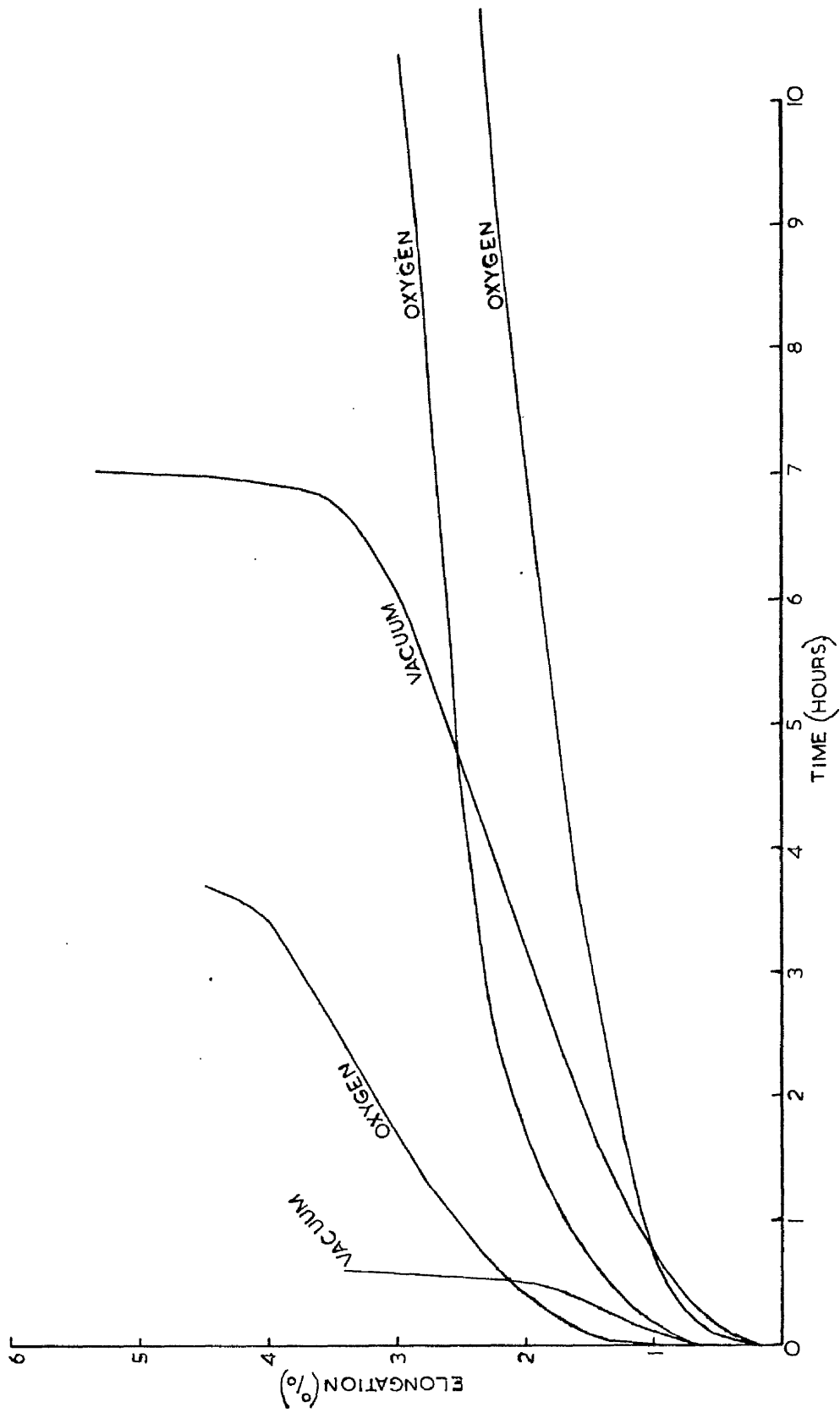
Interrupted Creep at 950°C and 11.0N/mm²

Fig. 28

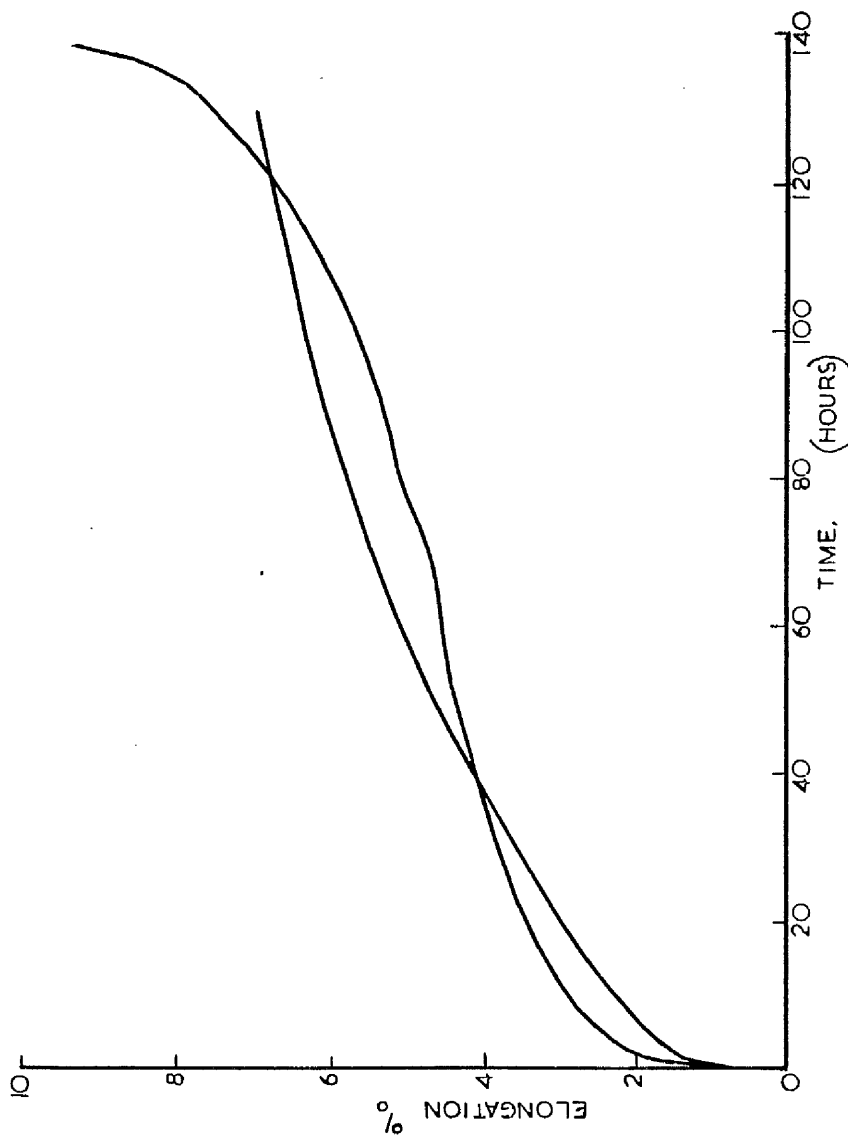


Creep of Pre Oxidised Nickel
at 950°C and 12.0 N/mm²

Fig. 29

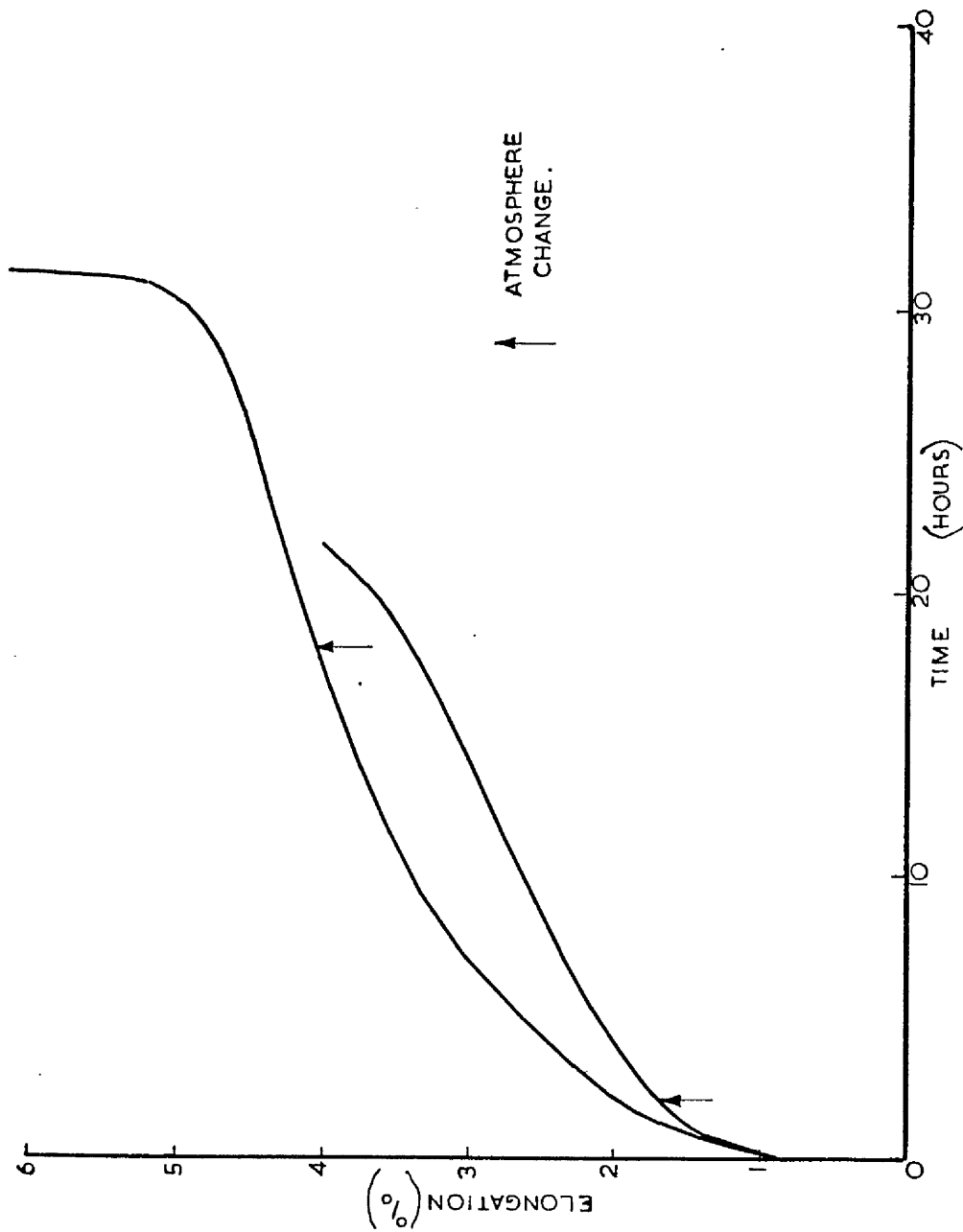


Creep of Pre Oxidised Nickel at 950°C Fig.30.
and 12·0N/mm² in oxygen.

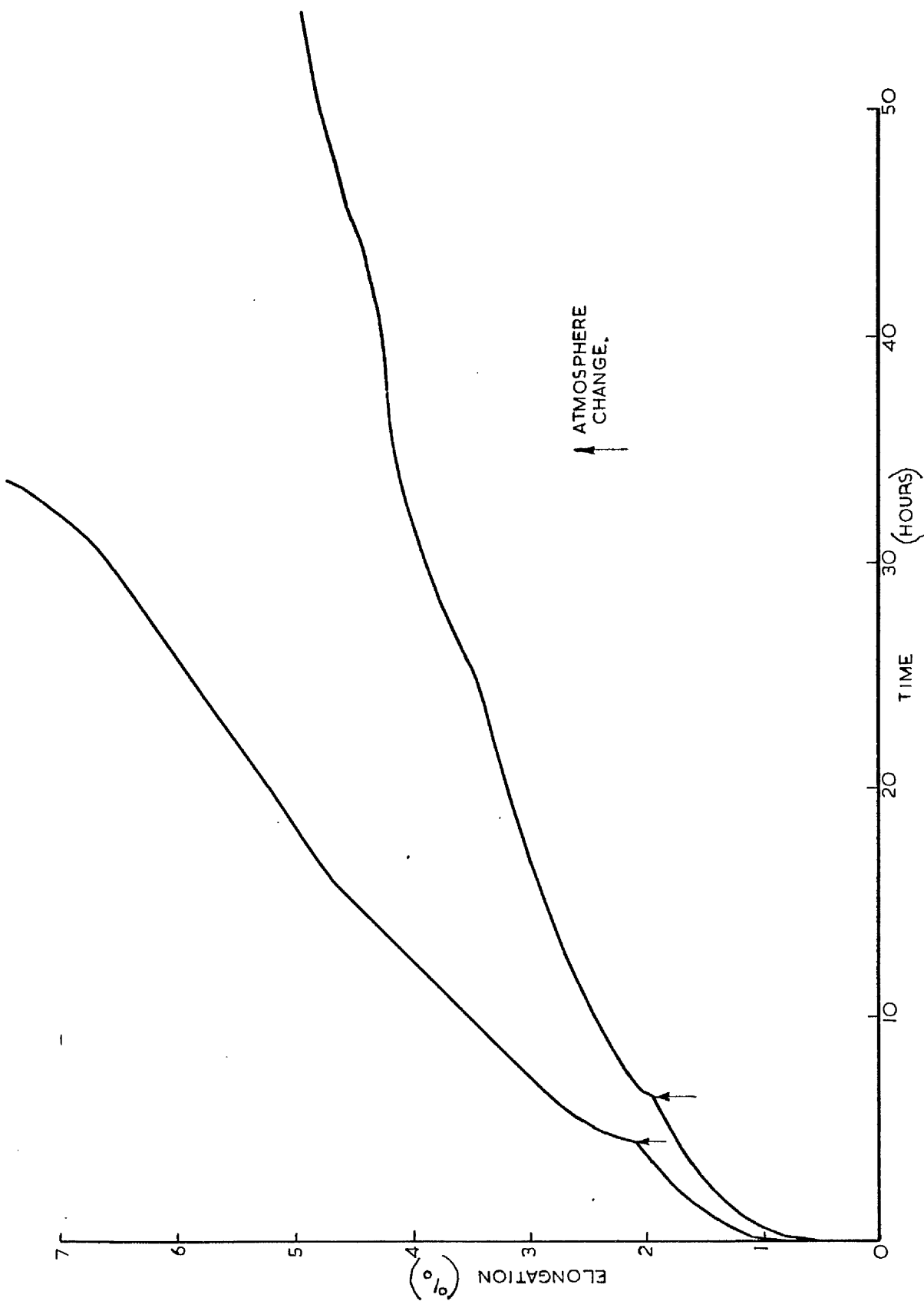


Creep of Nickel at 950°C and 10·0N/mm²
Oxygen Then Vacuum.

Fig. 31



Creep of Nickel at 950°C and 10.0N/mm^2 Fig.32
Vacuum then Oxygen.



Creep of Nickel at 950°C and 11.0N/mm^2
with Atmosphere change.

Fig.33

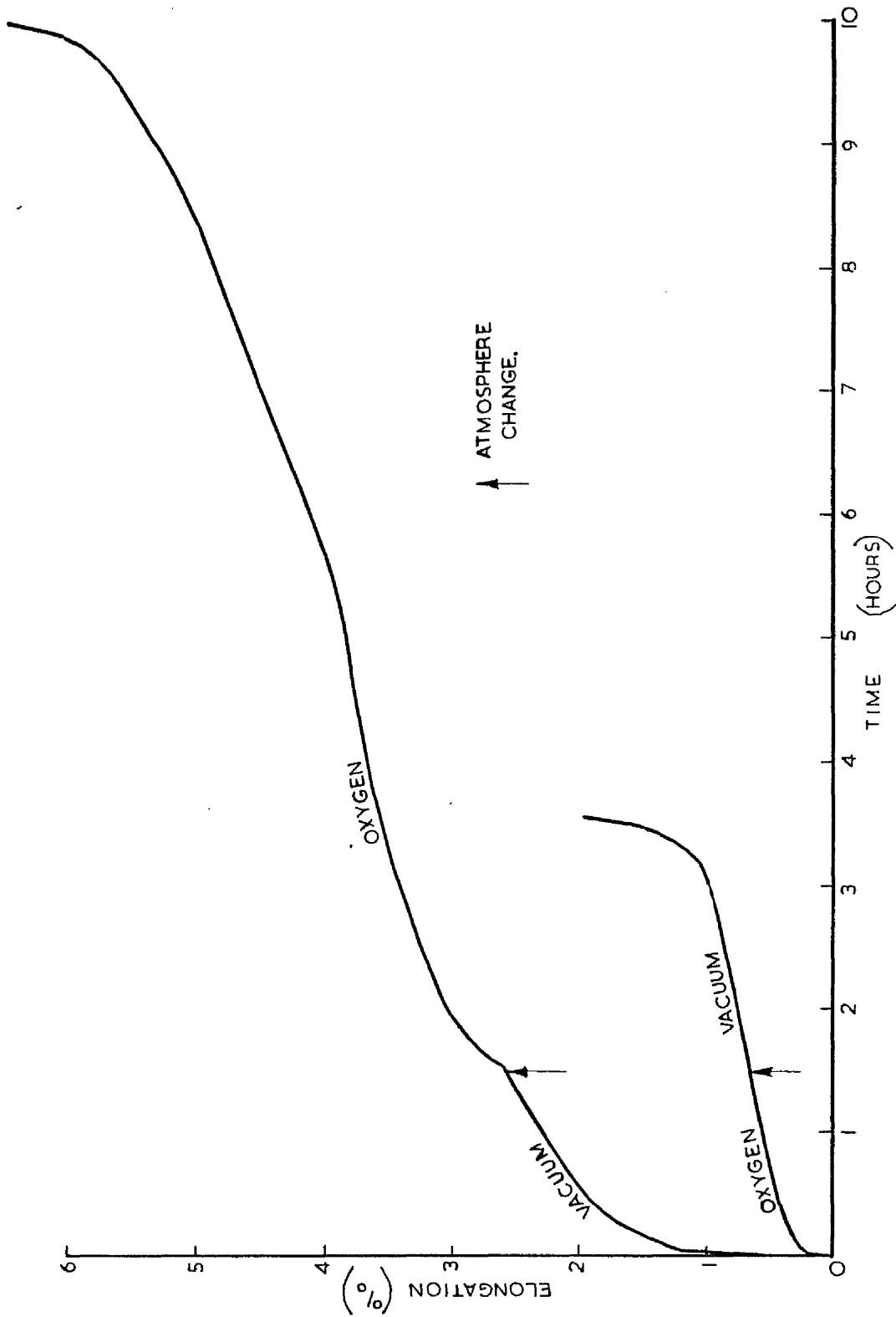


Fig. 34. Annealed Specimen after Creep Testing.
x 2 Oxygen. 950°C. 12 N/mm². 173 hours.



Fig. 35. Pre Oxidised Specimen after Creep Testing.
x 2 Oxygen. 950°C. 12 N/mm². 127.5 hours.



Fig. 36. Failed Specimen in Creep Rig.
x 2.5 Oxygen. 950°C. 12 N/mm². 10 hours.



Fig. 37. Voids near Specimen Surface.
x 90 Oxygen. 700°C 23 N/mm². 13.7 hours, R.L.



Fig. 38. Voids near Fracture Surface in Specimen Centre.
x 90 Oxygen. 700°C. 30 N/mm². 8.7 hours, R.L.

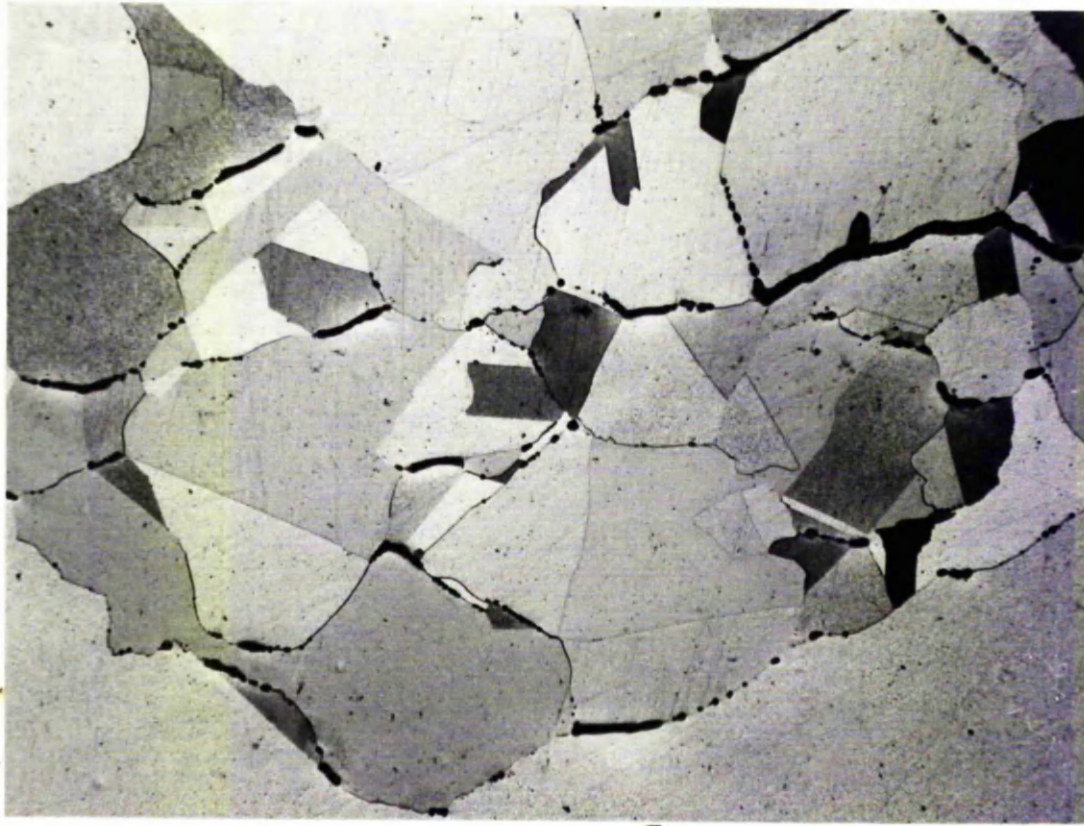


Fig. 39. Voids in Specimen Centre.
x 90 Vacuum. 700°C. 25 N/mm². 8.9 hours, R.L.

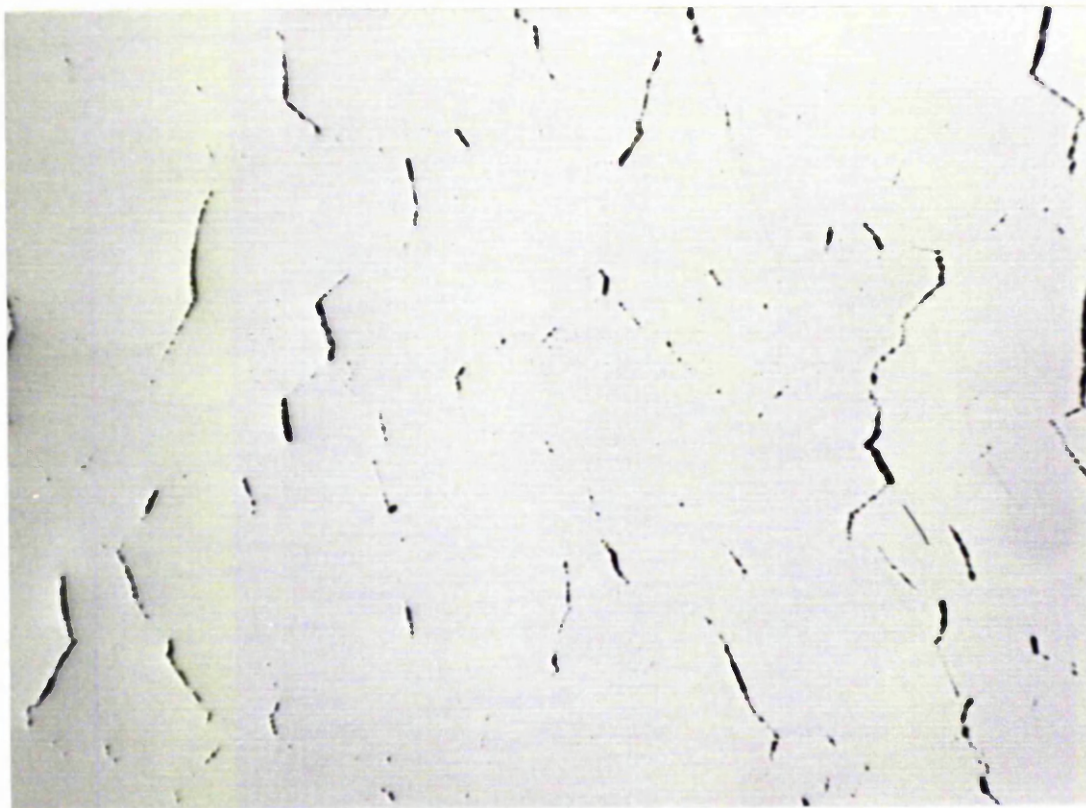


Fig. 40. Voids near Specimen Surface.
x 90 Vacuum. 700°C. 23 N/mm². 25.5 hours, R.L.

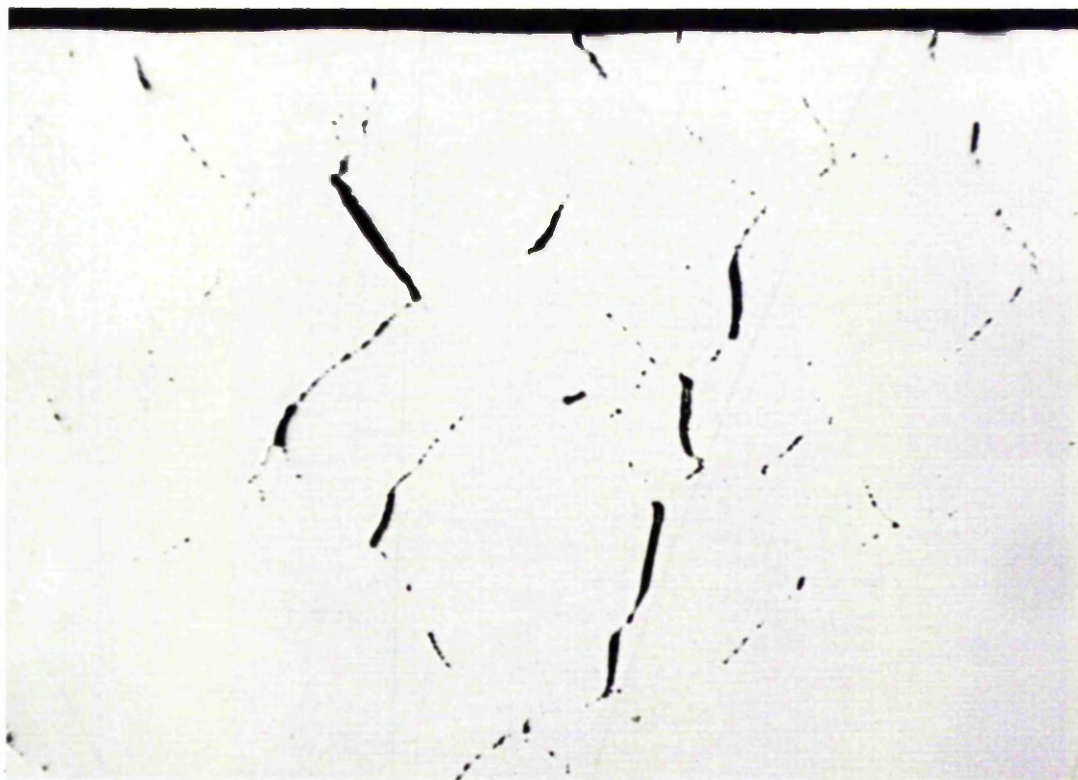


Fig. 41. Fracture Surface and Adjacent Cracking.
x 90 Vacuum. 700°C. 23 N/mm². 25.5 hours, R.L.

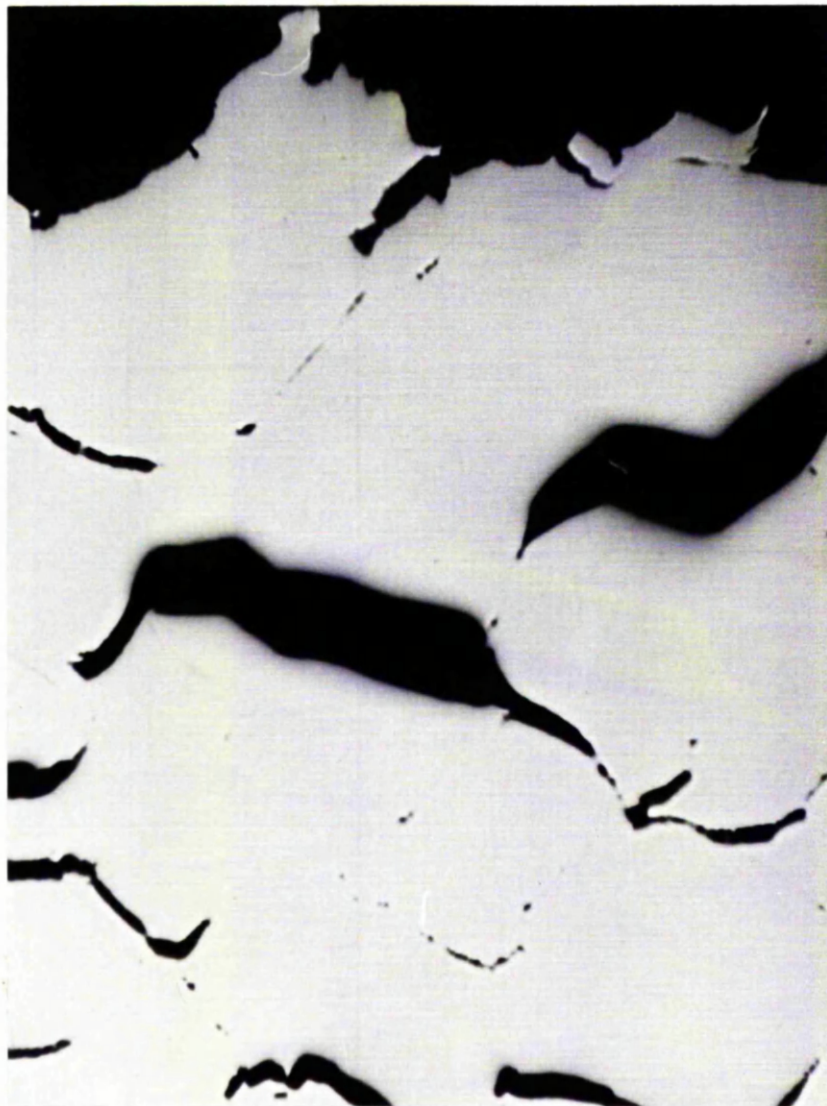


Fig. 42. Typical Grain Boundary Void Chain.
x 90 Vacuum. 950°C. 11 N/mm². 0.1 hours, R.L.

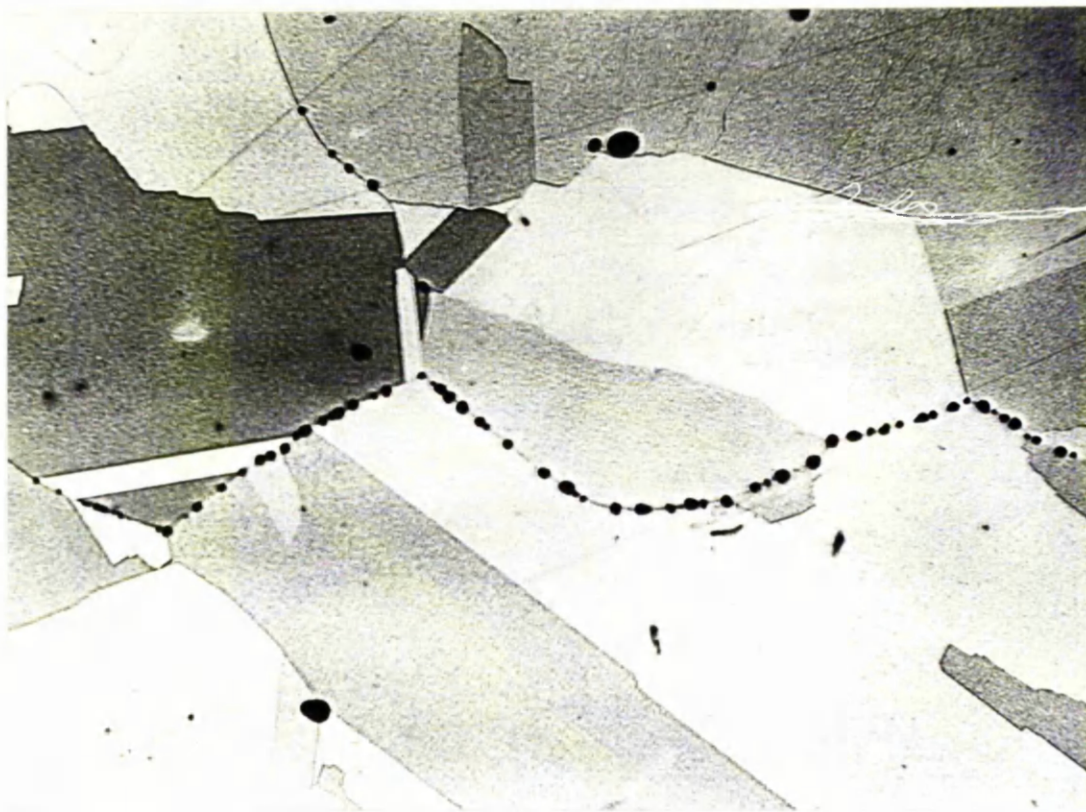
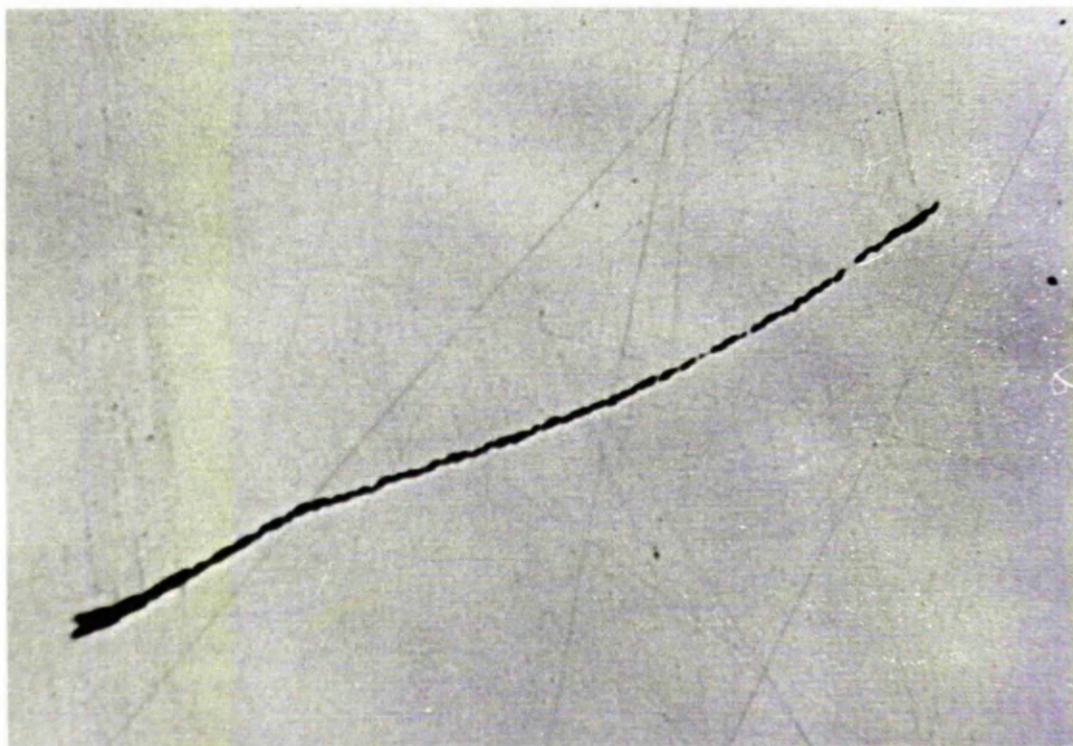


Fig. 43. Coalescence of Grain Boundary Void.
x 170 Vacuum. 950°C. 11 N/mm². 3.0 hours.





With Compliments

Department of Mechanical Engineering,
The University,
Glasgow, G12 8QQ.

Fig. 44. Serrations on Crack Faces.
x 170 Vacuum. 950°C. 10.5 N/mm². 21.5 hours, R.L.

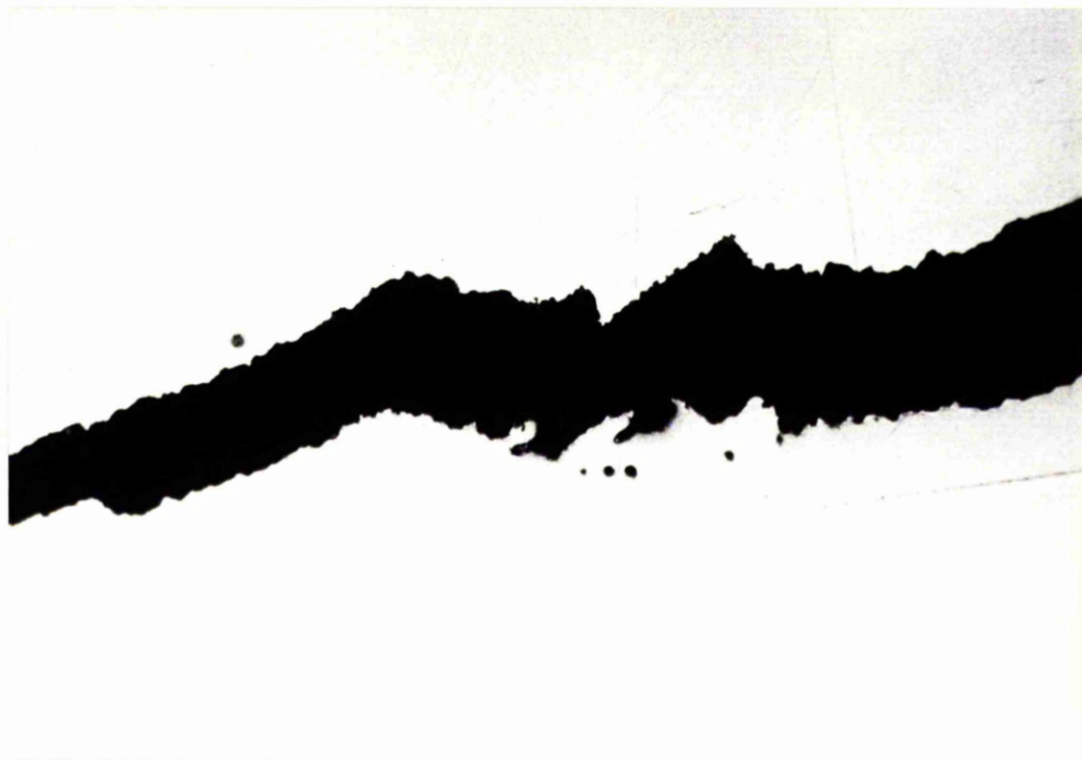


Fig. 45. Serrations on Fracture Surface.
x 170 Vacuum. 950°C. 11 N/mm². 2.1 hours, R.L.



Fig. 46. Void Formation near Specimen Surface.
x 175 Oxygen. 950°C. 11 N/mm². 1.5 hours.

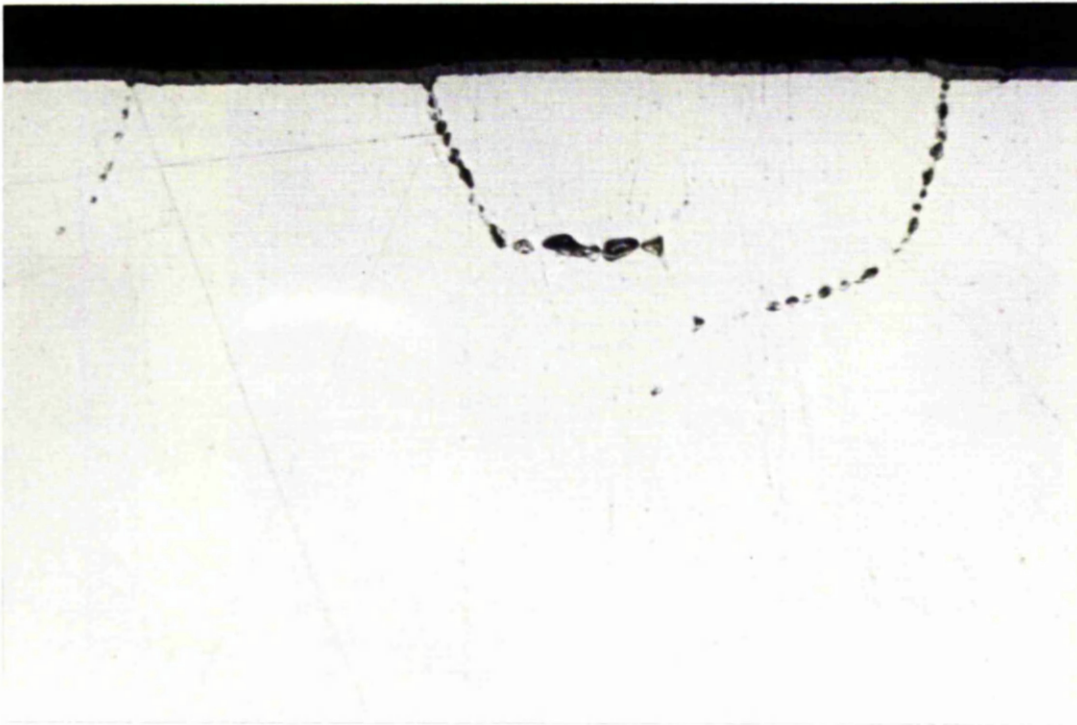


Fig. 47. Void Formation near Specimen Surface.
x 90 Oxygen. 950°C. 12 N/mm². 5.6 hours, R.L.

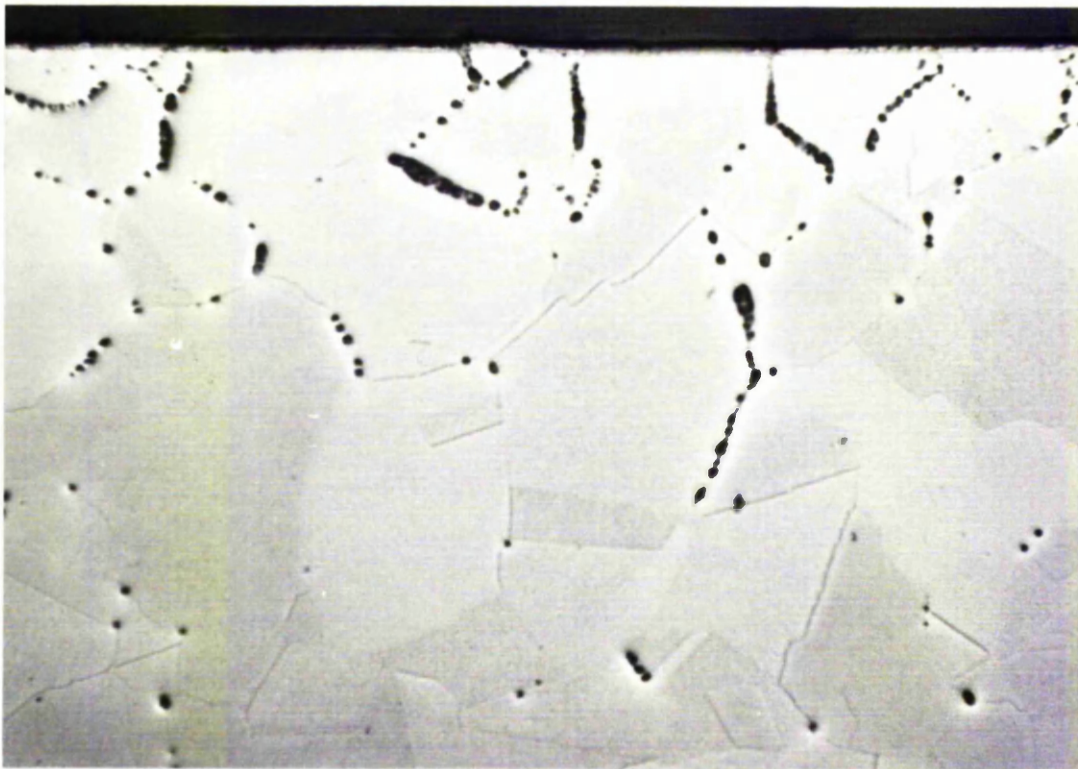


Fig. 48. Void Distribution across Specimen.
x 30 Oxygen. 950°C. 12 N/mm². 13 hours, R.L.



↔





With Compliments

Department of Mechanical Engineering,
The University,
Glasgow, G12 8QQ.

Fig. 49. Voids near Specimen Surface.
x 110 Oxygen. 950°C. 11 N/mm². 100 hours, R.L.



Fig. 50. Voids in Centre of Specimen.
x 90 Oxygen. 950°C. 11 N/mm². 100 hours, R.L.

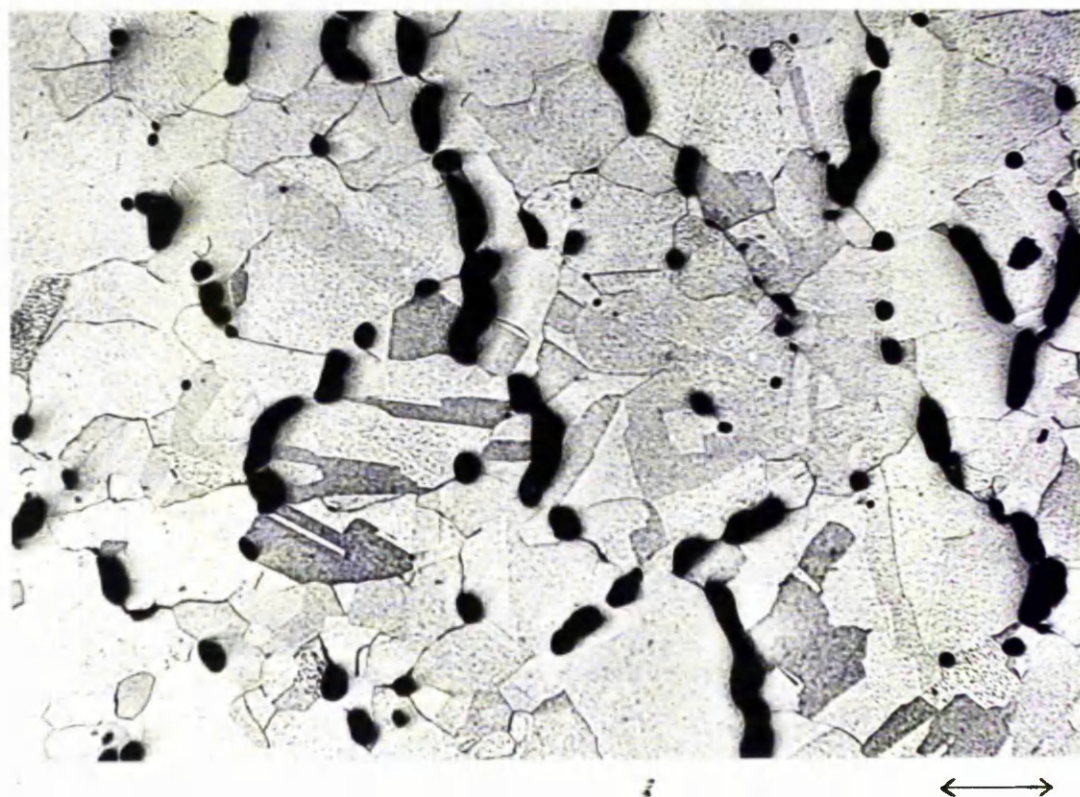


Fig. 51. Crack at Specimen Surface.
x 410 Oxygen. 950°C. 12 N/mm². 5.6 hours, R.L.

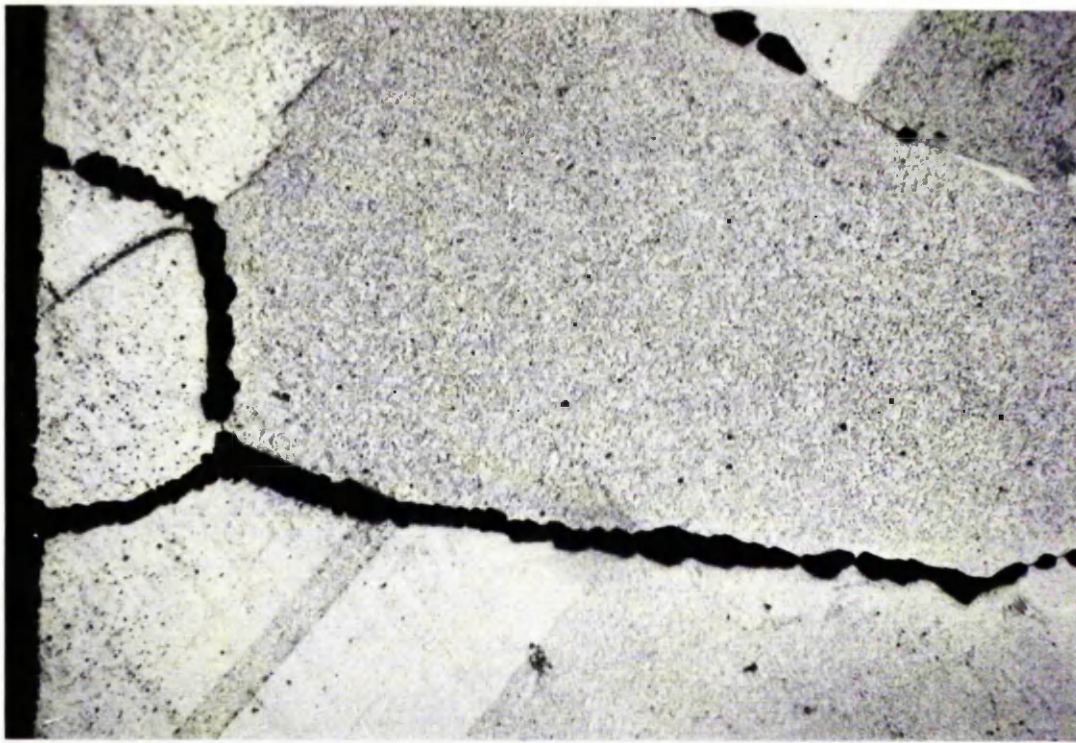


Fig. 52. Crack System near Specimen Surface.
x 40 Oxygen. 950°C. 12 N/mm². 24.1 hours.



Fig. 53. Crack System in Specimen Centre.
x 45 Oxygen. 950°C. 12 N/mm². 24.1 hours.



Fig. 54. Crack Formation at Specimen Surface.
x 90 Oxygen. 950°C. 11 N/mm². 100 hours, R.L.



Fig. 55. Fracture Surface.
x 90 Oxygen. 950°C. 11 N/mm². 101 hours, R.L.

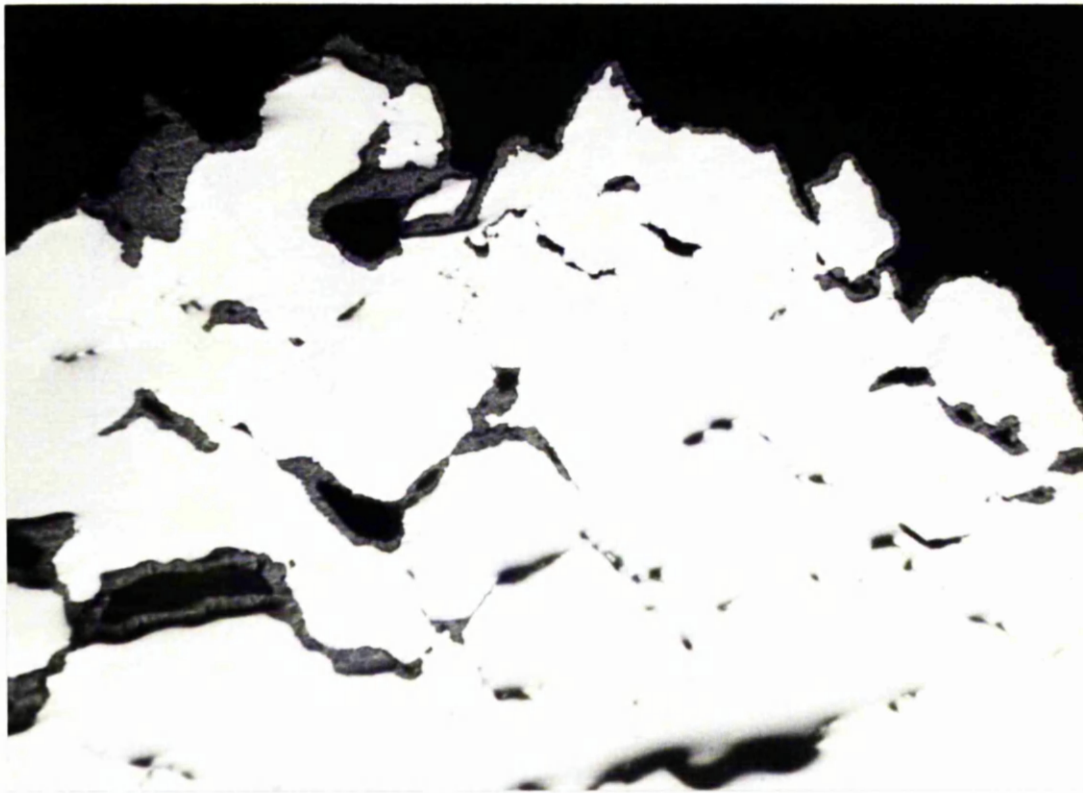


Fig. 56. Cracks and Voids at Specimen Surface.
x 175 Oxygen. 950°C. 11 N/mm². 122 hours, R.L.

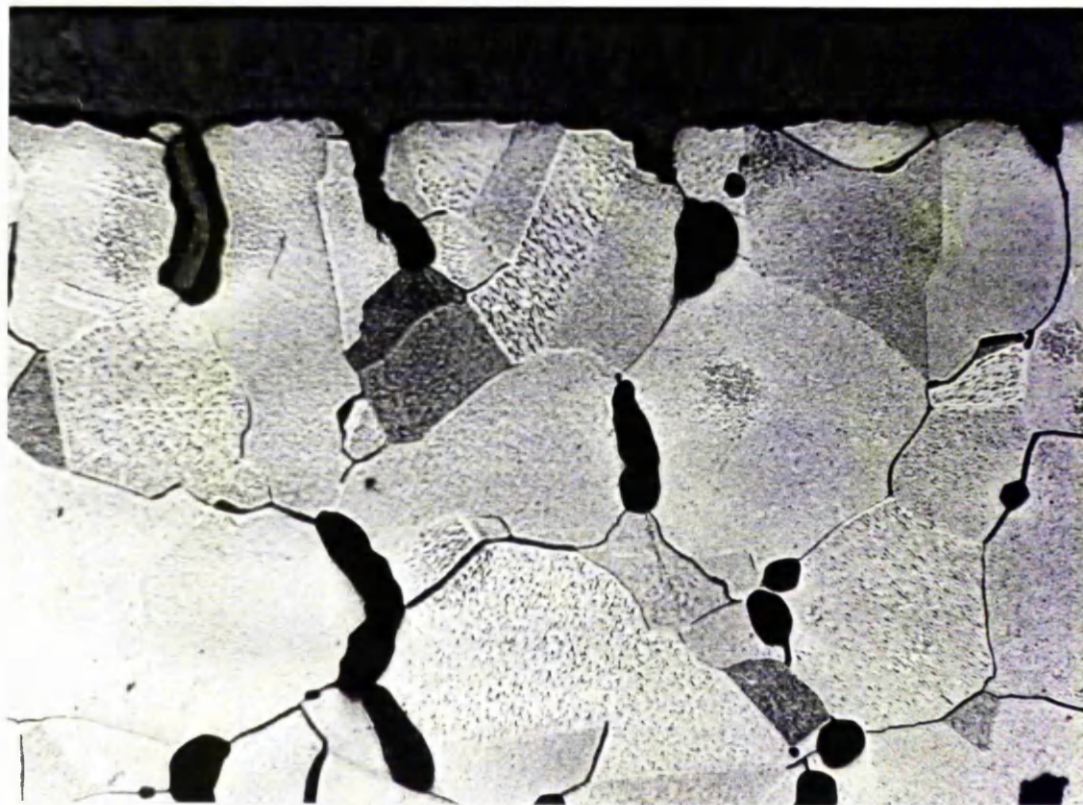


Fig. 57. Oxide Filled Crack at Specimen Surface.
x 440 Oxygen. 950°C. 11 N/mm². 122 hours, R.L.

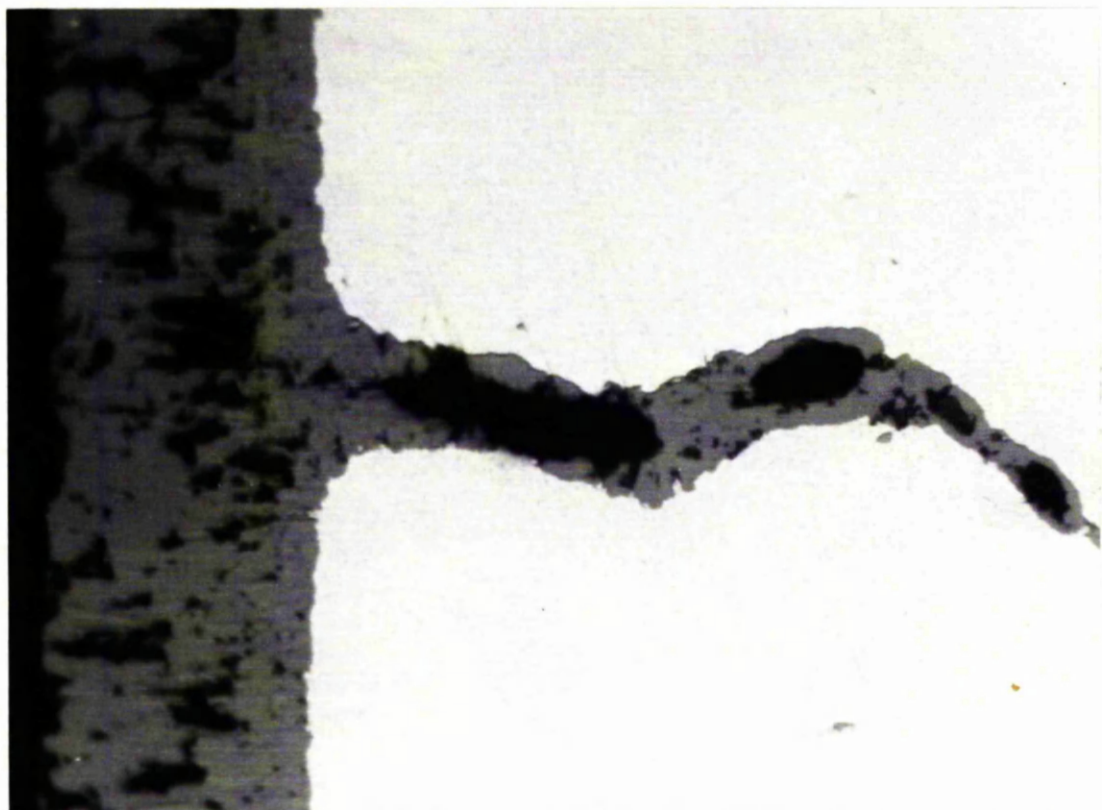


Fig. 58. Crack System at Specimen Surface.
x 90 Oxygen. 950°C. 11 N/mm². 169 hours, R.L.



Fig. 59. Void Distribution across Specimen.
x 30 Oxygen. 950°C. 10.5 N/mm². 332 hours.

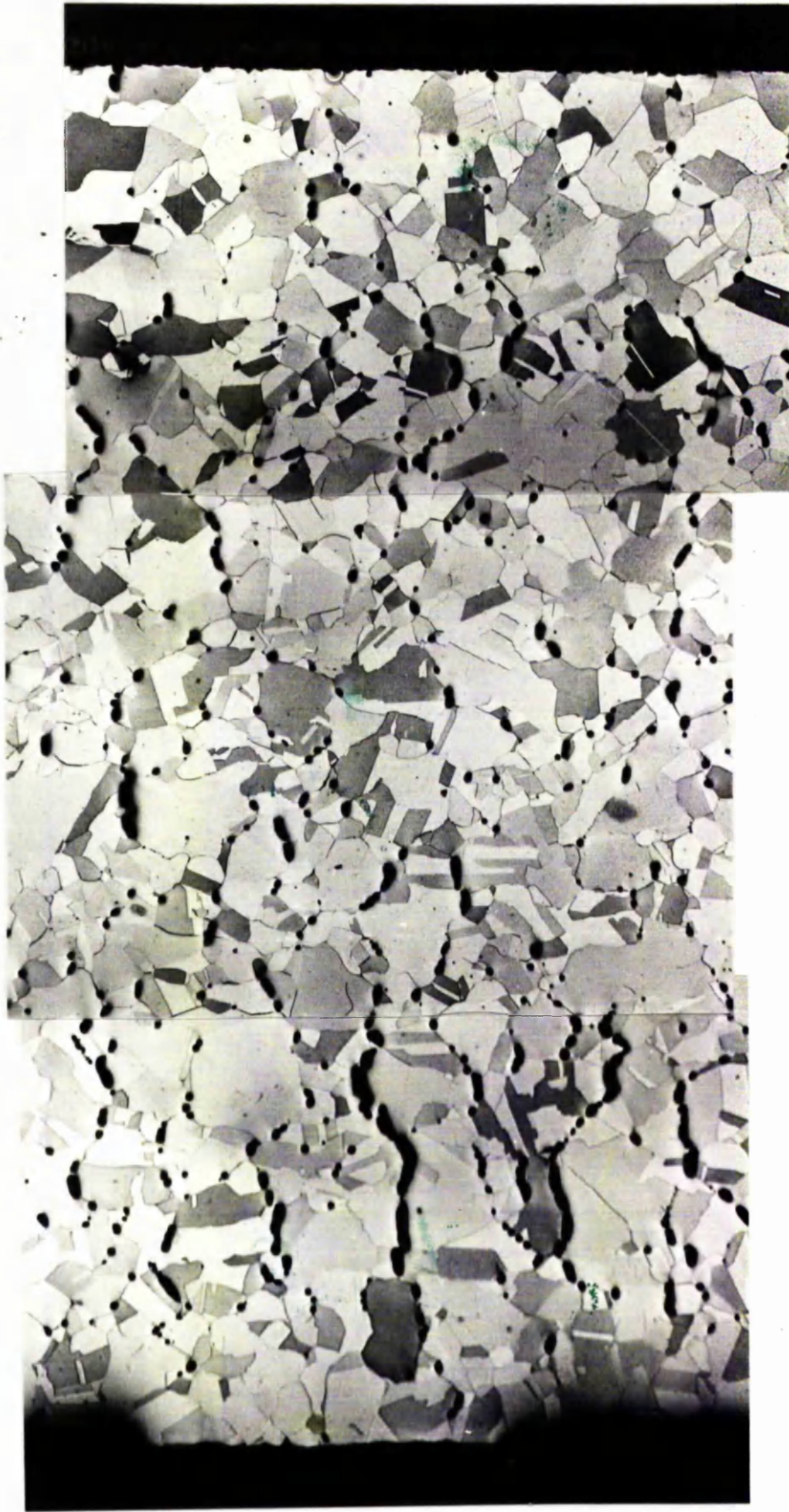


Fig. 60. Void Distribution across Specimen.
x 30 Oxygen. 950°C. 10.5 N/mm². 530 hours.

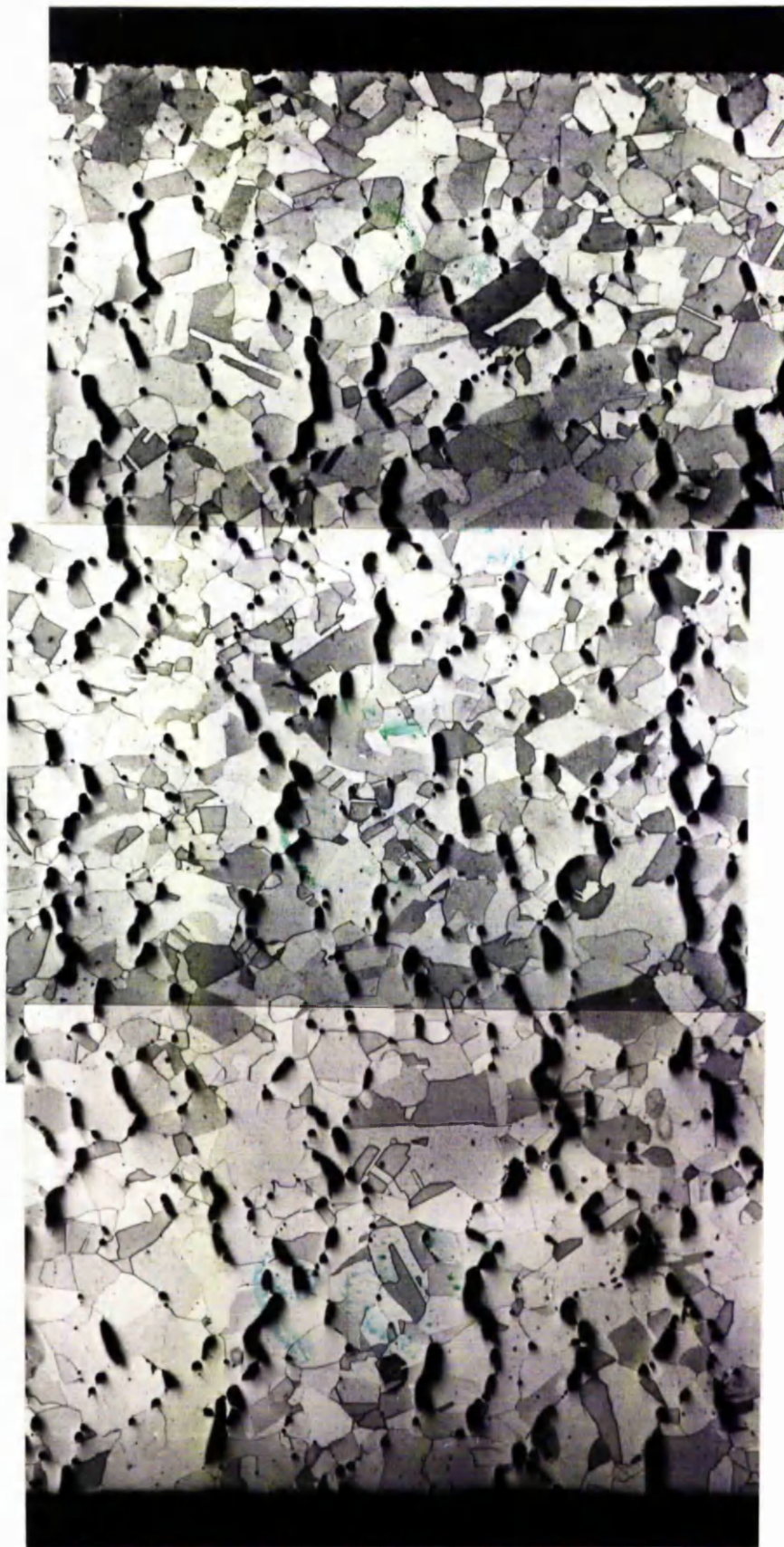


Fig. 61. Voids near Specimen Surface.
x 160 Oxygen. 950°C. Zero. 5.6 hours.

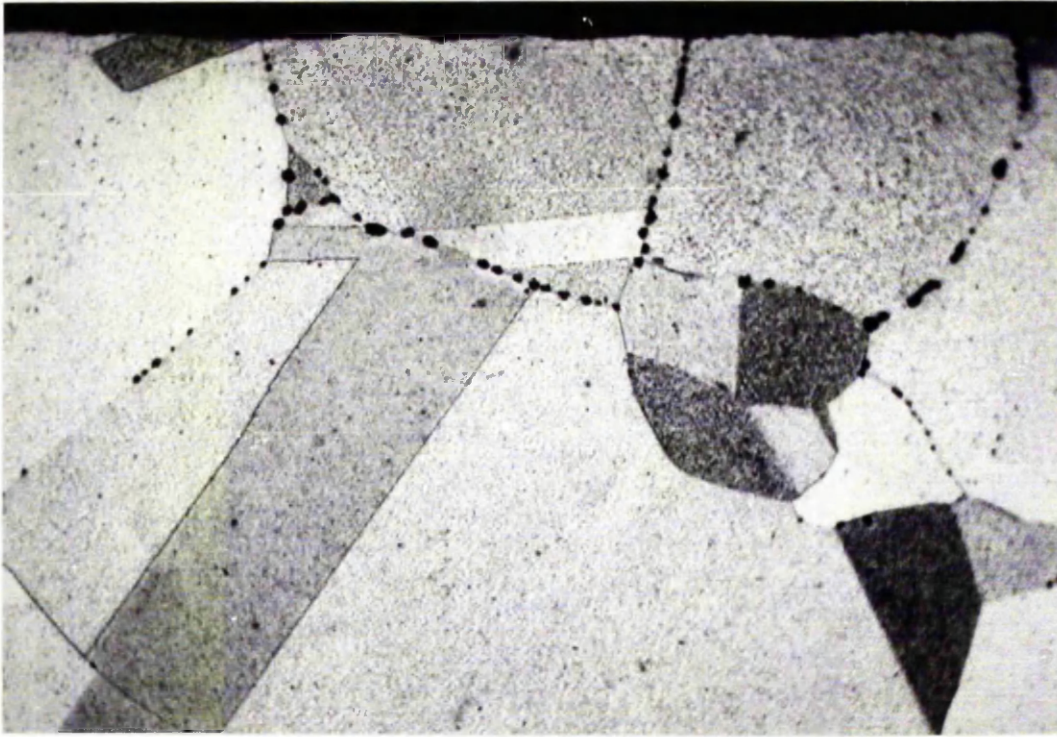


Fig. 62. Voids near Specimen Surface.
x 90 Oxygen. 950°C. Zero. 100 hours.

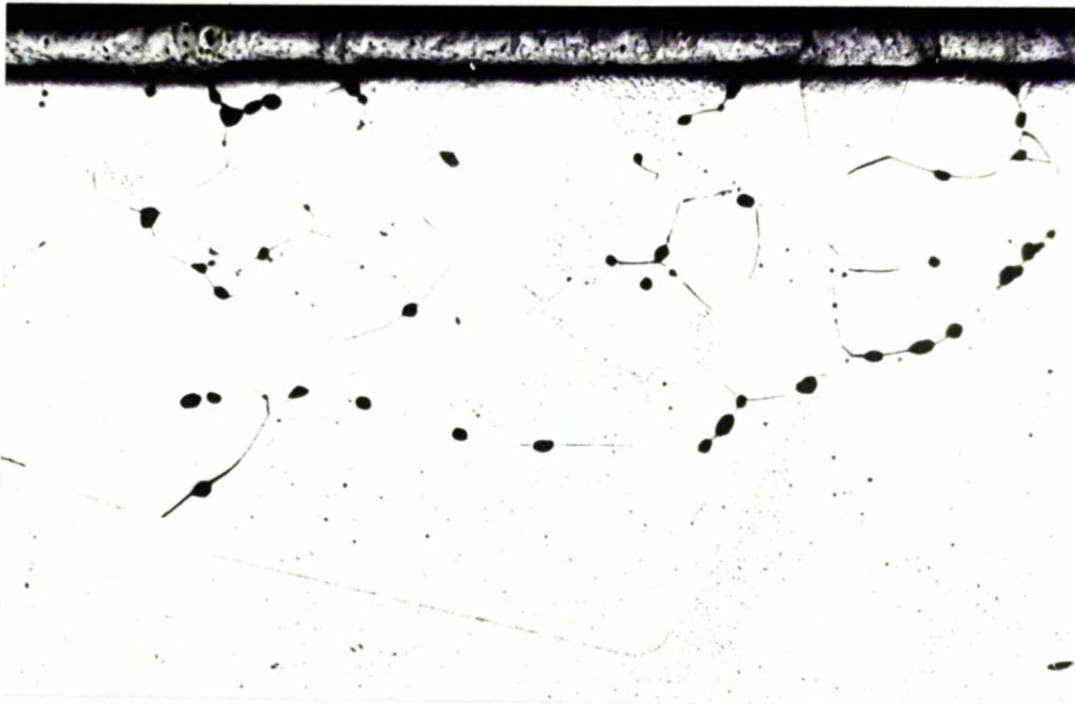


Fig. 63. Voids near Specimen Surface.
x 90 Oxygen. 950°C. Zero. 169 hours.



Fig. 64. Voids in Specimen Centre.
x 90 Oxygen. 950°C. Zero. 122 hours.

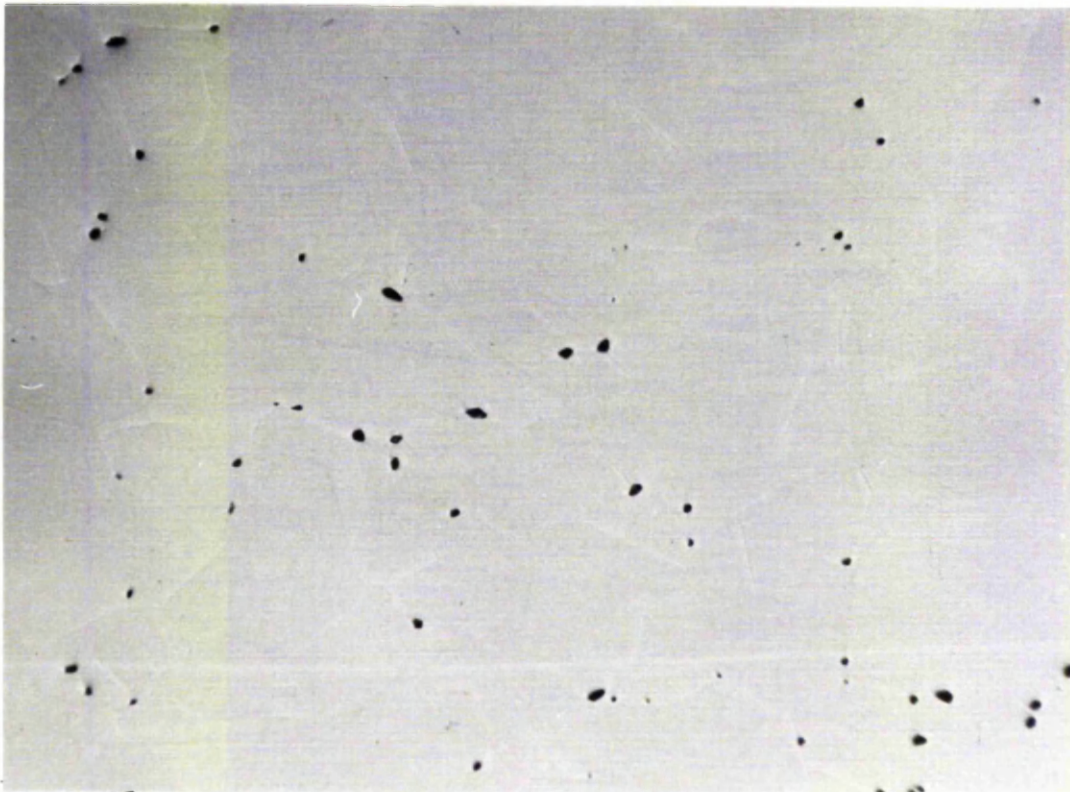


Fig. 65. Voids in Specimen Centre.
x 80. Oxygen. 950°C. Zero. 332 hours.

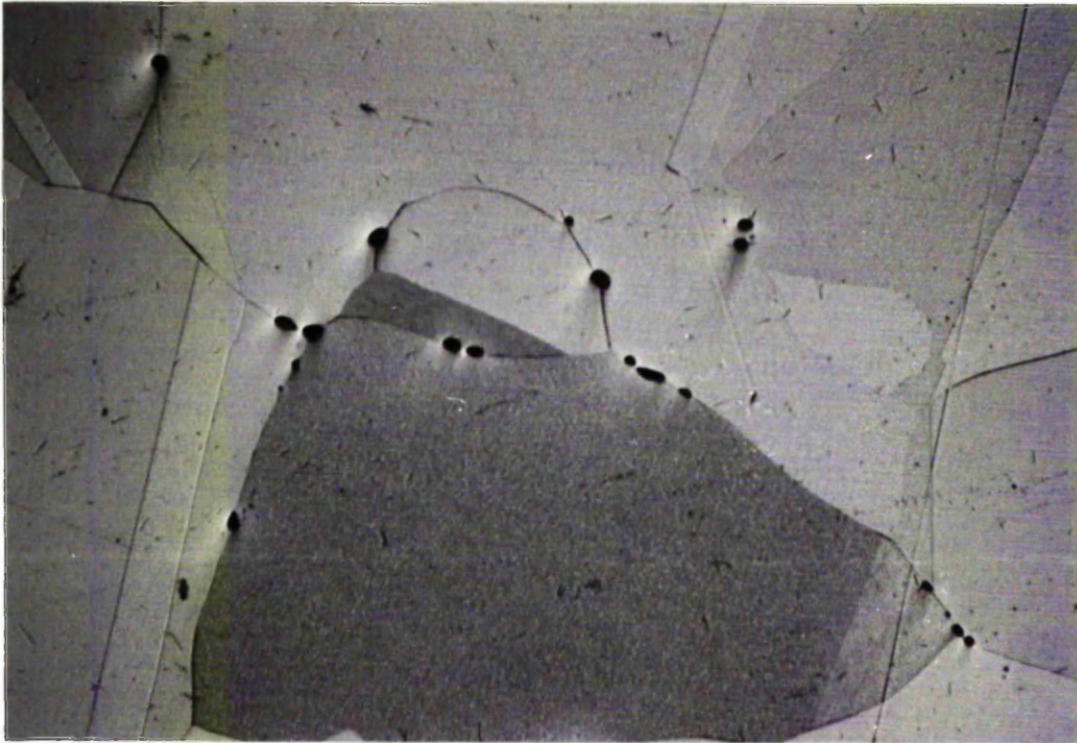


Fig. 66. Oxidation of Void Coalescence near Specimen Surface.
x 175. Oxygen. 950°C. Zero. 332 hours.

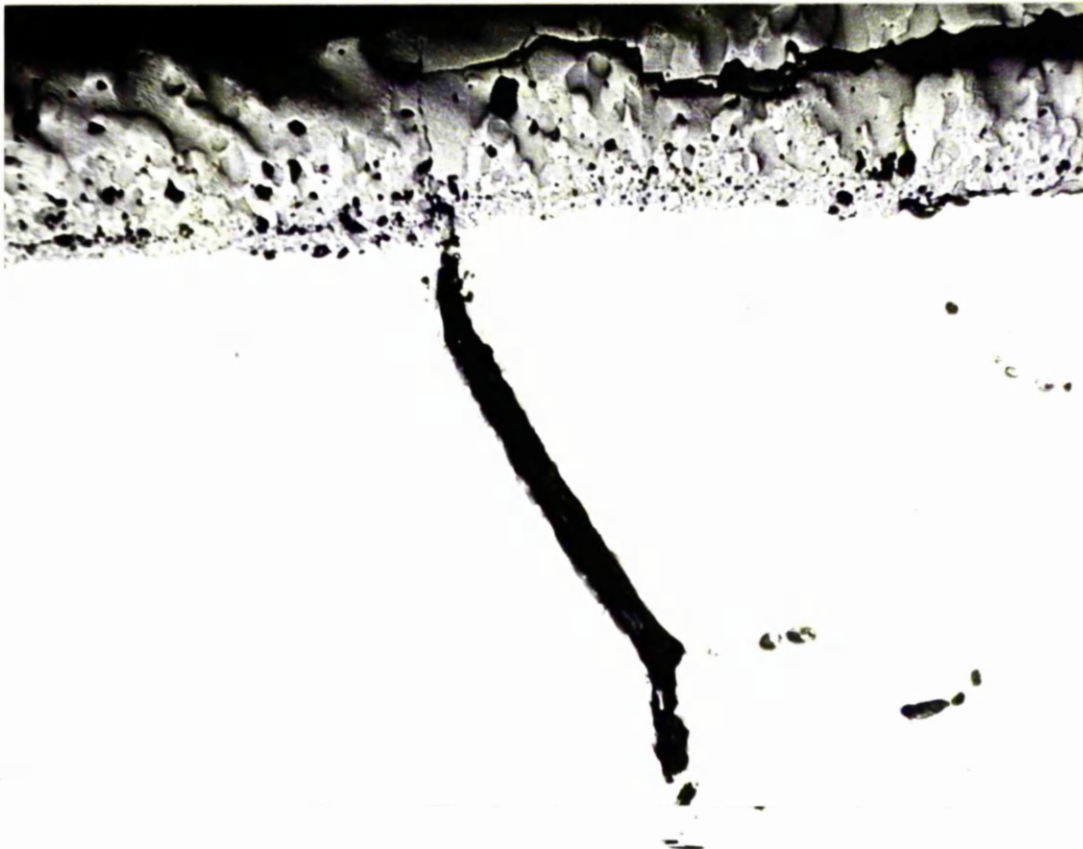


Fig. 67. Structure of Stressed Specimen.
x 45 Oxygen. 950°C. 5 N/mm². 49 hours.

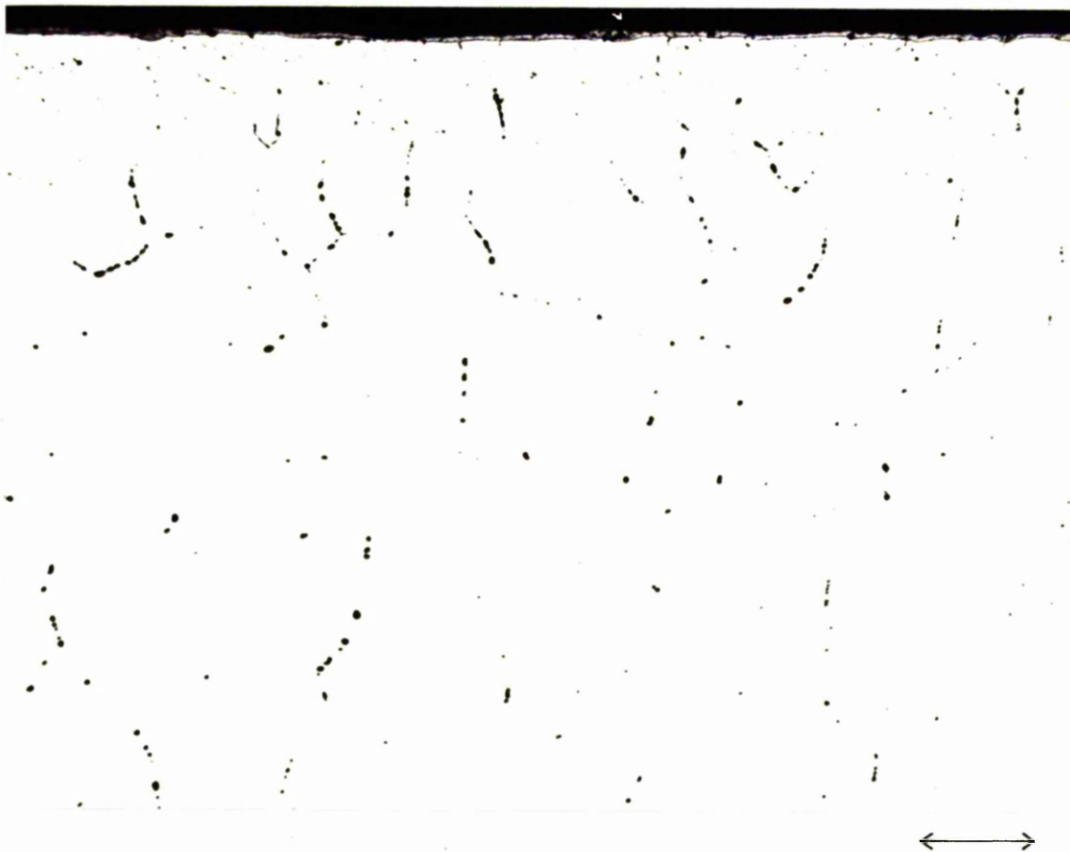


Fig. 68. Structure of Unstressed Specimen.
x 45 Oxygen. 950°C. Zero. 49 hours.

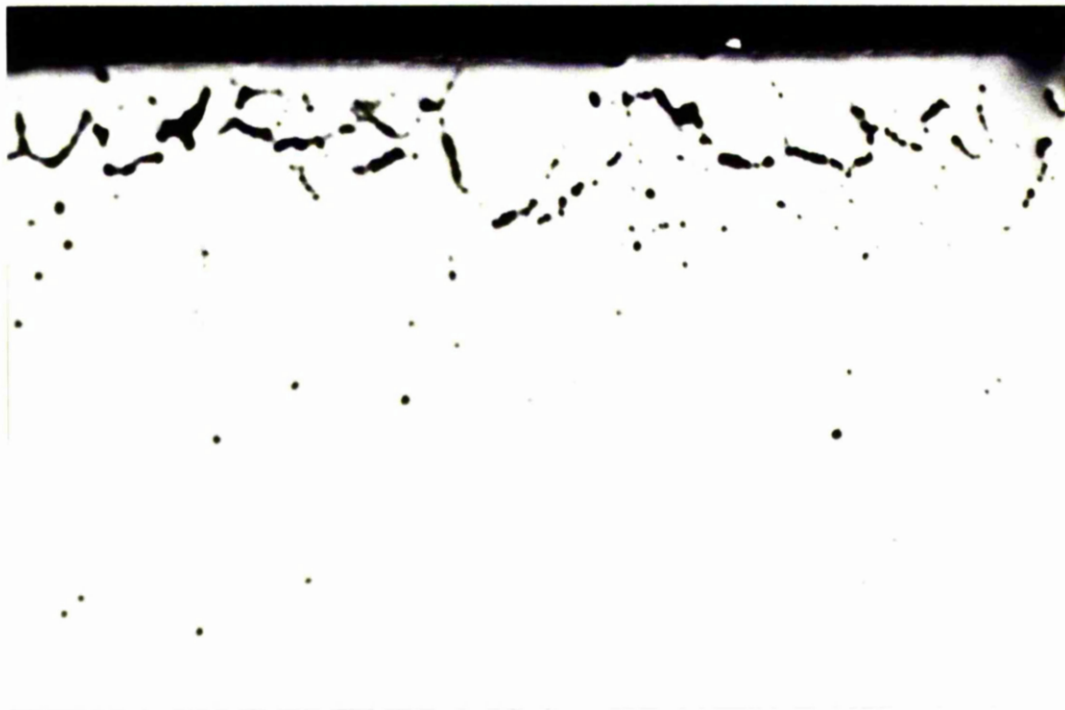


Fig. 69. Structure of Stressed Specimen.
x 45 Oxygen. 950°C. 5 N/mm². 120 hours.



Fig. 70. Structure of Unstressed Specimen.
x 45 Oxygen. 950°C. Zero. 120 hours.

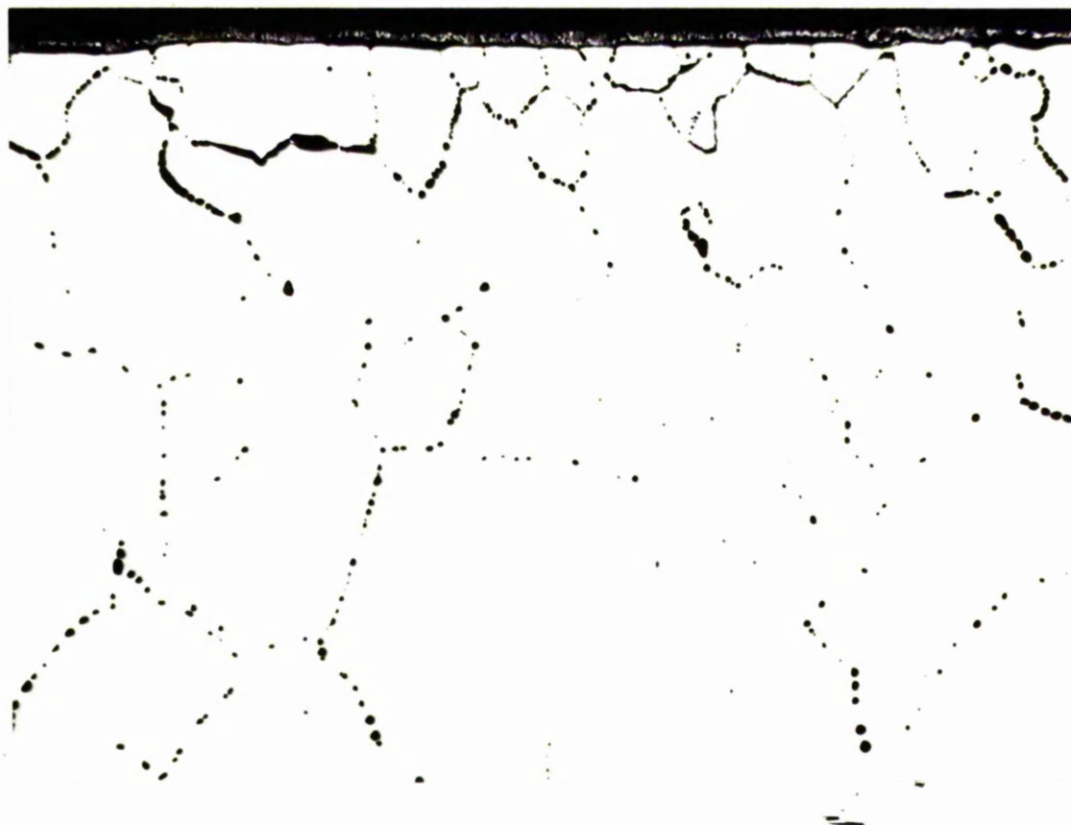


Fig. 71. Structure of Stressed Specimen.
x 45 Oxygen. 950°C. 5 N/mm². 144 hours.



Fig. 72. Structure of Unstressed Specimen.
x 45 Oxygen. 950°C. Zero. 144 hours.



Fig. 73. Structure of Stressed Specimen.
x 45 Oxygen. 950°C. 5 N/mm². 164 hours.



Fig. 74. Structure of Unstressed Specimen.
x 45 Oxygen. 950°C. Zero. 164 hours.

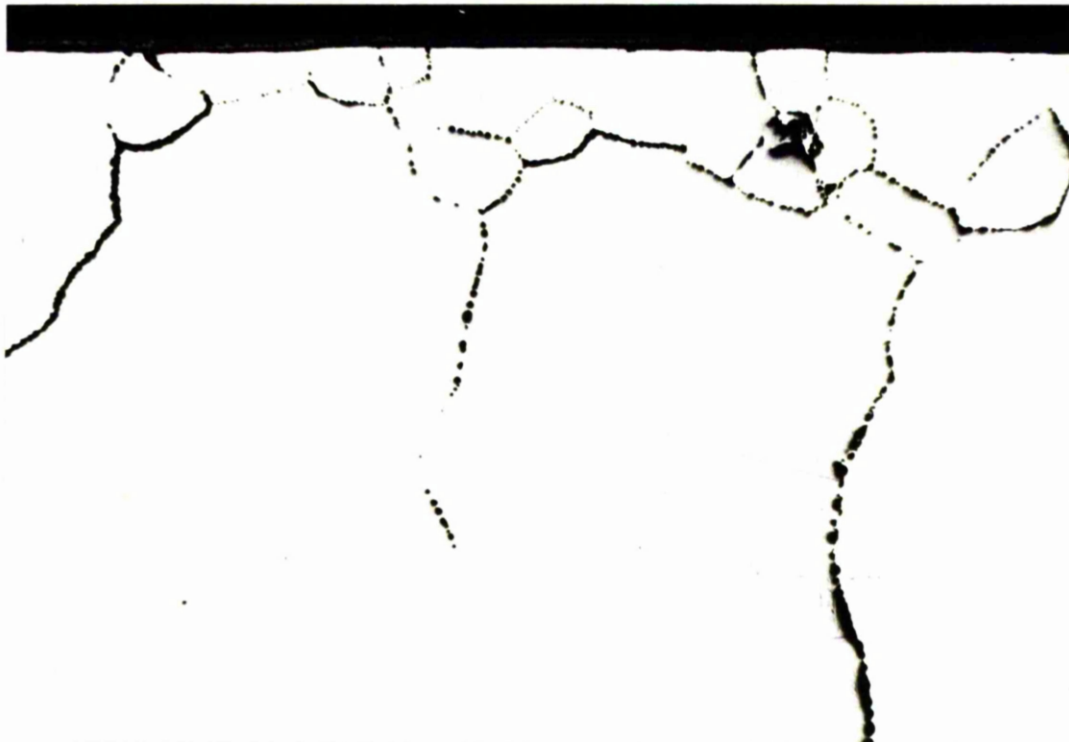


Fig. 75. Oxide Growth in Simulated Crack.
x 90 Oxygen. 950°C. Zero. 6 hours.

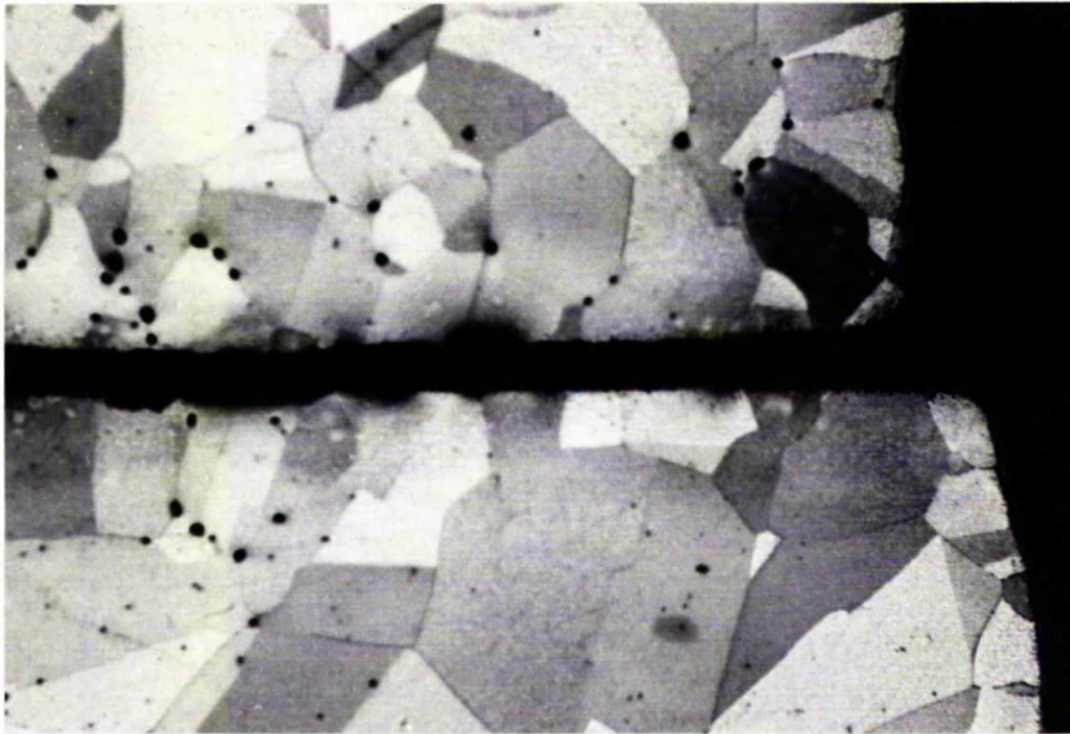


Fig. 76. Oxide Growth in Simulated Crack.
x 90 Oxygen. 950°C. Zero. 24 hours.

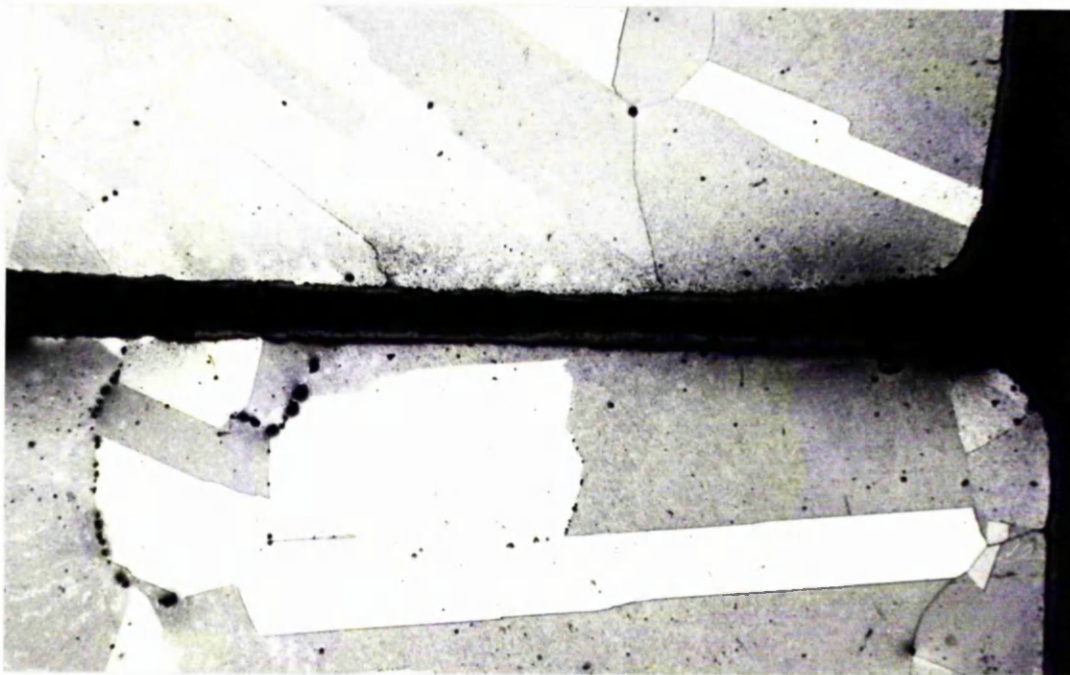


Fig. 77. Oxide Growth in Simulated Crack.
x 90 Oxygen. 950°C. Zero. 48 hours.

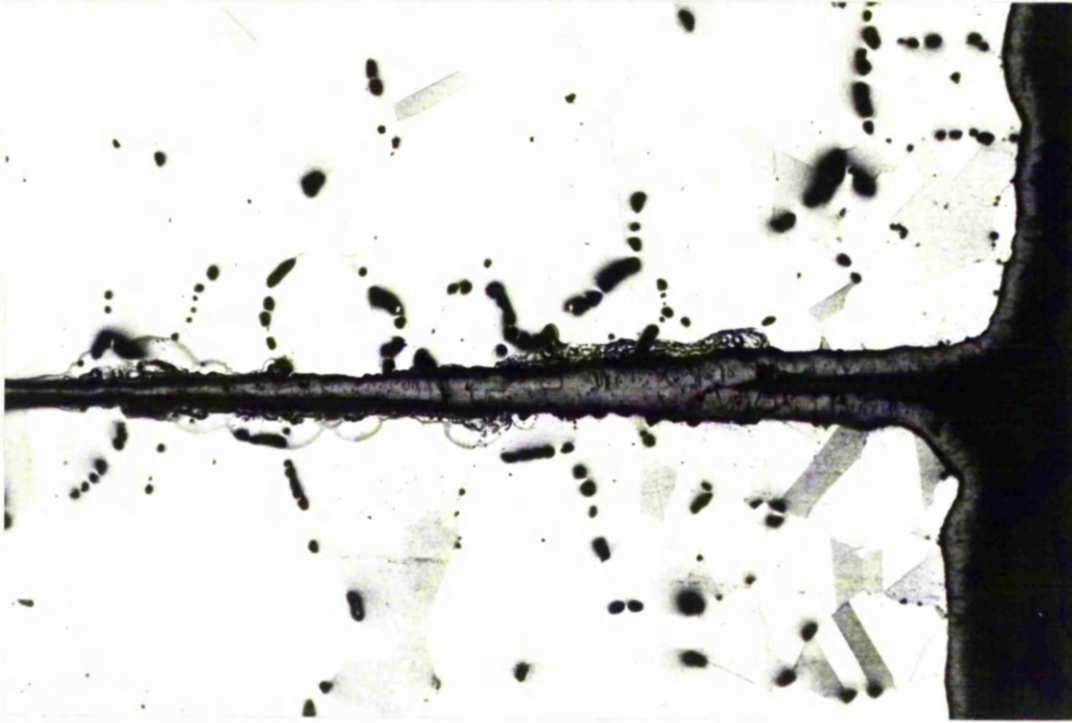


Fig. 78. Oxide Growth in Simulated Crack.
x 90 Oxygen. 950°C. Zero. 72 hours.



Fig. 79
x 550

Surface Oxide on Stressed Specimen.
Oxygen. 950°C. 11 N/mm². 101 hours, R.L.

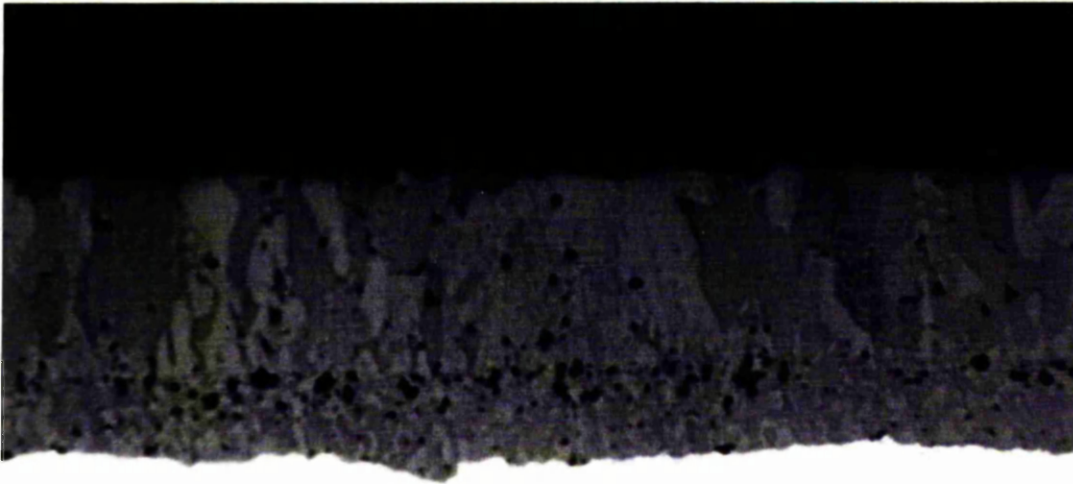


Fig. 80.
x 550

Surface Oxide on Unstressed Specimen.
Oxygen. 950°C. Zero. 101 hours.

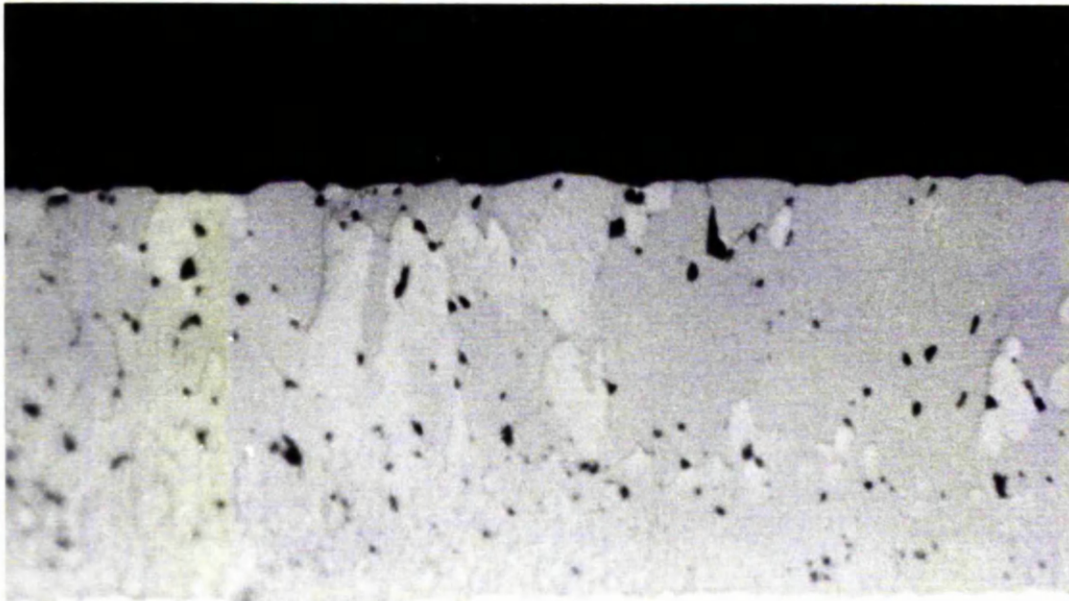


Fig. 81. Surface Oxide on Stressed Specimen.
x 220 Oxygen. 950°C. 11 N/mm². 169 hours, R.L.

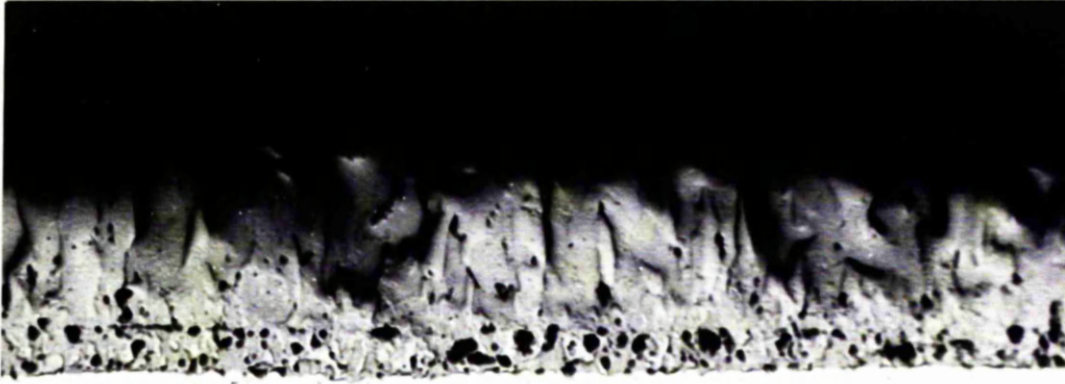


Fig. 82. Surface Oxide on Stressed Specimen.
x 175 Oxygen. 950°C. 10.5 N/mm². 332 hours.

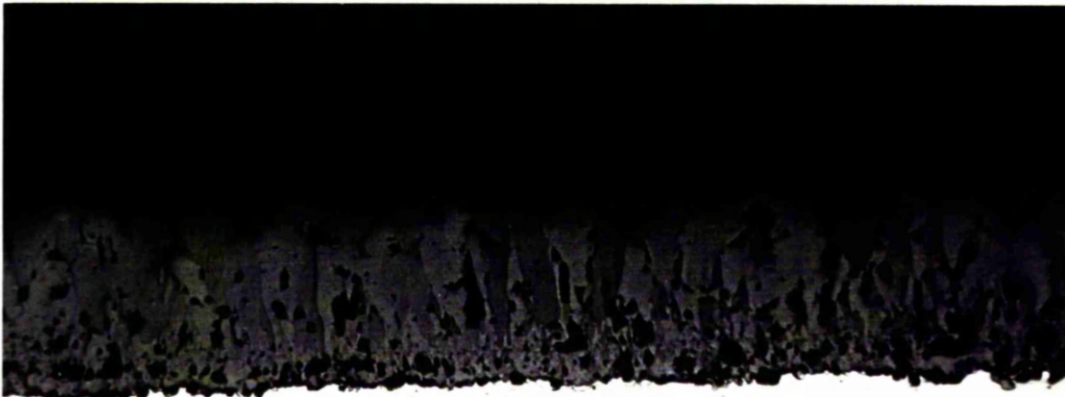


Fig. 83. Surface Oxide on Stressed Specimen.
x 175 Oxygen. 950°C. 10.5 N/mm². 530 hours.

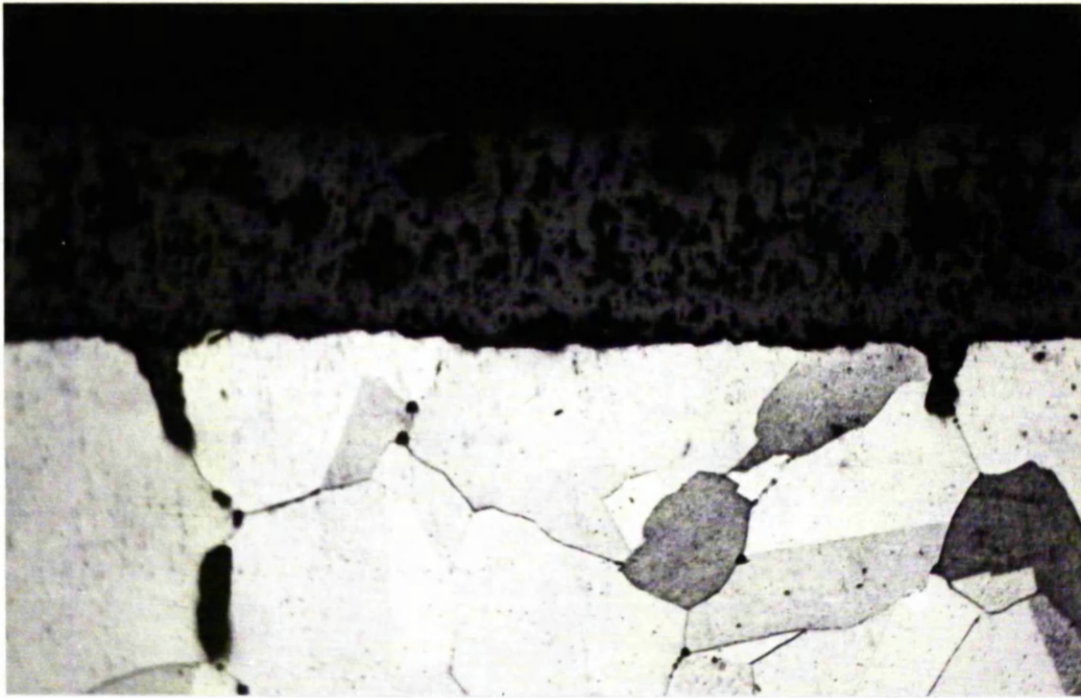


Fig. 84. Surface Oxide on Unstressed Specimen.
x 175 Oxygen. 950°C. Zero. 530 hours.



Fig. 85. Specimen after Creep Testing.
x 25 Oxygen. 950°C. 11 N/mm². 100 hours, R.L.



Fig. 86. Typical Region of Fracture Surface.
x 63 Oxygen. 950°C. 11.5 N/mm². 0.9 hours, R.L.



Fig. 87. Typical Region of Fracture Surface.
x 630 Oxygen. 950°C. 11.5 N/mm². 0.9 hours, R.L.

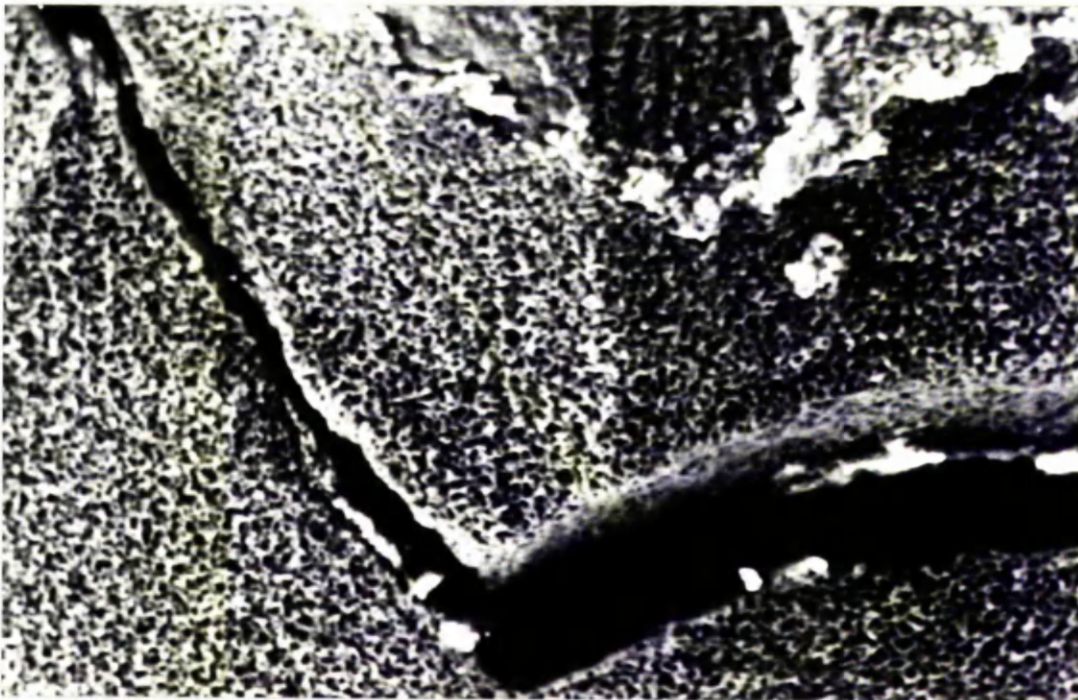


Fig. 88. Typical Region of Fracture Surface.
x 63 Oxygen. 950°C. 11.5 N/mm². 0.9 hours, R.L.



Fig. 89. Typical Region of Fracture Surface.
x 1260 Oxygen. 950°C. 11.5 N/mm². 0.9 hours, R.L.

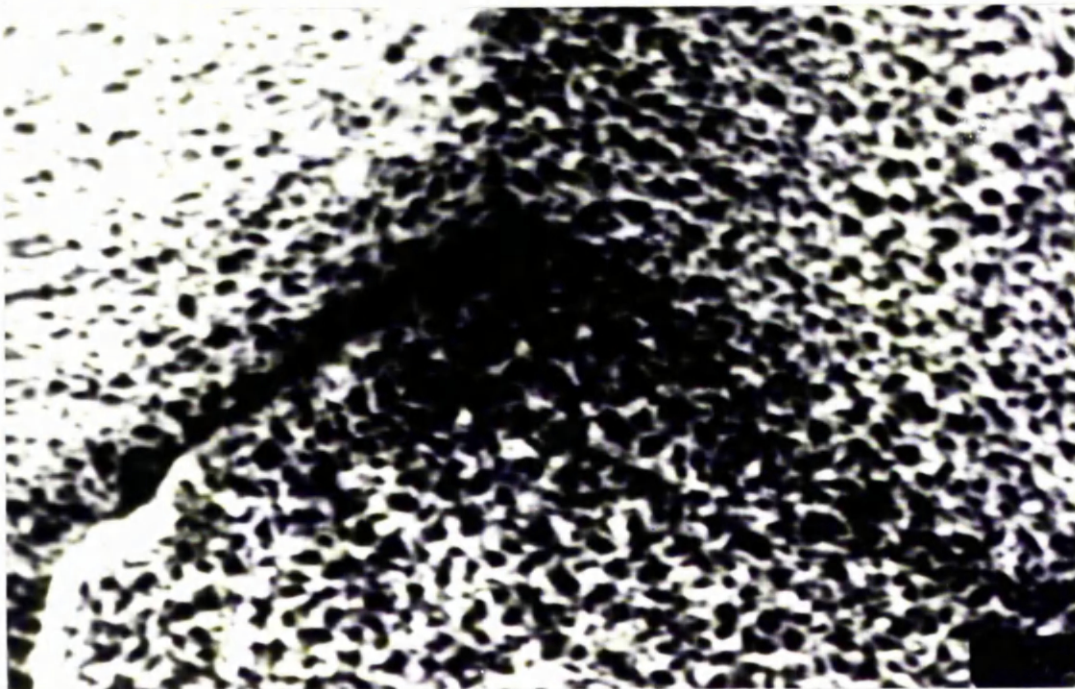


Fig. 90. Oxide on Fracture Surface.
x 2500 Oxygen. 950°C. 11 N/mm². 169 hours, R.L.

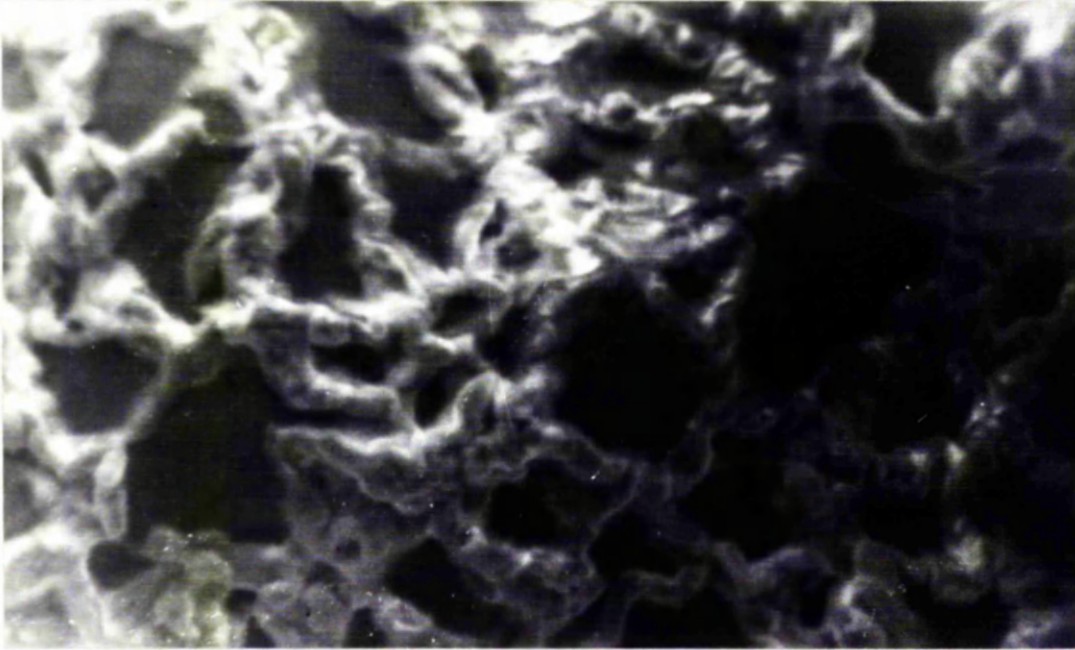


Fig. 91. Oxide on Fracture Surface.
x 2500 Oxygen. 950°C. 11 N/mm². 100 hours, R.L.

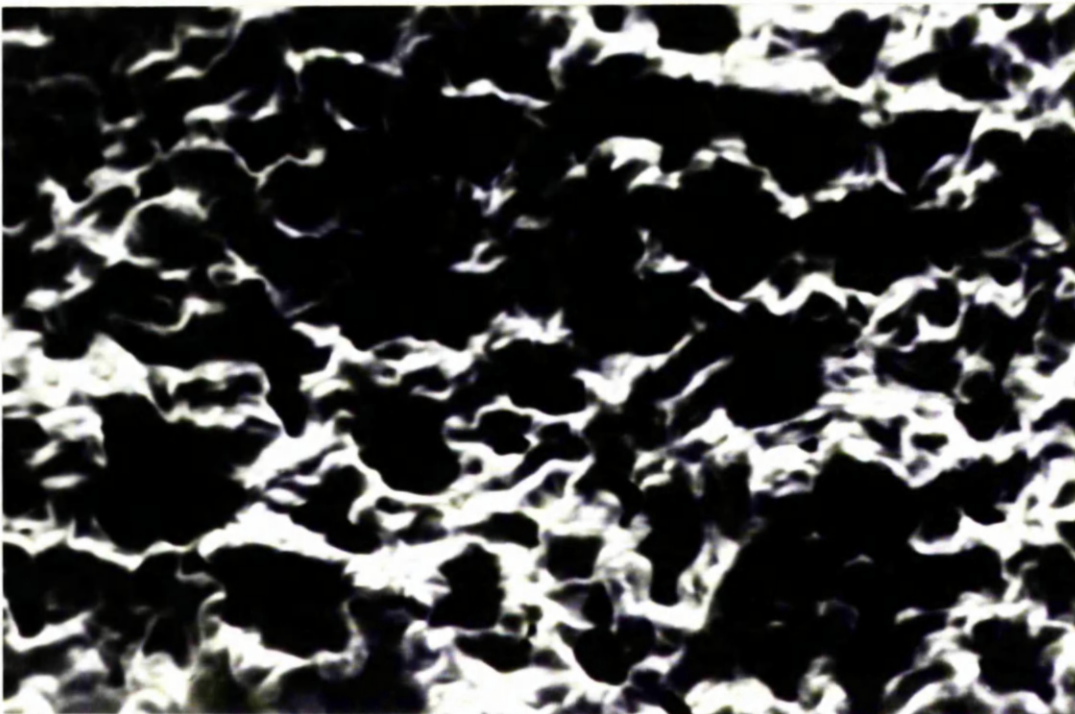


Fig. 92. Feature on Fracture Surface.
x 630 Oxygen. 950°C. 11 N/mm². 100 hours, R.L.

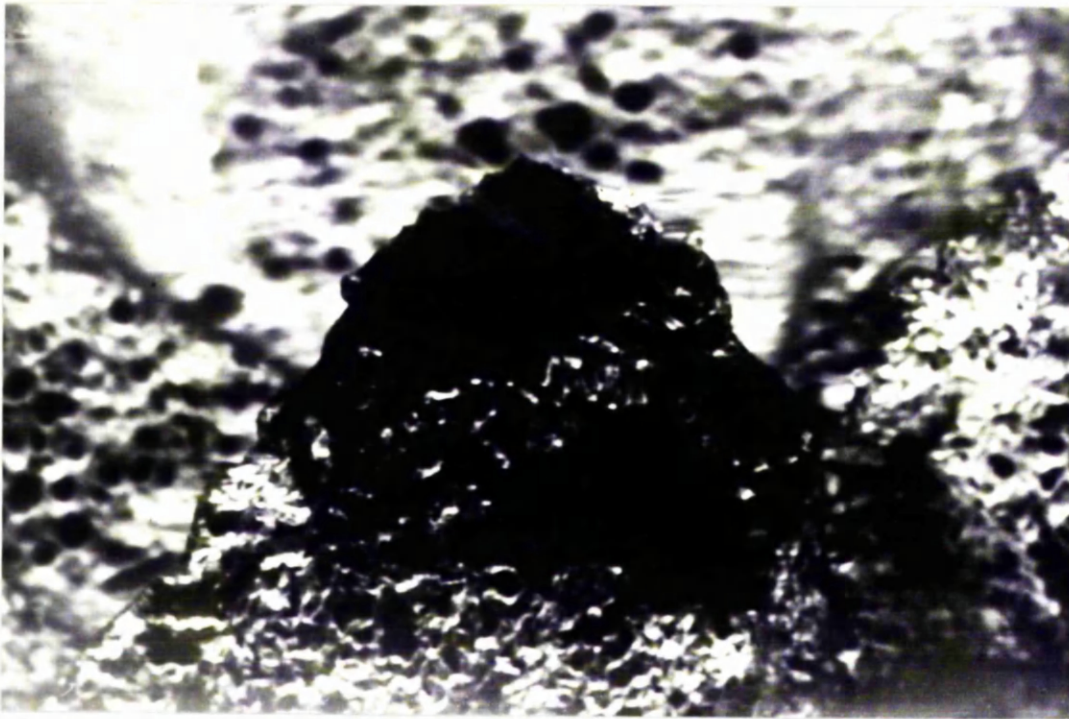


Fig. 93. Plan View of Oxide on Specimen Surface.
x 630 Oxygen. 950°C. 11 N/mm². 0.9 hours, R.L.

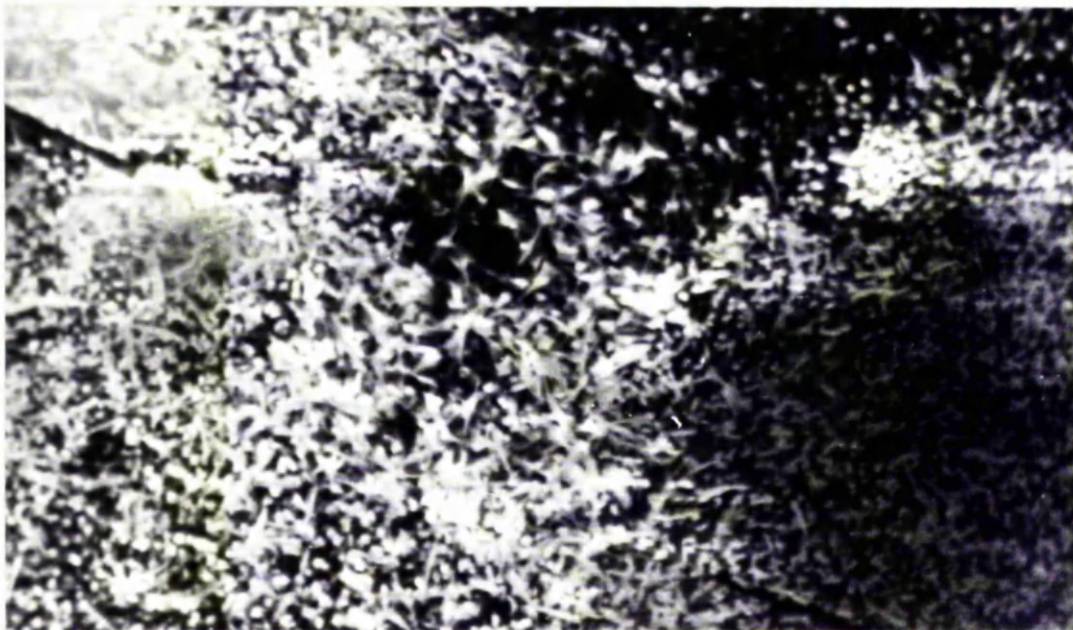


Fig. 94. Plan View of Oxide on Specimen Surface.
x 2500 Oxygen. 950°C. 11 N/mm². 0.9 hours, R.L.

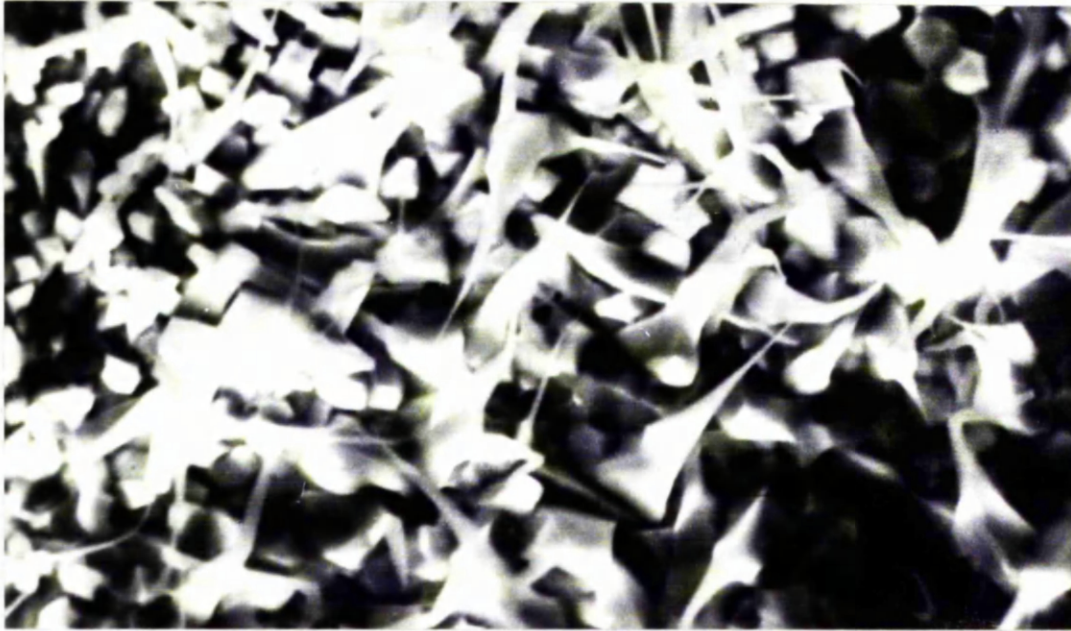


Fig. 95. Plan View of Oxide on Specimen Surface.
x 25000 Oxygen. 950°C. 11 N/mm². 0.9 hours, R.L.

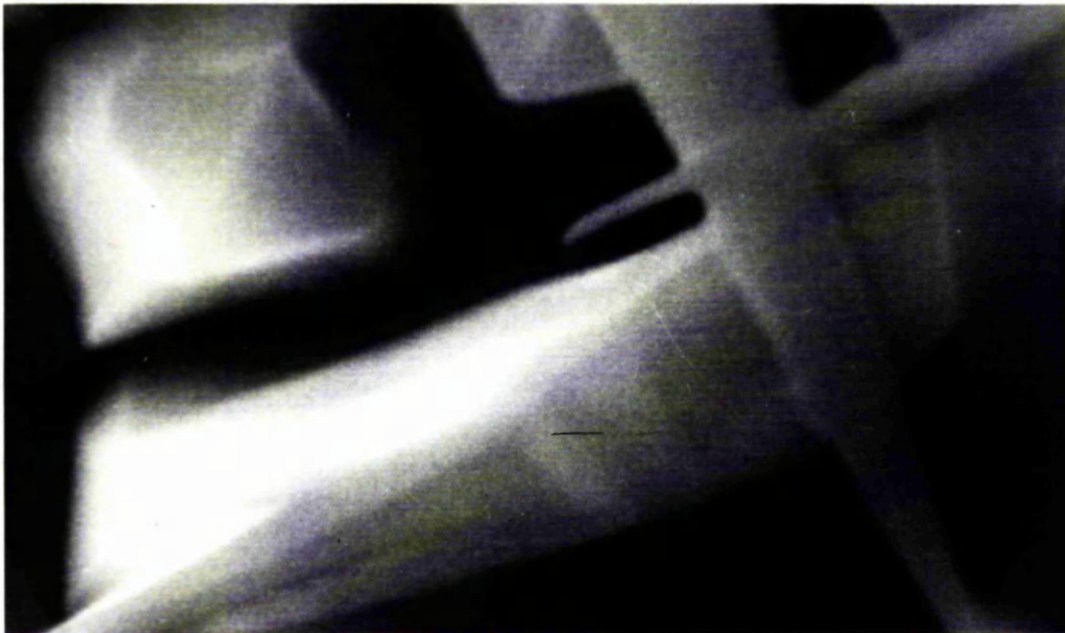


Fig. 96. Plan View of Oxide on Specimen Surface.
x 630. Oxygen. 950°C. 11 N/mm². 169 hours, R.L.



Fig. 97. Fractured Section of Two Layer Oxide.
x 1260. Oxygen. 950°C. 11 N/mm². 100 hours, R.L.

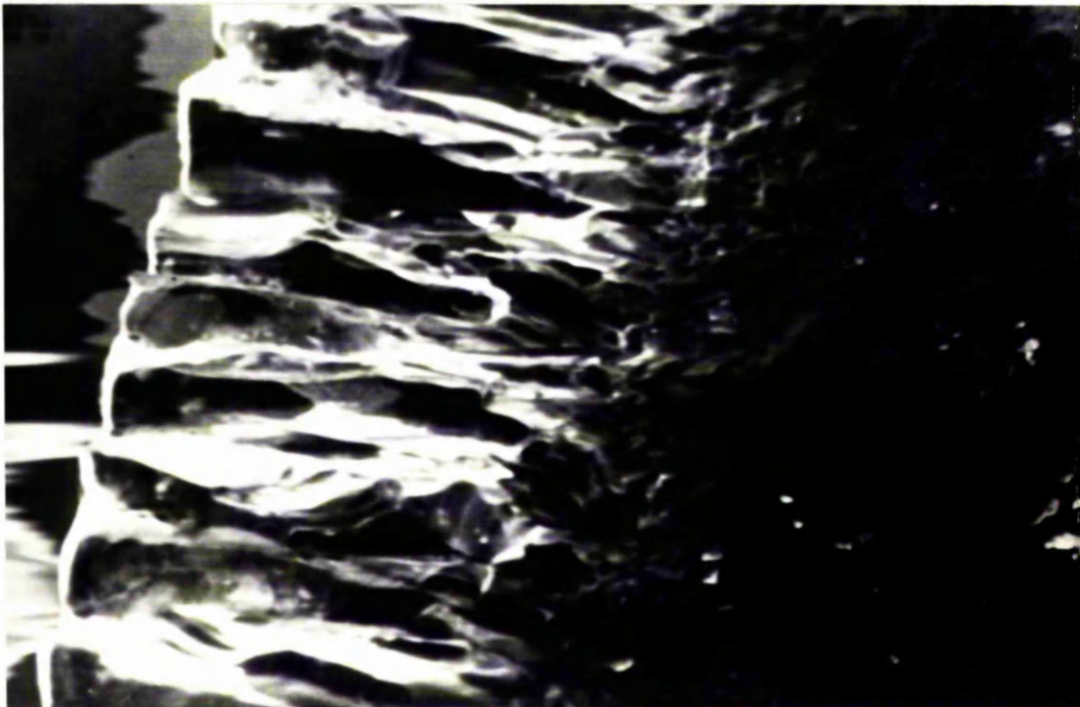
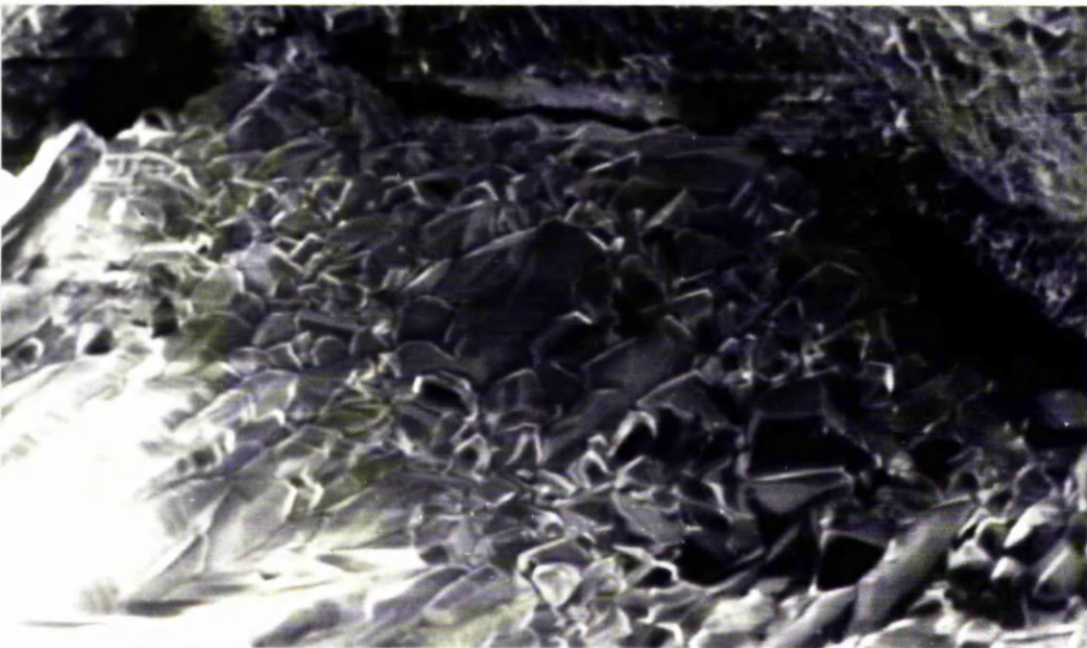


Fig. 98. Fractured Section of Outer Oxide Layer.
x 630 Oxygen. 950°C. 11 N/mm². 169 hours, R.L.



Fig. 99. Fractured Section of Inner Oxide Layer.
x 1260 Oxygen. 950°C. 11 N/mm². 169 hours, R.L.



DISCUSSION

5.1 Introduction

This experimental work has provided information which, in common with the prior work reviewed, is at times confusing if not contradictory. While the importance of individual results is recognised, it may provide a simpler path of explanation to concentrate on the major trends which have emerged.

The results of creep tests at 700°C showed essentially no difference in creep properties, whether carried out in oxygen or vacuum. Therefore these results provide little positive information on the actual mechanisms involved in the effect of an oxidising atmosphere on creep. By far the greater part of any explanation must be based on the results of the work carried out at 950°C where spectacular differences in creep behaviour were obtained in oxygen as opposed to vacuum. These differences were similar to those reported in the literature but as mentioned in 3.6 may be exaggerated due to the constant stress loading system used in the present work.

Overall at 950°C, creep resistance was considerably improved in an oxygen atmosphere. The most obvious sign of the effect was a marked increase in rupture life. This was not brought about by any single mechanism. The various factors, and their interdependence contributing to this increase are carefully outlined in this chapter.

The work showed little evidence of a reduction in creep resistance due to oxidation as has been reported previously⁽⁶⁾, albeit

at lower temperatures. It could be argued that the limited oxidation occurring at a pressure of 10^{-1} torr at 950°C might give rise to such an effect. However the single comparative test conducted in a vacuum of 10^{-6} torr did not show a significant variation in creep properties from the results in a vacuum of 10^{-1} torr (Table IV and Fig. 20). Therefore for the purposes of this work it is assumed that the creep results obtained in a vacuum of 10^{-1} torr are a fair representation of the creep properties of nickel where the occurrence of oxidation is absent.

5.2 Primary Creep

The accepted explanation of primary creep behaviour is in terms of a work hardening mechanism (2.3). As the metal is strained, the dislocation density increases and the mesh size of the dislocation network reduces. This strengthening effect forces a reduction in the creep rate. Recovery processes also act at this time. Their effect is to soften the metal and make the strengthening effect less than if work hardening alone operated. During primary creep, work hardening is dominant and the work hardening rate and creep rate fall with time.

Table VII and Figs. 25 to 27 strongly indicate that the creep rate in oxygen decreases more rapidly with time than in vacuum (4.5). An increase in work hardening rate or a decrease in recovery rate could produce this effect. Primary creep behaviour is more sensitive to work hardening rate than to recovery rate and therefore an increase in the former is the more likely cause. A reduction in creep rate due to the presence of an oxide film has been noted previously (4). An oxide layer of greater shear modulus than the underlying metal will exert a repulsive force on dislocations and therefore prevent their escape at the surface⁽⁸⁵⁾. This acts to increase the

dislocation density and hence work hardening rate of the metal.

Figs. 29 and 30 also gave indications that pre oxidised specimens had reduced primary creep extensions (4.6). The effect would be due to the pre-existing oxide layer and is in agreement with the above.

However the effect is not brought about by the mere presence of oxide on, or oxidation at, the metal surface. The vacuum level of 10^{-1} torr allowed slight oxidation to occur at 950°C . The effect was only found where there was a relatively thick pre-existing oxide layer or in oxygen where there was a high oxidation rate. Therefore this reflection of dislocations at the surface is affected by the thickness, nature and rate of formation of the oxide.

5.3 Secondary Creep

The title of this section is in a sense incorrect. It has already been demonstrated that a true secondary stage did not exist in oxygen at 950°C . Therefore what follows is a discussion of the absence of classic secondary or steady state creep in oxygen.

This classic steady state behaviour is brought about by a balance between work hardening rate and recovery rate (2.3). The declining work hardening rate of the primary stage eventually reaches a value at which it exactly balances the recovery rate and the creep rate becomes constant.

Figs. 19, 21, 23 and 24 show the continually declining creep rate in oxygen (4.5). A steady state creep rate is not achieved because the work hardening rate and recovery rate never reach a state of balance. It has therefore to be decided whether simultaneous oxidation affects work hardening, recovery, or both, in such a manner as to cause this non-balance.

It was suggested in the previous section (5.2) that the modification of primary creep behaviour was due to an increase in work hardening rate. If this was the sole effect and recovery was unaffected, then a steady state stage would be established, in a shorter time, at approximately the same value of creep rate as in vacuum. Figs. 25 to 27 show that, at equivalent time, the creep rate in oxygen is of the same order as the creep rate in vacuum but continues to decline thereafter (4.5).

It is assumed here and referred to later (5.12) that oxidation causes the injection of vacancies into the metal. The presence of these excess vacancies could additionally strengthen the material by various mechanisms, e.g. the condensation of vacancy atmospheres on dislocations and the collapse of condensed vacancies to form dislocation loops.

In order to prevent the establishment of steady state conditions an interference with the recovery process must occur. A simple decrease in the recovery rate would not prevent the onset of steady state. This would merely extend the time to onset and reduce the value of the steady state creep rate. The injection of excess vacancies into the nickel would be expected to increase the recovery rate. Recovery makes use of the processes of dislocation climb, lattice diffusion and therefore vacancy movement. Thus an explanation of how excess vacancies apparently decrease the recovery rate must be sought.

Creep rate results from a relation between work hardening and recovery. Recovery is affected by the vacancy concentration which is temperature dependent and also influenced by the creation of vacancies due to deformation and therefore work hardening. The relation between work hardening and recovery can then be said to be

inherently connected with vacancy concentration.

In vacuum the vacancy concentration can be regarded as a closed system dependent only on the creep process and ambient temperature. If oxidation occurs, a variable essentially independent of the creep process affects vacancy concentration. This alters the relation or balance between work hardening and recovery and changes the creep rate. The oxidation of nickel follows a parabolic rate law and initially causes a high rate of vacancy injection into the metal which thereafter declines parabolically. Therefore the initial balance between work hardening and recovery is set in relation to a high formation rate of vacancies in excess of that from creep alone. From that point, the balance is dynamic, due to an ever declining rate of excess vacancy formation. The work hardening rate chases an ever declining recovery rate which results in an ever declining creep rate.

Figs. 31 and 33 show that the cessation of oxidation did not alter the creep rate. Instead, steady state conditions were quickly established, dependent on the vacancy related balance at the time when vacancy injection ceased.

Figs. 32 and 33 show that where oxidation commenced after steady state conditions had been established in vacuum, an increase in creep rate was triggered (4.7). Oxidation increases both the work hardening rate and the recovery rate. The sudden increase in creep rate results from the greater sensitivity of the creep process to recovery at this stage. The important point is that the balance between work hardening and recovery is upset and never re-established.

5.4 Void Nucleation

The previous chapter showed that grain boundary voids were formed as a result of creep alone and oxidation alone (4.10 and

4.12). Voids due to the creep process were primarily nucleated in the body of the specimen on grain boundaries, perpendicular to the applied stress (Figs. 37 to 40). Voids due to oxidation were mainly nucleated close to the specimen surface on grain boundaries parallel to the surface (Figs. 61 to 63). Voids were also nucleated in the specimen body after long oxidation times (Figs. 64 and 65). When simultaneous oxidation and creep occurred, voids due to both processes were nucleated (4.11). Figs. 46 to 50 show that in this case voids were preferentially nucleated near to the specimen surface, on grain boundaries perpendicular to the applied stress. Only after relatively long times did void nucleation in the specimen body match that near the surface. Thus in the combined case, the processes of void nucleation, due separately to oxidation and creep, interfere. Oxidation causes the nucleation to occur close to the specimen surface, while creep causes that nucleation to take place on grain boundaries at high angles to the axis of stress.

Void nucleation rates can be assigned as being due to creep alone, and oxidation alone. It is uncertain whether their combination results in a simple summation and whether the same mechanisms apply. Voids have been said to be nucleated heterogeneously during oxidation⁽¹⁹⁾ but this gives little help in defining a mechanism. Assuming that vacancy injection plays a major part in void nucleation, then the nucleation rate will bear some relation to the oxidation rate and fall with time.

There is a clearer understanding of the nucleation of voids during creep (2.3). The nucleation rate due to creep is deformation controlled^(24,57,68,69) and nucleation commences very early in the creep life. The previous sections (5.2 and 5.3) have outlined differences in deformation rates between creep in oxygen

and creep in vacuum. Although these differences were relatively small, a lower void nucleation rate due to creep could be expected when simultaneous oxidation occurs.

Comparison of specimens tested in vacuum and in oxygen showed little difference in the numbers of voids formed over equivalent time intervals. Comparison of Figs. 42 and 43 with Figs. 46 and 47 illustrates this. The void nucleation rate due to oxidation would compensate for any decrease in that due to creep. Therefore the total numbers of voids formed and overall nucleation rates may, as observed, not be greatly different over that period of time which represents the creep life of vacuum specimens.

The time dependence of void nucleation rates in oxygen and vacuum, respectively, will differ. A constant nucleation rate associated with steady state conditions⁽⁶⁹⁾ will not occur in oxygen. Instead the void nucleation rate will continually decrease due to the declining creep and oxidation rates. The greater numbers of voids found in oxygen tested specimens are therefore a consequence of the extended creep lives and greater total deformations.

5.5 Void Growth and Coalescence

Once a stable void nucleus has been established, it increases in size both as a result of creep or oxidation. In the limit, growth continues until individual voids link up or coalesce.

It was observed that voids reached a noticeably larger size prior to coalescence, in oxygen tested specimens compared to those in vacuum (4.10). Figs. 59 and 60 show extreme examples of this. Relatively little coalescence had occurred after times in excess of 300 hours of creep in oxygen. Under equivalent conditions in vacuum, fracture had occurred in less than 30 hours. Thus coalescence

appeared to be retarded in oxygen.

Little attention has been given to void growth during oxidation and it can only be assumed that the injection of vacancies contributes to it. Void growth during creep is said to result from the absorption of vacancies from the grain boundary. The vacancies being generated by dislocation movement in the grain boundaries (68,69,74). When creep alone is compared with simultaneous creep and oxidation, the major difference, in this context, is the additional supply of vacancies due to oxidation. Although a connection between void nucleation rate and growth rate should not necessarily be expected, it could be assumed that an increase in vacancy concentration would increase both.

Void coalescence concerns the linking of existing voids. The number of voids already present is of more relevance than is the actual nucleation rate. Void growth rate would therefore be expected to play the more important role in void coalescence. In creep, void growth is more closely connected with vacancy generation than is void nucleation and, therefore, simultaneous oxidation would seem likely to increase growth rates. However, with similar numbers of existing voids, an increase in void growth rate should give more coalescence and not less, as observed. This assumes a similar mode of growth and it is herein that the reason may lie.

The observation that larger individual voids were found in oxygen tested specimens than in any vacuum tested specimen is important. This is interpreted as showing that a greater proportion of the void growth occurred outwith the grain boundary plane. Therefore, the grain boundary voids inherently had a lesser tendency to spread along the grain boundary and gave less coalescence when simultaneous creep and oxidation occurred.

This can be related to one theory of void growth kinetics during creep^(68,69) and an assumption that, during oxidation, void growth results from the flux of injected vacancies. Void growth during creep was said to result from the condensation of vacancies whose source was the grain boundary. This growth was initially in three dimensions. At some point growth outwith the grain boundary plane ceased and further void growth was spreading over the grain surface. This coincided with the onset of steady state creep. During creep in oxygen no steady state region existed (5.3). It could be argued therefore that the extended primary type creep behaviour would allow continual three dimensional void growth. In addition, the increased vacancy concentration due to oxidation could result in a tendency for greater vacancy condensation from the lattice rather than the grain boundary.

5.6 Crack Initiation and Propagation

The initiation of cracks could be regarded as being one and the same as void nucleation. However, in this section, the point of crack initiation is taken as being the start of propagation, i.e. the point at which a cleavage mechanism takes over from the vacancy absorption mechanism of void growth. Intergranular crack initiation therefore occurs when void formation has weakened the grain boundaries and caused sufficient stress intensification to produce cleavage. The cracks propagate through the grain boundaries, leading to complete parting and intergranular fracture. This then would be the situation in vacuum where initiation tends to occur in the specimen body and propagation is towards the free surface (4.10).

There are several important modifications to the above when simultaneous oxidation occurs. Individual voids are larger and void coalescence has a greater ratio of width to length. The

available "notches" for crack initiation are therefore less sharp than when creep alone occurs. Voidage is concentrated close to the specimen surface and crack propagation is directed into the specimen body. Taken in isolation, the compounding of damage close to the specimen surface, due to oxidation plus creep, might be expected to cause premature failure. However it is this very process of preferential crack formation at the free surface which ensures the delay of fracture.

The first cracks to be initiated are open to the surface. This allows unhindered penetration by atmospheric oxygen and oxide formation within the cracks. The propagation of cracks from the surface into the centre of a specimen rather than the reverse ensure that significant oxide free cracks do not develop (4.11 and Fig. 51).

The build up of oxide within the cracks interferes considerably with the mechanism of crack propagation. Figs. 75 to 78 showed the potential of the oxide to bridge and even fill cracks (4.14). Figs. 52 to 58 show bridged and filled cracks in crept specimens. For the oxide to play a major role in the prevention of failure, it must be load bearing. This provides a self healing mechanism in the nickel and lowers the stress intensity at the crack tip. This will act to reduce the crack propagation rate.

The crack propagation rate can also be reduced by crack tip blunting. Figs. 54 and 56 to 58 contain some examples of apparently blunt cracks in the nickel. The surface of the oxide within cracks usually had a rounded configuration and Fig. 58 shows a rare example of a sharp crack in the oxide. A further indication of crack tip blunting is obtained if a basic implication is borrowed from fracture mechanics. A certain crack opening displacement will result in crack propagation. Therefore some approximate ratio should be expected between crack width and crack length. Comparison

of vacuum tested and oxygen tested specimens revealed a tendency for the ratio of width to length to be greater in oxygen tested specimens (Figs. 40, 41, 43 and 44 with Figs. 52 to 55). One deduction is that crack tip blunting occurred in oxygen.

One further related obstacle to crack propagation can be proposed when simultaneous creep and oxidation occur. Grain boundary voids and void coalescence are larger and wider than when creep alone occurs. When a crack breaks into such voidage it will experience considerable instantaneous blunting. Figs. 51, 71 and 73 appear to show this effect. Thus the physical effect of oxide formation, existing voids and possibly vacancy injection allowing increased local deformation, may all contribute to crack tip blunting.

The process of crack formation and oxidation continues, developing extensive crack networks (Figs. 52, 53 and 69). This can lead to the formation of a complex composite material composed of an oxide matrix enclosing nickel grains or agglomerates of grains. There is then no reason why this material should show creep behaviour similar to the original nickel.

5.7 Fluctuating Creep Rate

Virtually no cracks were found in oxygen tested specimens which did not exhibit a fluctuating creep rate (Figs. 19 and 59). Cracks were invariably found in specimens which did experience a period of fluctuating creep rate (Figs. 21, 54, 55 and 58). This further suggests that secondary creep is non-existent in a strongly oxidising atmosphere at 950°C. Only the traditional primary and a modified tertiary stage exist (4.5). The final stages of creep in oxygen where a fluctuating creep rate occurred were predominantly concerned with crack propagation.

Any effect of oxidation on the creep deformation or void formation processes can be ruled out as a cause of fluctuating creep rate. In tests where an oxygen atmosphere was removed part way through a test, the subsequent creep in vacuum showed no evidence of a fluctuating creep rate (Figs. 31 and 33). It could be considered as a consequence of a structure consisting of metal grains in an oxide matrix. However, where creep in vacuum was interrupted in tertiary and the specimen oxidised for 24 hours, instant failure occurred on re-application of the load. The phenomenon of a fluctuating creep rate must therefore be regarded as a consequence of simultaneous dynamic oxide generation within propagating grain boundary cracks.

Consider the development of a single grain boundary crack in nickel. Void coalescence initiates a short crack originating from the free surface. Oxidation of the crack surfaces immediately occurs. Depending on the rate of crack propagation or, more directly, on the rate at which the crack walls move apart, after some time the oxide will bridge the crack. In the limit the oxide would completely fill the crack (Fig. 57). Assuming this bridge to be load bearing, it will reduce the stress intensity at the crack tip and the crack propagation rate. In the extreme propagation would cease. If crack tip oxidation is considered, free oxidation will initially cause a considerable blunting effect and relatively large reduction in propagation rate. The formation of an oxide bridge will restrict the access of atmospheric oxygen and reduce the oxidation rate. Crack tip blunting is lessened with a potential increase in crack propagation rate.

Consider now crack initiation at a relatively short distance away from the free surface. Crack propagation will be relatively unimpeded until the crack reaches the surface and allows free access

of oxygen. The above sequence of events will then ensue.

If crack propagation is halted and oxidation continues, then it is feasible that a jacking displacement due to the oxide wedge can be allowed for. This could restart crack propagation.

The period of fluctuating creep rate is, in effect a modified tertiary stage. As such the extension during this period mainly represents damage accumulation. The overall creep strain will consist of several components:

- (1) Creep within the nickel grains or agglomerates of grains.
- (2) Grain boundary crack formation.
- (3) Continual oxide formation within grain boundary cracks.
- (4) Creep of the oxide within grain boundary cracks.

The sum of these components will not necessarily result in a uniform increase in extension. Various reasons for cyclic crack formation have been suggested above. Localised conditions will dictate the extension due to the oxide. It was observed that damage from creep alone tended to accumulate in bands when creep alone occurred (4.10). When simultaneous oxidation occurred the damage was more uniformly distributed, especially after long times. Therefore the fluctuating creep rate may represent a different time base of damage accumulation in various areas of a specimen. Damage will accumulate in a certain region until saturation is reached. The strength of the composite metal/oxide type structure is sufficient to resist failure (5.6). Crack formation, etc., will then commence in a separate region of the specimen, producing a non-uniform overall strain rate.

5.8 Fracture

A failure mechanism must be sought for the situation of simultaneous creep and oxidation. In normal creep failure there is wide variation in the extent of damage prior to failure and in the propagation rate of individual cracks, i.e. the first crack to form and propagate may lead to failure, or many cracks may form before progressive damage leads to failure.

In the present case it could be conveniently suggested that, at some stage, a particular crack forms which propagates sufficiently quickly to cause failure. However many specimens showed extensive oxidised crack networks extending from surface to surface (Figs. 52 to 55). Invariably the full length of the fracture surface was oxidised (Fig. 55). It is possible that a crack could be initiated in the specimen centre and propagate, oxide free, to the surfaces but no significant unoxidised cracks were observed.

Consider an oxidised crack which extends completely through the specimen. The oxide layer must bear the entire load and therefore be subject to creep. There is little information on the creep of nickel oxide but it does occur and will lead to failure. However the consideration is not merely the creep of nickel oxide. The oxide is self healing in that fresh oxide is continually forming to repair any damage. As the oxide thickness increases, the oxidation rate and therefore generation rate of fresh oxide will diminish, until at some stage it cannot keep pace with damage and failure ensues. Initially, creep of the oxide is compensated by oxide growth but as the growth decreases, creep becomes dominant and fracture occurs. In support of this mechanism it was observed that oxide on the fracture surfaces (Figs. 87 to 92) had a structure typical of oxide which has undergone plastic deformation^(48,84).

An alternative mechanism for failure could be via the formation of a double layer oxide. Detachment of the oxide layer or a relatively weak bond between layers would cause failure. Such a mechanism would only operate after relatively long oxidation times and not be universally important. In addition it would give failure in a fixed time after the formation of the first oxidised crack, i.e. the formation time of a double layer oxide. Therefore the former theory seems more plausible.

5.9 Rupture Life

An explanation can now be given for the great increase in rupture life when creep occurs in oxygen as opposed to vacuum (Table IV and V). The interference of the creep and oxidation processes results in firstly, a delay of damage formation and secondly, an increase in the extent of damage prior to failure. A large proportion of the rupture life is therefore concerned with damage accumulation and this results in the high extension values and high products of rupture life and creep rate (Table V and Fig. 13).

5.10 Effect of Temperature and Stress on the Creep of Nickel in Oxygen

The experimental findings provide little direct information on temperature dependence as tests were only carried out at 700°C and 950°C. There was no apparent atmosphere effect at the lower temperature and a gross effect at the higher temperature. Quantitatively similar creep was induced at both temperatures by using different stress ranges to compensate for the temperature difference. Assuming qualitative similarity also, the differing atmosphere effect at the two temperatures can only be ascribed to the difference in oxidation rate.

In the early stages of creep the absence of an atmosphere effect at 700°C shows that the mere occurrence of an oxide film is not sufficient to modify the work hardening rate and that the rate of build up and thickness of the surface film is important in determining whether dislocation processes are interfered with (5.2). It can also be deduced that the rate of injection of vacancies has an important bearing on the upset of balance between work hardening and recovery as well as on the modification of void formation (5.3, 5.4 and 5.5). The effect of stress at 950°C (Table V) reveals that as the creep process is speeded up, so the influence of oxidation on the deformation and void formation processes is reduced.

A direct assessment of the effect of temperature on crack propagation and oxidation, and fracture is not possible as the creep behaviour was only modified by oxidation at 950°C . The results of tests in oxygen at 950°C (Table V) cover the complete effect of stress. At 12.0 N/mm^2 there was only a slight effect due to oxidation (Fig. 23) while at less than 10.5 N/mm^2 , oxidation effectively caused complete prevention of failure. Consideration of this hypersensitivity to applied stress will inherently predict the dependence on temperature.

The assumption is made that stress level has no effect on oxidation and that the oxidation rate is solely dependent on temperature. Creep rate and therefore crack propagation rate increase with increased stress. Crack propagation rate is related to the rate at which crack faces move apart and this must also increase with stress. Oxidation rate and therefore the rate at which the oxide increases in thickness is fixed with temperature. Thus as stress increases, the likelihood of oxide bridges forming within

cracks is reduced. Oxide bridging of cracks therefore depends on a balance of two competing processes. Only if the oxide thickening rate is the greater will bridging occur, after a time dependent on the difference between the two rates.

Blunting of the crack tip by oxidation also depends on crack propagation rate. The higher the propagation rate, the less is the opportunity for significant blunting.

There will be a wide variation in crack propagation rates in nickel at any given stress level. The situation is not therefore a simple effect or no effect. As stress level increases there is a greater proportion of relatively faster crack propagation. Therefore oxide formation will impede less cracks and be less effective in impeding the propagation of individual cracks. In addition, oxide formation does not simply reduce the crack propagation rate by a fixed amount or proportion. The mechanisms are compound. The slower the crack propagation/opening rate, the greater is the extent of blunting/bridging, the greater is the reduction in propagation rate and the greater is the blunting/bridging effect, etc.

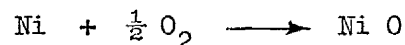
The oxide and oxide/metal bond will have certain rupture strengths of which the oxide is probably weaker⁽²¹⁾. When the stress across oxide bridges is of the order of the rupture strength of the oxide, a critical balance exists. Only if the acting stress is less than the rupture strength will the oxide provide a strengthening effect. This also relates back to the extent of oxide formation within a crack. The acting stress in the oxide will decrease as the number of bridges increase. The rupture strength of nickel oxide has been given as 28 N/mm^2 at 817°C . Allowing a reduction for increased temperature, it is quite possible the applied stress

used in this work approximated to the rupture strength of nickel oxide at 950°C.

Thus the extreme sensitivity to applied stress of rupture life under conditions of simultaneous creep and oxidation is explained in terms of the additive effect of various factors. These factors which contribute to the prevention of failure are themselves highly sensitive to stress.

Temperature obviously affects the process through its effect on oxidation rate. Increased temperature increases the oxide thickening rate. This raises the crack propagation rate which can be impeded. A quantitative assessment of this can be attempted.

Oxidation data are commonly given in terms of weight gain per unit area. This must be converted to an oxide thickening rate. Consider the oxidation of nickel.



A mass balance based on atomic weight gives

$$58.7 + 16 \longrightarrow 74.7$$

Let x mg be the weight gain per unit area. The corresponding weight of nickel transformed to nickel oxide is $x \times \frac{58.7}{16}$ mg.

If thermal expansion is ignored, the density of nickel can be taken as 8.9 g/cm³ at 950°C. The volume of nickel transformed to nickel oxide is then $x \times \frac{58.7}{16} \times \frac{1}{8.9 \times 10^3}$ cm³. The Pilling-Bedworth ratio for nickel oxide is 1.65⁽³³⁾. The change in volume in the transformation is then

$$\begin{aligned} & x \times \frac{58.7}{16} \times \frac{1}{8.9 \times 10^3} \times \frac{0.65}{1} \text{ cm}^3 \\ & = 2.68 \times 10^{-4} x \text{ cm}^3 \end{aligned}$$

Using this calculation, data given by Hancock and Fletcher⁽¹⁹⁾ for the oxidation of thick nickel specimens has been interpolated and converted from weight gain to surface advancement versus time and is shown in Fig. 100. The weight gain was given for a unit area of one square centimeter and surface advancement therefore becomes 2.68×10^{-4} x cm where the volume change is assumed to occur only in the direction normal to the surface.

When applied to the concept of crack bridging the surface advancement rate is doubled due to the oxidation of both surfaces. As a crack propagates, fresh surface is continually exposed to the oxidising atmosphere and the relevant oxidation rate is therefore that in the initial stages of Fig. 100. The sustained oxide surface advancement rate over the first hour is approximately 10^{-4} cm per hour. Unimpeded crack propagation should give failure in less than this time. Therefore the crack closing rate would be of the order of 2×10^{-4} cm per hour.

A crack opening rate is more difficult to quantify as it will vary considerably, even within a single specimen. No direct measurements are available, but an estimate can be made. Assume that crack propagation commences at the end of conventional secondary creep and that, at this time, the strain rate is entirely due to crack formation. Fig. 23 shows that a slight atmosphere effect existed and Figs. 52 and 53 show that some oxide bridging occurred where the applied stress was 12.0 N/mm^2 . In oxygen and in vacuum the relevant creep rates were 0.4 per cent per hour and 1.0 per cent per hour, respectively (Tables IV and V). This can be considered as an estimate of the creep rate range involved. These values represent actual extension rates of 1.1×10^{-2} cm per hour and 2.8×10^{-2} cm per hour, respectively. The crack closing rate

due to oxidation was calculated as 2×10^{-4} cm per hour. Therefore if all extension resulted from crack formation, a crack density of between 55 and 140 cracks per centimeter of gauge length would be required to allow oxide bridging. Metallography revealed that specimens had crack densities of up to 50 cracks per centimeter of gauge length.

Thus theory and experiment nearly equate in what was taken as a limiting case. Tables IV and V show that at a stress of 10 N/mm^2 where failure was effectively prevented in oxygen, the creep rates in oxygen and vacuum were 0.01 per cent per hour and 0.1 per cent per hour. In this case crack densities of between 1.4 and 14 cracks per centimeter of gauge length would allow oxide bridging of cracks. These values are well within those observed.

These effects of stress and temperature on the ability of oxidation to increase rupture life by inhibiting crack propagation, also explain why no effect was found at 700°C . While the creep rates were similar, the oxidation rate was markedly less. The oxidation rate at 700°C would be less by a factor of 20 than that at 950°C (19). Thus with a creep rate of 0.1 per cent per hour, the required crack density to allow oxide bridging would be 280 cracks per centimeter of gauge length.

5.11 Prediction of an Atmosphere Effect on Creep

Due to the complex nature of the processes involved, a quantitative statement of the conditions required to produce an alteration in creep behaviour cannot be made. However the results allow some qualitative guidelines to be given which assist in predicting the likelihood of interaction between oxidation and creep.

The extension of rupture life depends on the ability of the oxide to sustain a tensile load. Therefore the applied stress

requires to be less than the rupture strength of the oxide.

Conditions must allow the oxide to form load bearing bridges across cracks. The oxidation rate must be sufficient to enable such bridging to occur. Thus there will be a minimum critical ratio of oxidation rate to crack opening rate. Because speed of creep fracture is related to deformation rate, the ratio of secondary creep rate to oxidation rate may be significant. The real criterion is oxide thickening rate as opposed to weight gain and therefore must involve factors such as the Pilling-Bedworth ratio. The critical ratio will be peculiar to a single metal. From the work reported here, the minimum ratio of oxidation rate to secondary creep rate is of the order of $1.0 \text{ mg cm}^{-2} (\text{per cent})^{-1}$ for nickel.

Other necessary properties of the oxide can be defined. In order to form a load bearing bridge, the oxide must be firmly adherent to the metal. The oxide must sinter effectively and this would seem to require the formation of oxide at the outer surface, i.e. oxidation by the outward diffusion of metal ions.

Oxidation by the outward diffusion of cations will in addition produce a vacancy flow into the metal. While this may not be an essential feature of increased rupture life, it would assist in inhibiting creep fracture.

The requirements for oxidation to inhibit creep rupture are seen to depend on the oxidation mechanism and oxide properties. Knowing creep, oxidation and oxide characteristics, the theory would require verified for each individual metal, by conducting creep tests in oxygen. These guidelines can be used to predict the temperature/stress regime in which an effect would be expected.

5.12 The Oxidation of Nickel at 950°C

The nature of the apparatus used did not allow quantitative study of oxidation. It was not part of the programme that such

measurements should be attempted. Thus, information was entirely derived from metallography.

The oxidation of nickel was found to occur in the manner well documented in the literature (2.2). For short oxidation times, a single layer oxide was formed and in excess of 50 hours, a two layer structure formed (4.15). Metallography failed to establish the structure of single layer oxides but clearly showed the two layer structure to consist of an inner equiaxed layer with an outer columnar layer (Figs. 79 to 84 and 97 to 99). There was considerable porosity in the inner layer and concentrated along the junction of the two layers (Figs. 79 to 84). This gives support to the dissociation growth mechanism.

Figs. 93 to 95 show the initial stages of oxide growth to occur by whisker formation. This equates to columnar type growth in random orientation. If the dissociation mechanism is accepted, the single layer oxide should be of a columnar nature orientated perpendicular to the surface. Some time must therefore elapse in the initial stages of oxidation before columnar growth is established perpendicular to the nickel surface.

The majority of the oxide on internal crack surfaces was of a columnar nature (Fig. 53). This would arise from direct access of atmospheric oxygen into the cracks. In some short oxide filled cracks at the specimen surface, the oxide structure was similar to the inner surface layer (Figs. 57 and 58). This may show a limited potential for oxidation by the dissociation mechanism as the crack developed. Such oxidation would occur in step with crack development and not, as in the case of a columnar structure, after crack propagation. The high incidence of short oxide filled surface cracks suggests that a jacking displacement due to the oxide wedge

did not enhance crack propagation.

Comparison of stressed and unstressed specimens did not provide any evidence that oxidation under stress affected the formation of a double layer. All pairs of specimens showed a similar oxide structure in terms of double layer formation (Figs. 79, 80, 83 and 84). This observation must therefore question the role of compressive stresses in the mechanism of double layer oxide formation. An external tensile stress will cancel compressive growth stresses. It can only be assumed that tensile stress acts equally to allow double layer formation.

A lack of plasticity in the oxide was demonstrated in the creep tests on pre oxidised nickel (Fig. 35). The pre-formed oxide spalled to the extent that the damage was not repaired during the course of the creep test. However the complete absence of spalling on nickel specimens where all oxidation occurred simultaneously with creep, showed that a continuous adherent oxide can form on a deforming surface.

The consistency of the observation that the oxide layer on stressed specimens was thinner than that on unstressed specimens suggests that the effect was real (4.15). The creep process may therefore interfere with the vacancy flux at the specimen surface. In simplistic terms the vacancy flux due to creep will be a net flow of vacancies to the longitudinal specimen surface, which is in direct opposition to the flux away from this surface due to oxidation. The vacancy concentration gradient will be reduced and act to reduce the oxidation rate. In addition oxidation at internal crack surfaces will further inhibit free surface oxidation. This effect is analogous to the reduction in oxidation rate as the thickness of sheet specimens is reduced⁽¹⁹⁾.

Grain boundary void formation occurred due to oxidation alone (4.12 and 4.13). As all specimens were previously annealed, this contradicts the suggestion that prior vacuum annealing removed potential sites for the heterogeneous nucleation of voids during oxidation⁽¹⁹⁾.

After long oxidation times the structure of the nickel was similar to that which had undergone creep (Fig. 74). However void coalescence did not occur to the extent found in crept specimens and there was little oxide penetration into the grain boundaries. It could therefore be suggested that, during simultaneous oxidation and creep, the more discreet void formation was due to an oxidation type mechanism of void growth.

The creep process, however, appeared to control the void nucleation mechanism during simultaneous oxidation and creep. In unstressed specimens voids were concentrated on grain boundaries parallel to the specimen surface. In stressed specimens voids were concentrated on boundaries perpendicular to the axis of stress and therefore to the surface (Figs. 67 to 74).

This evidence strongly suggests that vacancy injection into the metal does occur during the oxidation of nickel. Grain boundary void formation during oxidation has been said to be due to either vacancy injection^(19,41), or creep induced by stresses set up in the metal⁽⁴²⁾. Due to the different position of void nucleation sites during creep alone and oxidation alone, such a stress system must be dissimilar to that caused by an applied tensile stress. During simultaneous oxidation and creep a stress due to oxidation would only affect void nucleation on grain boundaries parallel to the surface. However the present evidence showed a marked increase in void nucleation on grain boundaries perpendicular to the surface.

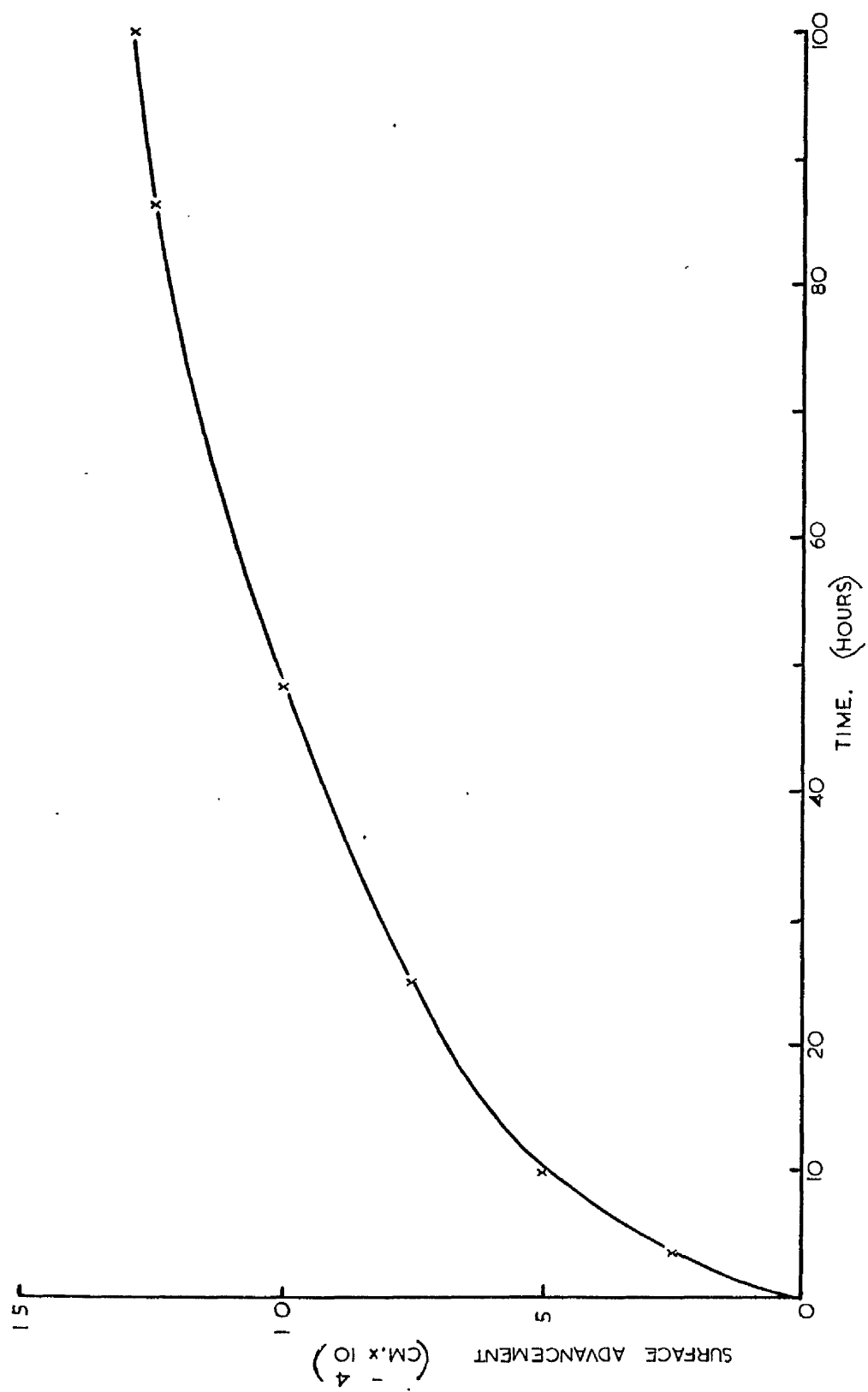
Therefore, creep and oxidation had combined to enhance void nucleation close to the specimen surface. This is not possible by a combination of the stress systems. The logical explanation is then an increased vacancy concentration due to oxidation, resulting in enhanced void nucleation at sites made favourable by the creep process.

5.13 Conclusions

1. At 950°C and over a stress range of 8.0 N/mm^2 to 12.0 N/mm^2 , considerable differences were found between the creep behaviour of high purity nickel in an oxygen atmosphere and vacuum.
2. A faster decrease of creep rate during primary creep was found in oxygen. It is suggested that this was caused by an increase in work hardening rate resulting from an increased dislocation density due to the formation of a surface oxide film.
3. No steady state creep rate was found in oxygen and the creep rate continued to decline. It is suggested that the injection of vacancies due to oxidation prevented the establishment of a balance between work hardening and recovery.
4. In oxygen, the coalescence of grain boundary voids was suppressed. It is suggested that the injection of vacancies due to oxidation altered the growth characteristics of voids to give a greater proportion of growth outwith the grain boundary plane.
5. In oxygen, the extended primary stage of decreasing creep rate led directly into an extended tertiary stage of fluctuating creep rate. This latter effect resulted from the formation of oxide within grain boundary cracks. The formation of load bearing bridges inhibited crack propagation.

6. These effects combined to increase the rupture life in oxygen relative to vacuum. This extension of rupture life was highly sensitive to stress.

Plot of Nickel Oxide Surface Advancement at 950°C.
Derived from data given by Hancock and Fletcher. (19) Fig.100



LIST OF REFERENCES

- (1) H. H. Bleakney. Proc. ASTM. vol. 47. p 575. 1947.
- (2) O. C. Shepard & W. Schalliol. ASTM. STP. 108. p 34. 1951.
- (3) H. T. McHenry & H. B. Probst. Tech. Note. No. 3987. National Advisory Committee for Aeronautics. Lewis Laboratory. 1957.
- (4) E. D. Sweetland & E. R. Parker. J. App. Mech. Trans. ASME. vol. 20. p 30. 1953.
- (5) P. Shahinian. Trans. Am. Soc. Metals. vol. 49. p 862. 1957.
- (6) R. L. Stegman, P. Shahinian & M. R. Achter. Trans. Met. Soc. AIME. vol. 245. p 1759. 1969.
- (7) R. R. Hough & R. Rolls. Metal Sci. J. vol. 5. p 206. 1971.
- (8) I. N. Bogachev, Y. G. Veksler & V. G. Sorokin. Prot. Metals (USSR) New York. vol. 7. p 19. 1971.
- (9) P. Shahinian & M. R. Achter. Trans. Met. Soc. AIME. vol. 215 p 37. 1959.
- (10) R. J. Sherman & M. R. Achter. Trans. Met. Soc. AIME. vol. 224. p 144. 1962.
- (11) T. C. Reuther, P. Shahinian & M. R. Achter. Proc. ASTM. vol. 61. p 956. 1961.
- (12) P. Shahinian. J. Basic. Eng. Trans. ASME. paper no. 64. Met. 6. 1964.
- (13) D. J. Duquette. Scripta Met. vol. 4. p 633. 1970.
- (14) J. S. Steele. Univ. of Glasgow. Dept. of Mech. Eng. Final Year Project. 1972.
- (15) P. Shahinian & M. R. Achter. Trans. Am. Soc. Metals. vol. 51 p 244. 1959.
- (16) P. Shahinian & M. R. Achter. Proc. ASTM. vol. 58. p 761. 1958.
- (17) R. Widmer & N. J. Grant. J. Basic Eng. Trans. ASME. vol. 82 p 882. 1960.
- (18) P. N. Chaku & C. J. McMahon. Metall. Trans. vol. 5. p 441. 1973.
- (19) P. Hancock & R. Fletcher. Metallurgie VI. vol. 1. p 1. 1966.
- (20) E. T. Denisenko & V. V. Shorokhod. Sov. Powder Metall. Met. Ceram. vol. 11. p 322. 1972.

- (21) T. R. Cass & M. R. Achter. *Trans. Met. Soc. AIME.* vol. 224 p 1115. 1962.
- (22) G. J. Richardson, C. M. Sellars & J. Tegart. *Acta. Met.* vol. 14. p 1225. 1966.
- (23) P. W. Davies, T. C. Finniear & B. Wilshire. *J. Inst. Metals.* vol. 91. p 289. 1962/3.
- (24) D. McLean. *Rep. Prog. Phys.* vol. 29 (1). p 1. 1966.
- (25) H. H. Bleakney. *Canada J. Tech.* vol. 30. p 340. 1952.
- (26) D. L. Douglass. *Mat. Sci. Eng.* vol. 3. p 255. 1968/9.
- (27) R. Lagneborg. *Met. Sci. J.* vol. 1. p 172. 1967.
- (28) R. Widmer & N. J. Grant. *J. Basic Eng. Trans. ASME.* vol. 82 p 829. 1960.
- (29) M. R. Achter. *ASTM. STP.* 415. p 181. 1967.
- (30) H. H. Smith & P. Shahinian. *ASTM. STP.* 462. p 217. 1970.
- (31) C. J. McMahon & L. E. Coffin Jr. *Metall. Trans.* vol. 1 p 3443. 1970.
- (32) J. D. Frandsen, N. E. Paton & H. L. Marcus. *Metall. Trans.* vol. 5. p 1655. 1974.
- (33) D. R. Holmes & R. T. Pascoe. *Werkstoffe u. Korrosion.* vol. 23. p 859. 1972.
- (34) M. R. Pickus & E. R. Parker. *J. Metals. Trans. AIME.* vol. 3. no. 9. p 792. 1951.
- (35) J. L. Meijering & M. J. Druyvestyen. *Philips Research Reports* vol. 2. no. 2. p 81. 1947.
- (36) A. U. Seybolt. *Quart. Supp. Phil. Mag.* vol. 12. no. 45. p 2. 1963.
- (37) G. C. Wood, I. G. Wright & J. M. Ferguson. *Corros. Sci.* vol. 5. p 645. 1965.
- (38) S. Mrowec. *Corros. Sci.* vol. 7. p 563. 1967.
- (39) G. C. Wood & I. G. Wright. *Corros. Sci.* vol. 5. p 841. 1965.
- (40) G. C. Wood, I. G. Wright, T. Hodgkiess & D. P. Whittle. *Werkstoffe u. Korrosion.* vol. 21. p 900. 1970.
- (41) R. Hales & A. C. Hill. *Corros. Sci.* vol. 12. p 843. 1972.
- (42) J. E. Harris. *Acta. Met.* vol. 26. p 1033. 1978.
- (43) G. B. Gibbs & R. Hales. *Corros. Sci.* vol. 17. p 487. 1977.

- (44) R. Hales. Corros. Sci. vol. 12. p 555. 1972.
- (45) K. N. Strafford & G. Smith. AIME. Proc. Mat. Sci. Symp. p 177. 1975.
- (46) G. C. Wood & T. Hodgkiess. Werkstoff u. Korrosion. vol. 23 p 766. 1972.
- (47) F. N. Rhines & J. S. Wolf. Metall. Trans. vol. 1. p 1701. 1970.
- (48) F. N. Rhines & R. G. Connell Jnr. AIME. Proc. Mat. Sci. Symp. p 94. 1975.
- (49) M. V. Speight & J. E. Harris. Acta. Met. vol. 26. p 1043. 1978.
- (50) D. R. Holmes & W. H. Whitlow. Werkstoffe u. Korrosion. vol. 23. p 741. 1972.
- (51) P. Hancock. Werkstoffe u. Korrosion. vol. 21. p 1002. 1970.
- (52) P. Hancock. AIME. Proc. Mat. Sci. Symp. p 155. 1975.
- (53) V. V. Levitin & L. K. Orzhitskaya. Phys. Met. Metall. vol. 30. p 172. 1970.
- (54) E. E. Badiyan & A. F. Sirenko. J. Mat. Sci. vol. 6. p 1479 1971.
- (55) W. J. Evans & B. Wilshire. Trans. Met. Soc. AIME. vol. 242 p 1303. 1968.
- (56) S. K. Mitra & D. McLean. Proc. Roy. Soc. Ser. A. vol. 292 p 288. 1966.
- (57) B. Wilshire. Scripta Met. vol. 4. p 361. 1970.
- (58) J. Weertman & P. Shahinian. J. Metals. Trans. AIME. vol. 206 p 1223. 1956.
- (59) C. R. Barrett & O. D. Sherby. Trans. Met. Soc. AIME. vol. 233 p 1116. 1965.
- (60) S. Karashima, H. Oikawa & T. Motomiya. Trans. Jap. Inst. Met. vol. 10. p 205. 1969.
- (61) S. K. Mitra & D. McLean. Met. Sci. J. vol. 1. p 192. 1967.
- (62) E. C. Norman & S. A. Duran. Acta. Met. vol. 18. p 723. 1970.
- (63) J. P. Dennison & B. Wilshire. J. Inst. Met. vol. 91. p 343 1962/3.
- (64) J. E. Harris, M. O. Tucker & G. W. Greenwood. Met. Sci. vol. 8. p 311. 1974.
- (65) D. A. Woodford. Met. Sci. J. vol. 3. p 234. 1969.
- (66) C. E. Price. Acta. Met. vol. 15. p 1249. 1967.

- (67) R. C. Boettner & W. D. Robertson. Trans. Met. Soc. AIME. vol. 221. p 613. 1961.
- (68) B. J. Cane & G. W. Greenwood. Met. Sci. vol. 9. p 55. 1975.
- (69) B. J. Cane. Met. Sci. vol. 12. p 102. 1978.
- (70) R. Resnick & L. Seigle. J. Metals. Trans. AIME. vol. 209 p 87. 1957.
- (71) P. W. Davies & B. Wilshire. Phil. Mag. vol. 11. p 189. 1965.
- (72) E. Smith & J. T. Barnby. Met. Sci. J. vol. 1. p 1. 1967.
- (73) J. W. Hancock. Met. Sci. vol. 10. p 319. 1976.
- (74) Y. Ishida & D. McLean. Met. Sci. J. vol. 1. p 171. 1967.
- (75) P. W. Davies & K. R. Williams. Phil. Mag. vol. 18. p 137. 1968.
- (76) W. R. Johnson, C. R. Barrett & W. D. Nix. Metall. Trans. vol. 3. p 695. 1972.
- (77) R. Fletcher. J. Phys. E. Sci. Inst. vol. 4. p 821. 1971.
- (78) R. L. Fullman, R. P. Carreker Jnr. & J. C. Fisher. J. Metals. Trans. AIME. vol. 197. p 657. 1953.
- (79) E. N. Thrower. J. Sci. Inst. vol. 29. p 91. 1952.
- (80) E. N. da C. Andrade. Proc. Phys. Soc. vol. 60. p 304. 1948.
- (81) A. J. Kennedy. J. Sci. Inst. vol. 30. p 371. 1953.
- (82) A. J. Kennedy. J. Sci. Inst. vol. 31. p 28. 1954.
- (83) F. Garofalo, O. Richmond & W. F. Domis. J. Basic Eng. Trans. ASME. vol. 84. p 287. 1962.
- (84) J. S. Wolf & J. M. Grochowski. AIME. Proc. Mat. Sci. Symp. p 274. 1975.
- (85) J. Weertman. & J. R. Weertman. "Elementary Dislocation Theory" Macmillan Series in Materials Science, 3rd Ed. p 170. 1966.



